

UNIVERSITY OF ALBERTA

Numerical Simulation of Hydrocarbon and Oxygen Transport and Microbial
Biodegradation During Bioventing: Application to a Field Study and Sensitivity
Analysis

BY

Sheri Lynn Gilmour



A thesis submitted to the Faculty of Graduate Studies and Research in partial fulfillment of the requirements for the degree of Master of Science.

DEPARTMENT OF GEOLOGY

Edmonton, Alberta
Fall 1996



National Library
of Canada

Acquisitions and
Bibliographic Services Branch

395 Wellington Street
Ottawa, Ontario
K1A 0N4

Bibliothèque nationale
du Canada

Direction des acquisitions et
des services bibliographiques

395, rue Wellington
Ottawa (Ontario)
K1A 0N4

Our file / Votre référence

Our file / Notre référence

The author has granted an irrevocable non-exclusive licence allowing the National Library of Canada to reproduce, loan, distribute or sell copies of his/her thesis by any means and in any form or format, making this thesis available to interested persons.

L'auteur a accordé une licence irrévocable et non exclusive permettant à la Bibliothèque nationale du Canada de reproduire, prêter, distribuer ou vendre des copies de sa thèse de quelque manière et sous quelque forme que ce soit pour mettre des exemplaires de cette thèse à la disposition des personnes intéressées.

The author retains ownership of the copyright in his/her thesis. Neither the thesis nor substantial extracts from it may be printed or otherwise reproduced without his/her permission.

L'auteur conserve la propriété du droit d'auteur qui protège sa thèse. Ni la thèse ni des extraits substantiels de celle-ci ne doivent être imprimés ou autrement reproduits sans son autorisation.

ISBN 0-612-18262-2

Canada

UNIVERSITY OF ALBERTA

LIBRARY RELEASE FORM

NAME OF AUTHOR: Sheri Lynn Gilmour

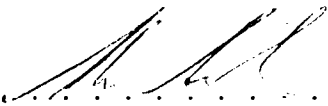
TITLE OF THESIS: Numerical Simulation of Hydrocarbon and Oxygen Transport and Microbial Biodegradation During Bioventing: Application to a Field Study and Sensitivity Analysis

DEGREE: Master of Science

YEAR THIS DEGREE GRANTED: 1996

Permission is hereby granted to the University of Alberta Library to reproduce single copies of this thesis and to lend or sell such copies for private, scholarly or scientific research purposes only.

The author reserves all other publication and other rights in association with the copyright in the thesis, and except as hereinbefore provided neither the thesis nor any substantial portion thereof may be printed or otherwise reproduced in any material form whatever without the author's prior written permission.

(Signed) 

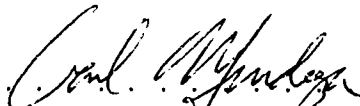
Sheri Lynn Gilmour
1619 - 89 Street
Edmonton, Alberta
Canada, T6K 2A8

Date: *Oct. 3, 1996* . . .

UNIVERSITY OF ALBERTA

FACULTY OF GRADUATE STUDIES AND RESEARCH

The undersigned certify that they have read, and recommend to the Faculty of Graduate Studies and Research for acceptance, a thesis entitled **Numerical Simulation of Hydrocarbon and Oxygen Transport and Microbial Biodegradation During Bioventing: Application to a Field Study and Sensitivity Analysis** submitted by Sheri Lynn Gilmour in partial fulfillment of the requirements for the degree of Master of Science.



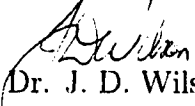
Dr. C. A. Mendoza (Supervisor)



Dr. W. B. McGill (External)



Dr. K. Muchlenbachs (Examiner)



Dr. J. D. Wilson (Chair)

Date: . 1/10/96 . . .

For A. Kathleen Gilmour.
my grandma
and
Pamela Gilmour.
my sister

Abstract

Studying the processes that are thought to occur during biodegradation of hydrocarbon contaminants in the unsaturated zone is important in order to implement bioventing as an effective remediation technique. A conceptual model to describe hydrocarbon and oxygen transport and microbial utilization in the unsaturated zone is developed. Steady-state laminar flow of air due to pressure gradients imposed by extraction wells is assumed. The advection-dispersion equation combined with Monod kinetics define transport and biodegradation for hydrocarbon and oxygen. The microbial utilization rates as well as the availability of hydrocarbon and oxygen may limit the biodegradation of the organic contaminant.

An axisymmetric finite-element model of the conceptual model is used to simulate a series of bioventing field trials and is applied to perform a sensitivity analysis. The match between the numerical results and the field data is very good, indicating that the processes occurring at the site are adequately represented by the numerical model. Exact representation of the field data is not possible due to the inability to fully quantify the heterogeneities in the subsurface at the field site. Initial concentrations of the hydrocarbon, oxygen, and microbial population were found to significantly affect the amount and distribution of hydrocarbon biodegradation. These initial concentrations at field sites need to be extensively measured to understand biodegradation during bioventing.

A sensitivity analysis reveals that the size of the microbial population, the maximum hydrocarbon utilization rate, and the hydrocarbon and oxygen half-saturation constants highly affect the amount of hydrocarbon biodegraded. The chemical prop-

erties, such as the Henry's constant and the organic partitioning coefficient, influence whether the contaminant is available for microbial biodegradation in the aqueous phase. In terms of minimizing off-gas treatment while maximizing mass removal, primarily by biodegradation, a reasonable low flow rate is preferred. For optimal remediation results during bioventing, a small well screen close to the hydrocarbon contaminant source should be implemented; sites without a lower permeable unit overlying the zone of contamination should have some sort of surface cover in order to increase the radius of influence of the extraction well thereby increasing the amount of oxygen circulating through the system.

Acknowledgements

First, and most important, I must thank my supervisor, Carl Mendoza. His support, caring, and understanding will never go unnoticed with his graduate students. During my degree, your door was always open and you always had time to help me with any problems, even if it involved sitting down with me to tackle coding errors for an afternoon. Your guidance has vastly increased my scientific knowledge.

I must thank the former Department of Geology and the new Department of Earth and Atmospheric Sciences for the funding I received through Graduate Teaching Assistantships and a Research Assistantship. I also appreciate the funding I received through Carl's NSERC Research Grant. I extend a thank you to James Armstrong and Brent Moore at Komex International Ltd. for the data provided by them for this thesis and their insight on the field site.

Thank you to my supervisory committee for answering all my inquiries and helping me when possible. Having obtained my undergraduate degree at the University, I would like to mention several professors that added to my academic career: Dr. Rutter, Dr. Chacko, Dr. Erdmer, Dr. Pemberton, and of course, Dr. Tóth. However, it was in Mr. Everitt's grade eight class that my interest in science truly began.

I would like to acknowledge the people in the Hydrogeology group that helped make my time here an enjoyable one: Ben, Kent, Liane, Morris, and Melody. I would especially like to thank Leroy for his computer expertise and general enthusiasm. He never did convince me that 'changing a couple lines of code' would truly solve the problem. Thank you to Darlene for her support, help, and being a good friend. Hang in there and before you know it, you too will be writing this page. Thanks to Brent

for the laughs we've shared this past year and for future ones that are to come. Your keen interest in science is a delight to watch. I would also like to thank the friends I have made past and present in the Geology Department. Unfortunately, you all made the ESB feel like a second home.

Thank you to a couple of great friends Debbie and Deanna. Debbie never complained about late night phone calls updating her on my latest successes and failures. Deanna was the person who knew everything that was happening during my progress and I thank her for always being interested in how things were going.

I would like to say thank you to a very special group of people in my life. You have helped me find my laughter, my feelings, my confidence, my strengths, and my inner happiness. Thank you for the experiences. I feel privileged to know you all.

I need to extend a thank you to all the members of my immediate family: Mom, Dad, Paula, Jolene, John, Pam, Doug, Nicholas, and Emilie. Without the support from my parents, I would not have made it through my first degree. Without the support from Doug and Pam, I would not have been able to finish this degree with a 'relatively' low stress level. I must say a special thank you to my sister Pam for all her support over the last three years. You've been a good ear (and a great distraction when I needed to play). Also, thank you to my grandparents: Nana, Grandpa Bill, and Grandma. You've always shown interest in my schooling and progress. I wish Papa was still with us to see my accomplishment. Thank you Auntie Bev for encouraging me through my entire post secondary career. Also, thanks so much to the Bechtels for all their cheers and Sunday night suppers.

Finally, thank you David. You were the one who suggested I should enter Graduate Studies. Three years ago, you helped me start the path to many wonderful changes in my life, supported me when things got a little rough, and encouraged me to travel and finish the road with my own abilities. Here's to our recent accomplishments and to the end of commuting on Highway Two. I look forward to our travels together.

Contents

1	Introduction	1
1.1	Bioventing	1
1.2	Monod Kinetics	5
1.3	Literature Review	8
1.4	Objectives/Purpose	13
2	Theory	16
2.1	Conceptual Model	16
2.2	Mathematical Model	18
2.2.1	Air Flow	19
2.2.2	Transport	23
2.2.3	Biodegradation Reaction	26
3	Numerical Model	28
3.1	Model Description	28
3.2	Mass Balance and Mass Fate	31
3.3	Accuracy and Stability Criteria	33
3.4	Analytical Solution Comparison	34
4	Comparison of the Numerical Model Results to Field Data	38
4.1	The Field Site	38
4.1.1	Site Location and Characterization	38
4.1.2	Temperature	42

4.1.3	Data Collection	42
4.1.4	Site Parameters	43
4.1.5	Microbial Population	46
4.2	Conceptual Model	48
4.2.1	Grid and Domain	48
4.2.2	Boundary Conditions	48
4.3	Modelling Results	50
4.3.1	Setup for Comparison to Field Data	50
4.3.2	Air Flow Comparisons	50
4.3.3	Biodegradation Comparisons	57
4.4	Summary	77
5	Sensitivity Analysis	79
5.1	Approach	79
5.2	Methods of Presenting Results	81
5.3	Base Case	82
5.4	Till Layer Thickness and Permeability	94
5.5	Extraction Rate, Size and Position of the Well Screen	103
5.6	Initial Microbial Concentrations	107
5.7	Soil Moisture Content	111
5.8	Biodegradation Parameters	114
5.9	Different Hydrocarbon Contaminants	118
5.10	Dispersivities	122
5.11	Unconstrained Source	123
6	Conclusions	125
	References	129

List of Figures

1.1	The relationship of the microbial growth rate and the hydrocarbon concentration.	7
2.1	The conceptual model of the physical situation and processes.	17
2.2	Approximation of the fluid distribution in the porous media when free product floats above the watertable.	18
2.3	The boundary conditions of the conceptual model.	22
3.1	Summary of the boundary conditions and the parameters for the analytical solution comparison.	36
3.2	Comparison of the numerical model to the analytical model.	37
4.1	Location of the field site.	39
4.2	The numerical grid.	49
4.3	Distribution of the wells at the field site.	51
4.4	Pressure distribution comparison.	52
4.5	Distribution of pressure along the extraction well screen.	54
4.6	Comparison of the pressure distribution that results from having the well radius equal to 0 <i>cm</i> versus 10 <i>cm</i>	55
4.7	Comparison of the pressure distribution when the extraction well is defined as a constrained pressure versus a constrained flux.	56
4.8	Results for the Recovery Test.	60
4.9	Comparing the difference between different half-saturation constants and initial microbial populations.	63

4.10	The difference between simulations with and without biodegradation.	64
4.11	Results for the Variable Flow Rate Test for ML 4A.	66
4.12	Results for the Variable Flow Rate Test for ML 3A.	67
4.13	Results for the Variable Flow Rate Test for ML 1A.	68
4.14	The different hydrocarbon trends for wells ML 1A and ML 3A for both with and without biodegradation.	70
4.15	Results for the Respiration Test for well ML 4A.	71
4.16	Results for the Respiration Test for well ML 3A.	72
4.17	Results for the Respiration Test for well ML 1A.	73
4.18	Hydrocarbon trends for ML-3A with and without biodegradation.	75
4.19	Hydrocarbon trends for ML-1A with and without biodegradation.	76
5.1	Hydrocarbon distributions for the base case simulation.	85
5.2	Hydrocarbon concentration profile for the base case simulation.	86
5.3	a) Pressure and b) velocity distributions for the base case simulation.	87
5.4	Oxygen distributions for passive transport for the base case simulation.	88
5.5	Oxygen distributions for advective-dispersive transport for the base case simulation.	89
5.6	Oxygen concentration profile for the base case simulation.	91
5.7	Microbial concentration profile for the base case simulation.	93
5.8	Hydrocarbon distributions for the base case simulation without biodegradation.	95
5.9	a) Pressure and b) velocity distributions for the no till layer simulation.	97
5.10	a) Pressure and b) velocity distributions for the thicker till layer simulation.	98
5.11	Hydrocarbon distribution for advective-dispersive transport for a) no till layer and b) a thicker till layer.	99
5.12	Oxygen distribution for advective-dispersive transport for a) no till layer and b) a thicker till layer.	100

5.13	Hydrocarbon concentration profile for two different extraction rates, 25 and 75 ℓ/s	104
5.14	Oxygen concentration profile for two different extraction rates, 25 and 75 ℓ/s	105
5.15	Oxygen distribution for advective-dispersive transport for the simulations where the smaller wellscreen is a) near the watertable and b) near the base of the till unit.	108
5.16	Oxygen distribution for a) passive transport and b) advective-dispersive transport for the increased microbial population size simulation.	110
5.17	Microbial concentration profile for the increased microbial population size simulation.	112
5.18	Comparison of the oxygen concentration profiles for the simulations with an increased and decreased soil moisture content.	113
5.19	Hydrocarbon distribution for advective-dispersive transport for a) an increased biodegradation rate and b) a decreased biodegradation rate.	116
5.20	Oxygen distributions for dodecane at 1800 hours.	121

List of Tables

4.1	Parameters used to describe the site properties.	44
4.2	Parameters used for transport simulations.	45
4.3	Acceptable ranges of the biodegradation parameters.	47
4.4	Parameters ranges for the three field tests.	61
5.1	Properties for the base case simulation.	83
5.2	Mass fate for the base case simulation.	92
5.3	Mass fate for the no till layer and the thicker till layer simulations. . .	101
5.4	Mass fate the two different extraction rates, 25 and 75 ℓ/s	106
5.5	Mass fate for a higher microbial concentration.	109
5.6	Mass fate for the increased soil moisture content simulation.	115
5.7	Biodegradation parameter ranges for the sensitivity analysis.	116
5.8	Mass fate for the increased rate of biodegradation and hexane transport.	117
5.9	The chemical properties for hexane, dodecane, and benzo[a]pyrene. . .	119

Notation

Flow

r	radial coordinate direction	[L]	m
z	vertical coordinate direction	[L]	m
k_{ij}	intrinsic permeability	[L ²]	m^2
k^*	relative permeability	[L ²]	m^2
ρ_0	density of the uncontaminated soil gas	[M/L ³]	kg/m^3
g	gravitational constant	[L/T ²]	m/s^2
μ_c	gas viscosity of the compound	[M/LT]	$Pa \cdot s$
μ_a	gas viscosity of air	[M/LT]	$Pa \cdot s$
h	equivalent head	[L]	m
P	gas pressure relative to atmospheric pressure	[M/LT ²]	Pa
t	time	[T]	s

Biodegradation

λ	Monod decay term	[-]	-
C_w	concentration of aqueous hydrocarbon	[M/L ³]	mg/ℓ
O_w	concentration of aqueous oxygen	[M/L ³]	mg/ℓ
M_t	total aerobic microbial concentration	[M/L ³]	mg/ℓ
h_u	maximum hydrocarbon utilization rate	[T ⁻¹]	s^{-1}
Y	microbial yield coefficient	[M/M]	mg/mg
K_C	hydrocarbon half-saturation constant	[M/L ³]	mg/ℓ
K_O	oxygen half-saturation constant	[M/L ³]	mg/ℓ
k_c	first order decay rate of natural organic carbon	[T ⁻¹]	s^{-1}
C_{oc}	natural organic carbon concentration	[M/L ³]	mg/ℓ
b	microbe death rate	[T ⁻¹]	s^{-1}
G	ratio of oxygen to hydrocarbon consumed	[M/M]	mg/mg

Notation

Transport

θ	total porosity	$[-]$	-
θ_a	air-filled porosity	$[-]$	-
θ_w	water-filled porosity	$[-]$	-
D_{ij}	hydrodynamic gaseous dispersion tensor	$[L^2/T]$	m^2/s
D_{ai}	air-phase diffusion coefficient	$[L^2/T]$	m^2/s
D_{wi}	aqueous effective diffusion coefficient	$[L^2/T]$	m^2/s
D_w	free-solution aqueous diffusion coefficient	$[L^2/T]$	m^2/s
α_l	longitudinal dispersivity	$[L]$	m
α_t	transverse dispersivity	$[L]$	m
δ_{ij}	Kronecker delta	$[-]$	-
τ_a	air-phase tortuosity	$[-]$	-
τ_w	water-phase tortuosity	$[-]$	-
v_i	average linear velocity of the gas mixture	$[L/T]$	m/s
q_i	gaseous Darcy flux	$[L/T]$	m/s
MW	molecular weight	$[M/M]$	g/mol
C	concentration of gaseous hydrocarbon	$[M/L^3]$	ppm
O	concentration of gaseous oxygen	$[M/L^3]$	ppm
R_C	retardation factor for hydrocarbon	$[-]$	-
R_O	retardation factor for oxygen	$[-]$	-
H_C	Henry's constant for hydrocarbon	$[-]$	-
H_O	Henry's constant for oxygen	$[-]$	-
ρ_b	porous medium bulk density	$[M/L^3]$	g/cm^3
K_D	distribution coefficient	$[L/M]$	ml/g
f_{oc}	soil organic content	$[-]$	-
K_{oc}	organic carbon partitioning coefficient	$[L/M]$	ml/g

Chapter 1

Introduction

Contamination of the environment is of increasing concern. In particular, hydrocarbon contamination of geologic material due to the leakage of petroleum products from underground and/or above-ground storage tanks or accidental releases is considered to be a major threat to groundwater supplies and has led to the development of various remediation techniques for subsurface cleanup. One technique for remediation of the unsaturated zone is vacuum extraction, also known as soil vapour extraction. One refinement of the method is known as bioventing.

1.1 Bioventing

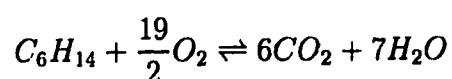
In its simplest form, vacuum extraction is the process whereby air is extracted from the subsurface to enhance volatilization of organic chemicals found in the unsaturated zone. These chemicals may exist in a number of phases, including the pure phase, the gas phase, the dissolved phase, or the sorbed phase. The liquid portion of the contaminant often can not be directly removed by vacuum extraction; however, continual extraction of vapours allows more liquid to vapourize, causing it to be removed in the gas phase (Massmann, 1989).

A beneficial side effect of vacuum extraction often appears to be the natural enhancement of petroleum product biodegradation. This occurs because increasing the supply of oxygen with vacuum extraction stimulates microbial activity which in turn

increases the amount of organic substances that are broken down. This process of enhanced biodegradation is commonly referred to as 'bioventing' and its degree of success depends on several factors, such as the type of contaminant, the microbial population, and the environmental conditions. Field studies have demonstrated the effect of air flow on the amount of contamination removed due to volatilization versus the amount removed due to biodegradation (Hinchee and Olfenbuttel, 1991). Low air flow rates provide only enough oxygen to sustain microbial activity by the addition of an external electron acceptor (oxygen), but limit the amount of direct volatilization. Due to the low volatilization rate, bioventing may be a more cost effective and beneficial remediation technique because it eliminates the need for expensive off-gas treatment facilities normally required for vacuum extraction.

Biodegradation can be either an aerobic or an anaerobic process. Aerobic biodegradation uses oxygen as an electron acceptor; anaerobic biodegradation often uses nitrogen as an electron acceptor. This study is only concerned with aerobic biodegradation which tends to be prevalent in the unsaturated zone and will focus on this aspect from this point forward.

In general, from a macroscopic viewpoint, microbial degradation can be described by a stoichiometric reaction. The reactants are the hydrocarbons of interest and oxygen, and the products are carbon dioxide and water (Beausoleil *et al.*, 1993). The reaction is driven by microbial metabolism of the hydrocarbon and oxygen; hydrocarbon biodegradation is essentially an oxidation-reduction reaction where the hydrocarbon is oxidized (donates an electron) and an electron acceptor, oxygen in this case, is reduced (accepts an electron). The wide variety of contaminants that can be biodegraded during bioventing include: pesticides, herbicides, solvents, heating oil, creosote, transmission fluid, jet fuel, diesel fuel, and others. Hexane has been chosen here as the hydrocarbon contaminant because it best represents the range of hydrocarbons being biodegraded at the field site in this study (Komex, 1994c). According to Riser-Roberts (1992), the stoichiometric reaction for hexane is:



Thus, for every 3.5 grams of oxygen utilized, approximately 1 gram of hydrocarbon is degraded.

In the field, oxygen utilization is generally used to estimate the biodegradation rate for several reasons. Firstly, the hydrocarbon degrades to both carbon dioxide and biomass; therefore, not all the carbon will be converted to carbon dioxide (Hinchee and Olfenbittel, 1991). In addition, some carbon dioxide may dissolve in water to form carbonic acid or bicarbonate. Thirdly, intermediate by-products other than carbon dioxide may form when hydrocarbons are only partially degraded (Hinchee and Olfenbittel, 1991).

The physical and chemical characteristics of the subsurface environment and the available electron acceptors and donors typically determine which types of microorganisms will be active (Beak, 1990). In general, the majority of the subsurface indigenous microbes are bacteria, but fungi and protozoa are also found (Fetter, 1993). Because the microbes are heterotrophic (meaning they derive energy and carbon for survival and growth from the decomposition of organic materials (Riser-Roberts, 1992)), there is a minimum substrate concentration of naturally occurring carbon or hydrocarbon contaminant required for a microbial community to be active (Fetter, 1993). This growth-limiting substrate concentration, sometimes referred to as the threshold concentration, has been estimated at approximately 1.0 to 5.0 μg of substrate *per kg* of soil (Alexander, 1994). The growth of a microbial population is therefore restricted by the concentration of the growth-limiting substrate. The distribution of the microbes in an uncontaminated soil profile may differ greatly as a function of soil type; however, for any one particular type of soil with a uniform substrate concentration, there is usually a fairly consistent population density of the microorganisms vertically and laterally. The size of the microbial population does not appear to affect its ability to degrade hydrocarbon (Beausoleil *et al.*, 1993) and occasionally several distinct populations may have a cooperative relationship in the destruction of hydrocarbons (NRC, 1993). Some chemicals are toxic to microbes at high concentrations and thus may inhibit microbial growth or hydrocarbon utiliza-

tion (Rittmann *et al.*, 1994), even though these chemicals are often readily degraded at lower concentrations. When a mixture of hydrocarbons is present, microbes may preferentially degrade the one hydrocarbon that provides the most energy and is easiest to digest (NRC, 1993).

The biodegradation rate of a contaminant refers to some measure of substrate mass loss or change in concentration over time (Rafai and Bedient, 1990). Miller *et al.* (1993) present an equation which is often used in the field to calculate a first approximation of the biodegradation rate from the oxygen utilization rate, the air filled porosity, the density of oxygen, and the mass ratio of oxygen to hydrocarbon required for mineralization. Knowing the biodegradation rate, the volume of soil aerated by the bioventing system, and the bulk density of the soil, an estimate of the total mass of hydrocarbon biodegraded can be determined. The rate of microbial degradation generally decreases for compounds of higher molecular weight, for aromatic compounds, and for compounds with a large amount of branching, and/or halogen atoms (Hemond and Fechner, 1994). Low biodegradation rates could also be due to the lack of oxygen, low microbial biomass, or some other factor(s).

From field studies, the sites best suited to bioventing of hydrocarbons are those which have aerobic conditions, sufficient air flow, neutral to slightly acidic pH, adequate soil moisture, enough background nutrients, and relatively warm temperatures (Riser-Roberts, 1992). The electron acceptor, oxygen, must be supplied in high enough concentrations to sustain aerobic biodegradation. For bioventing applications the amount of available oxygen is largely a function of the flow rate. The optimal pH range of a remediation site for microbial activity is six to eight, although microbial respiration has been observed outside this range as well (Riser-Roberts, 1992). The pH can also influence the mobility, the activity, and the solubility of the contaminants. An optimal soil moisture content for each specific site to sustain the microbial community exists; too little soil moisture will inhibit microbial activity, while too much soil moisture will limit the air permeability, thus decreasing the oxygen transfer capacity of the soil. The essential macro-nutrients for microorganisms

are nitrogen, phosphorous, sulphur, and potassium. Some previous site studies have found that background concentrations of the nutrients are sufficient for biodegradation and no nutrient addition is required (Miller *et al.*, 1991). Microbial metabolism may occur between -2 to $110\text{ }^{\circ}\text{C}$ [(Riser-Roberts, 1992; Pederson, 1996), as reported by (Fyfe, 1996)]; however, different types of bacteria have specific preferred temperature ranges over which they metabolize. Within the allowable temperature range, the rate of biodegradation tends to increase with increasing temperature (Chapelle, 1993). The metabolism rate has been shown to be directly related to temperature and can be estimated by the van't Hoff-Arrhenius equation (Miller *et al.*, 1993). For simplicity, the pH and background nutrients are assumed to be constant at optimum concentrations and are not investigated in this study.

Environmental factors influencing the availability of oxygen to the microbes affect the implementation of bioventing. The success of any venting remediation technique will depend on the ability to induce an air-flow field which will intersect the distributed hydrocarbon contaminant in a heterogeneous unsaturated zone. Heterogeneities may lead to preferential flow paths, meaning, for example, oxygen may only reach certain areas where residual is trapped (*e.g.*, fine-grained clay and silt lenses) by passive transport. The geologic material must have a permeability which allows sufficient air flow through the field site area. In finer materials with lower permeabilities, fracturing may increase the number of potential air flow paths. Remediation will also depend on the rate of contaminant mass transfer from the immiscible and air phases to the water phase (Baehr *et al.*, 1989). Since biodegradation occurs in the water, the amount of both hydrocarbon and oxygen in the aqueous phase will influence the amount of biodegradation occurring.

1.2 Monod Kinetics

To adequately describe biodegradation, the kinetics of the biotransformation of the hydrocarbon contaminant along with the transport of the oxygen and hydrocarbon must be investigated. This requires coupled equations to describe the removal of

hydrocarbon and the consumption of oxygen by microbes, and the growth and death of the microbes. Monod kinetics relate the change in density of microbes on a hydrocarbon substrate to the hydrocarbon and oxygen concentrations.

One modified equation of the Monod function to describe microbial growth is (Fetter, 1993):

$$\frac{\partial M_t}{\partial t} = h_u Y \left(\frac{C_w}{K_c + C_w} \right) \left(\frac{O_w}{K_o + O_w} \right) M_t - b M_t + k_c Y C_{oc} \quad (1.1)$$

where M_t is the total aerobic microbial concentration; h_u is the maximum hydrocarbon utilization (or growth) rate per unit mass of microorganisms; Y is the microbial yield coefficient; C_w , O_w are the aqueous hydrocarbon and oxygen concentrations, respectively; K_C , K_O are the hydrocarbon and oxygen half-saturation constants; b is the microbial death rate; k_c is the first-order decay rate of natural organic carbon; and C_{oc} is the natural organic carbon concentration. The equations which describe hydrocarbon consumption and oxygen utilization are discussed in the following chapter.

Once a microbial population has become acclimated to its environment, it will either grow or die based on the kinetic coefficients and the hydrocarbon and oxygen concentrations. The size of the initial microbial population is generally determined from analysis of field samples collected for the various geologic material present. The increase in mass of new microbes during biodegradation needs to be predicted, which can be calculated by Equation 1.1. The number, and from there the mass, of new microbes can also be determined from measurements of microorganisms in pure cultures (Alexander, 1994). The microbial yield, Y , is then calculated by dividing the mass of the new microbes grown by the mass of the chemical degraded. The microbial death rate is generally not measured, but can be obtained from measuring the rate at which the microbial population decreases when the substrate concentration is below the minimum concentration. The death rate has little effect on the amount of hydrocarbon biodegraded and thus the reasons why the microbial population is decreasing are more important than the actual death rate. Some reasons of microbial death include: freeze/thaw periods, predation of protozoans, changes in soil moisture

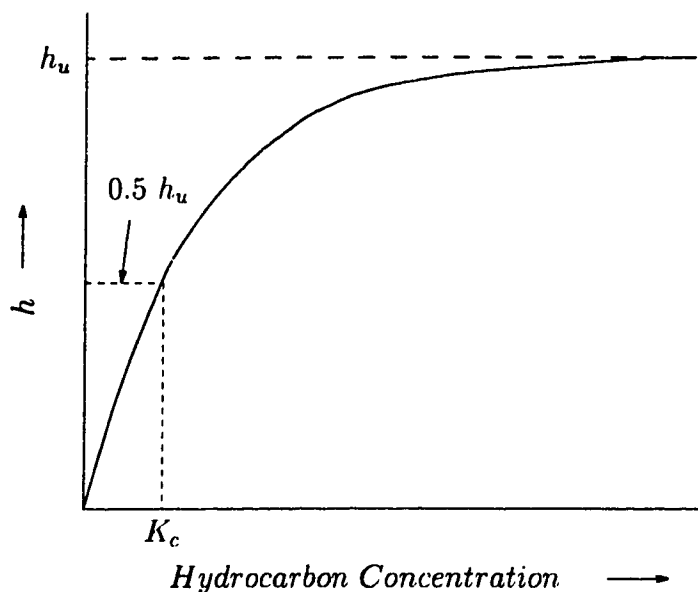


Figure 1.1: The relationship between the microbial growth rate and the hydrocarbon concentration (based on Fig. 6.1, Alexander, 1994).

content, and influxes of toxic gases (pers. comm. McGill, 1996).

An understanding of the kinetic degradation coefficients is essential in order to describe microbial degradation with some certainty. The following briefly describes the more significant kinetic degradation coefficients and, briefly, discusses how these coefficients are calculated. The specific growth rate, h , of the microbes is simply the product of the microbial yield coefficient, Y , and the rate at which the hydrocarbon is degraded. For a given oxygen concentration, at low hydrocarbon concentrations, the specific growth rate of microbes, h , is low; however, as the hydrocarbon concentration increases, the growth rate of the microbes also increases to some maximum (Alexander, 1994) where little change in the growth rate occurs (see Figure 1.1). The maximum utilization rate, h_u , is basically the maximum growth rate of the microbes. Figure 1.1 also shows that the half-saturation constant, K_C , is calculated when the growth rate is at half the maximum. This constant, K_C , varies with the affinity or attraction of the microbe to the hydrocarbon substrate (Alexander, 1994). The lower the value of the half-saturation constant, the greater the attraction the

microbe has for the hydrocarbon substrate. For a single substrate, this constant may extend over a considerable range; for a single microbe, this constant may differ for different hydrocarbons (Alexander, 1994). The oxygen half-saturation constant, K_O , is calculated in a similar fashion as the hydrocarbon half-saturation constant, K_C .

1.3 Literature Review

To date, the study of enhanced subsurface biodegradation has primarily been focused on saturated porous media. Many of these studies used numerical modelling techniques. For the most part, the models were verified analytically or by comparison to laboratory tests; only a few studies have used field data for model verification (Rafai *et al.*, 1991; Rafai *et al.*, 1988; Widdowson and Aclion, 1991; Borden *et al.*, 1986). Biodegradation in the saturated zone has been shown to enhance hydrocarbon remediation (Borden *et al.*, 1986; Sleep and Sykes, 1991; MacQuarrie *et al.*, 1990; Molz *et al.*, 1986); however, oxygen supply is usually insufficient to prevent significant contaminant migration (Sleep and Sykes, 1991).

Parameters that affect biodegradation, the rate of biodegradation, and the success of bioremediation have been investigated in these studies. The heterogeneity structure of the porous medium was found to be a very sensitive parameter (MacQuarrie and Sudicky, 1990; Schafer and Kinzelbach, 1991; Brusseau, 1991; Borden and Bedient, 1986). Variations in hydraulic conductivity (Rafai *et al.*, 1988) and average linear groundwater velocity (MacQuarrie and Sudicky, 1990) also affected the predictive ability of most models. When applying their model BIOPLUME II, Rafai *et al.* (1988) found the lower the hydraulic conductivity value used, the higher the rate of biodegradation was required to match the decline in hydrocarbon concentrations observed at their field site. The microbial parameters deemed to be important were the maximum hydrocarbon utilization rate per unit mass of microorganisms (Rafai *et al.*, 1988), the initial microbial concentrations, and the half-saturation constants for the hydrocarbon and the oxygen (Chen *et al.*, 1992). Most importantly, in most studies of biodegradation in the saturated zone the key limiting factor was deter-

mined to be oxygen availability (Borden and Bedient, 1986; Sleep and Sykes, 1991; Wu *et al.*, 1990; MacQuarrie and Sudicky, 1990).

Depending upon the transport mechanisms and the relative rates of transport, biodegradation can be described as either an instantaneous reaction or a kinetic reaction. Due to the slow transport of oxygen in most saturated zones, oxygen supply is rate limiting and biodegradation can be described as an instantaneous reaction applicable when the advective transport of oxygen is slower than biodegradation. For saturated zones with high groundwater flow rates and for unsaturated zones with high permeabilities, oxygen transport is relatively fast and biodegradation must be described as a kinetic reaction. Thus, a kinetic reaction is applicable for slowly degradable hydrocarbons, in areas close to the hydrocarbon plume, or in situations where the natural microbial populations have yet to adapt to the foreign hydrocarbon (Borden and Bedient, 1986). Borden and Bedient (1986) developed equations for simulating the growth, death, and transport of microorganisms, as well as the transport and removal of hydrocarbon and oxygen within an aquifer. They assumed biodegradation could be approximated as either modified Monod kinetics, as discussed previously, where the first-order decay rate is strongly dependent on the saturated thickness (influencing the oxygen accessibility and the vertical dispersion coefficient), or approximated as an instantaneous reaction between oxygen and hydrocarbon when the amount of oxygen required for the degradation of the hydrocarbon plume is rate limiting. In this study, a kinetic reaction is used to describe biodegradation because there is sufficient oxygen supply and the area of bioremediation is close to the hydrocarbon source.

Rafai and Bedient (1990) compared the two conceptual models for biodegradation in groundwater as discussed by Borden and Bedient (1986). Biodegradation described by an instantaneous reaction between the hydrocarbons and the oxygen required less biotransformation data and was simpler to model than biodegradation described by a dual substrate Monod kinetic model. The main difference between the two models was that the instantaneous model assumed oxygen transport was

limiting the biodegradation process while the kinetic model allowed for the fact that the oxygen utilization might be considered to be as significant as oxygen transport (Rafai and Bedient, 1990). The differences between the results of the two models were a function of the initial concentration of oxygen, the distribution of both the hydrocarbon and oxygen (MacQuarrie *et al.*, 1990), the half-saturation constants, and the Damköhler number (which represents the effect of heterogeneity or structure of the porous medium (Brusseau, 1991)). As discussed above, when the rate of advective transport is slower than the rate of biodegradation, Chen *et al.* (1992) indicate that no microbial parameters need to be employed and degradation may be computed directly from a stoichiometric reaction.

Few studies have considered the problem of describing the distribution of microorganisms in the subsurface. Baveye and Valocchi (1989) compared and contrasted three different conceptual frameworks for bacterial growth: (a) uniform coverage of the matrix by microorganisms; (b) distribution of microorganisms into microcolonies; and (c) variable spatial distribution of the microorganisms. Molz *et al.* (1986) modelled microbial growth degradation processes using the concept of a microcolony. Widdowson *et al.* (1988) extended the model by Molz *et al.* (1986) and incorporated organic carbon biodegradation by facultative bacteria. They found that both nutrient availability and the mode of respiration are important factors when simulating biodegradation.

Research into biodegradation of contaminants in the unsaturated zone is starting to expand; however, most studies assume diffusion to be the only mode of contaminant and oxygen transport. Aelion and Bradley (1991) confirmed the existence of an actively growing and respiring microbial community through a field and laboratory study. Bachr and Corapcioglu (1987) developed a one-dimensional model for multiphase transport for any multiconstituent immiscible contaminant in the unsaturated zone. In this model, biodegradation was not based on kinetic mass transfer, but rather equilibrium partitioning of oxygen between air and water phases. Their study found that although oxygen replenishment to the contaminated soil steadily

increased as the air-phase tortuosity increased, the total biodegradation in the soil did not increase to the same extent as the associated increased availability of oxygen. They concluded this may be due to the fact the conditions favorable to increased biodegradation were also favorable to increased volatilization of the volatile mass, resulting in losses to the atmosphere. Ostendorf and Kampbell (1991) modelled hydrocarbon and oxygen vapor concentrations in a microbiologically active, geologically simple vadose zone with diffusion and Monod kinetics. Volatilization was found to be a significant long-term transport mechanism for the contaminant, but biodegradation did prevent the escape of the contaminant to the atmosphere at certain site locations. Baehr and Baker (1995) presented a mathematical model which simulates both the transport and reaction of gas-phase constituents when applied to column experiments or field sites. This model can be used to determine hydrocarbon production and consumption rates and thus the hydrocarbon biodegradation rate.

Vacuum extraction is similar to bioventing in that both involve advective-dispersive transport in the unsaturated zone. Only the relevant studies dealing with vacuum extraction are summarized here (Massmann, 1989; Baehr *et al.*, 1989; Brusseau, 1991; Armstrong *et al.*, 1994). These studies did not address the issue of biodegradation. Massmann (1989) showed that vapour extraction systems can be described by differential equations developed to model groundwater flow since the equations are good approximators to gas transport. These equations can only be used if the maximum pressure difference is less than half of an atmosphere. Baehr *et al.* (1989) developed an equilibrium-based, steady-state mathematical model to predict radially symmetric air flow and advective-dispersive transport when venting from a single well in the unsaturated zone. They then successfully applied this model to describe remediation of a contaminated site. Air-phase permeability was found to be a key parameter required to predict the air-flow field. Brusseau (1991) developed a one-dimensional, finite-difference model describing vacuum extraction which incorporated the effects of physical heterogeneity and rate-limited sorption on the transport of chemicals by gas-phase advection and dispersion. The model used both instantaneous and rate-

limited mass transfer between the water and solid phases. The model assumed both advective and non-advective domains within a soil and allowed for both equilibrium and non-equilibrium phase transfer in each domain. A disadvantage in this model was the large amount of input data required. Armstrong *et al.* (1994) numerically modelled the rate-limited extraction of volatile compounds to describe vacuum extraction. They assumed with high extraction rates, non-equilibrium phase partitioning occurred. Their experiment and simulations showed that there is a critical airflow rate beyond which a decrease in remediation time did not occur and that pulsed pumping was less effective than continuous pumping.

Rathfelder *et al.* (1995) give a good overview of the research completed in the area of bioventing as well as vacuum extraction. More studies involving transport in the unsaturated zone and the biodegradation process are required to better understand the relationship between the two. Chapelle (1993) noted that the unsaturated zone between the root zone and the water table is probably the least studied of any subsurface environment. To date studies dealing with biodegradation in the unsaturated zone have generally dealt with natural degradation and therefore assume diffusion to be the mode of contaminant and oxygen transport. However, in bioventing remediation sites, as in vacuum extraction remediation sites, advective-dispersive transport occurs and this transport has not yet been widely studied with respect to bioremediation. Hinchee and Ong (1992) discuss an in-situ test method to determine rates of hydrocarbon degradation to provide a quick assessment of bioventing at a field site. The work by Lang *et al.* (1995) involves the development of a two-dimensional numerical model specifically designed to simulate the bioventing process. Biodegradation appears to increase the rate of dissipation of the hydrocarbons above the rates from volatilization and diffusion to the atmosphere. Transport and biodegradation processes need to be described numerically and verified with field data from more bioventing sites to gain a better understanding of the processes that occur at these sites.

Based on the results from previous studies, biodegradation appears to be primar-

ily affected by numerous factors for each individual site. For each study performed, due to parameter uncertainty and variability, sensitivity analyses were important in order to determine which processes and parameters dominate at that particular site. As a result, the following aspects may need to be considered when investigating biodegradation: quantification of the biodegradation process as being either an instantaneous reaction or a kinetic reaction; determination of the distribution of the microbial population; adequate representation of the oxygen distribution, utilization, and transport; and, good representation of the hydrocarbon distribution and its input/output from the system. It is important to quantify heterogeneities within study areas in order to establish an understanding of the subsurface and its processes. Other aspects to be considered that may affect biodegradation are the air-phase permeability and the microbial parameters.

Based on the findings of previous studies, the sensitivity analysis for this study focuses on site properties, hydrocarbon contaminant properties, and microbial parameters. Determining the effects of layer thickness, permeability, soil moisture content, dispersivity, and extraction well set up help define the importance of certain site properties. To determine the importance of the contaminant and its properties, the transport and biodegradation of two different contaminants, dodecane and benzo[a]pyrene, are also modelled in order to compare to hexane transport. The microbe parameters vary over a range of values to help determine the effects they have on the outcome. These parameters include: the half-saturation constants, the microbe death rate, the hydrocarbon utilization rate, and the microbe distribution.

1.4 Objectives/Purpose

Bioventing is currently being applied to various sites across North America without a complete understanding of the underlying processes. Thus, there is a need to gain a better understanding of the bioventing remediation technique. To this end, there are three primary objectives of this project:

- to develop a comprehensive description of the processes involved in the bioventing remediation technique;
- to numerically simulate field results from a bioventing remediation pilot test; and,
- to perform a sensitivity analysis of various parameters affecting bioventing.

The primary tool for the investigation is a finite-element numerical model that simulates the physical, chemical, and biological processes that are thought to occur during bioventing. In particular the processes that are represented are the flow of air, the advective-dispersive transport of oxygen and hydrocarbon, the growth of microbes, and the biodegradation of hydrocarbon. The interactions between oxygen, hydrocarbon, and microbes are fully coupled through kinetic interaction terms describing biodegradation.

The numerical model was used to examine a bioventing remediation strategy for existing subsurface contamination at a sour gas plant located near Strachan, Alberta. Contamination of both the saturated and unsaturated zones at the site is the result of condensate leakage over the past couple of decades. Natural-gas condensate is the portion of gas at reservoir temperature and pressure which reverts to a liquid upon production. In the near-surface environment the condensate exists as light non-aqueous phase liquid (LNAPL) that floats as a pool on the watertable. At this site, the LNAPL pool has an areal extent of about 65 000 m^2 and a vertical thickness up to 3 m (Moore *et al.*, 1995). The condensate found at Strachan is mainly composed of intermediate light hydrocarbons (C_5 to C_{12}), but may contain some C_{12} to C_{22} components (Moore *et al.*, 1995). Site characterization and pilot testing of the remediation scheme using vacuum extraction with bioventing has been performed by Komex International Ltd. Extensive temperature, pressure, and concentration measurements have been recorded as part of the pilot study. The concentrations of oxygen, carbon dioxide, and total hydrocarbon have been collected. The numerical results were compared to the analytical data obtained in the field. Once a reasonable

representation of the field observations had been obtained, a sensitivity analysis was performed to determine which parameters likely have the greatest effect on biodegradation and thus to elucidate ways in which the bioventing efficiency of the technique may be optimized at this site.

Chapter 2

Theory

2.1 Conceptual Model

The physical scenario under consideration is illustrated in Figure 2.1. A spill of non-aqueous-phase-liquid (NAPL) has occurred at some time resulting in the development of a condensate layer in the vicinity of the watertable. Through time, this free product has migrated laterally down the slope of the watertable causing widespread contamination. Watertable fluctuations have further increased the volume of sediment contaminated since NAPL was smeared across previously clean geologic material resulting in residual being trapped above and below the watertable (see Figure 2.2).

Also shown in Figure 2.1 is an extraction well that has been installed for site remediation. Passive vapour transport, primarily by diffusion, occurs when the well is not functioning. Vapourization of the hydrocarbon in the condensate layer and the residual zones to the gaseous phase and volatilization from the dissolved phase to the gaseous phase result in vapour migration dominated by gaseous diffusion. Both sorption from and dissolution into the soil moisture may retard the diffusion process. The lack of air flow leads to the rapid depletion of oxygen in the system as the microbial population, pre-existing in the subsurface, utilizes the oxygen for biodegradation. In many cases this decrease in oxygen concentration will limit the biodegradation process because oxygen replenishment by diffusion is slow. Advective-dispersive trans-

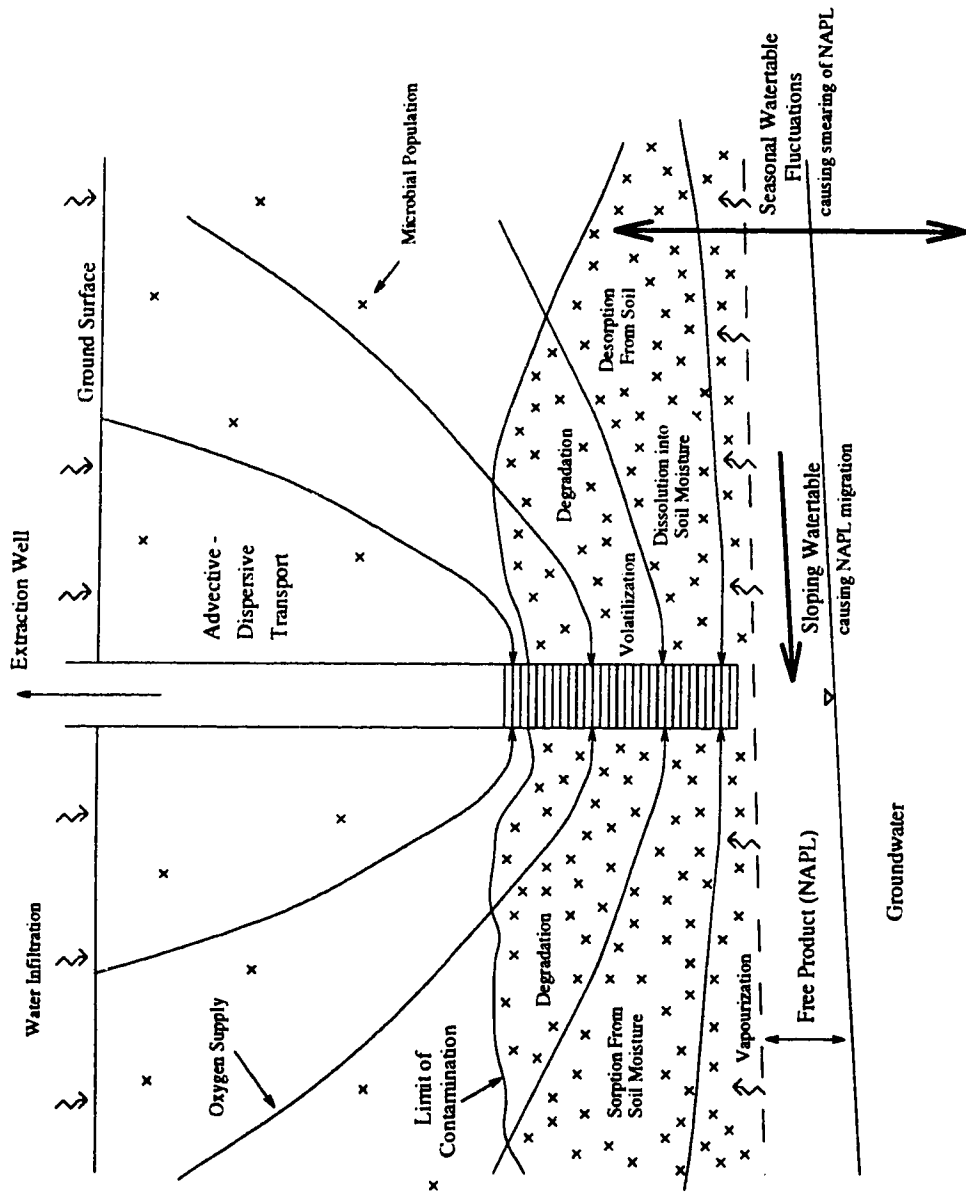


Figure 2.1: The conceptual model of the physical situation and processes.

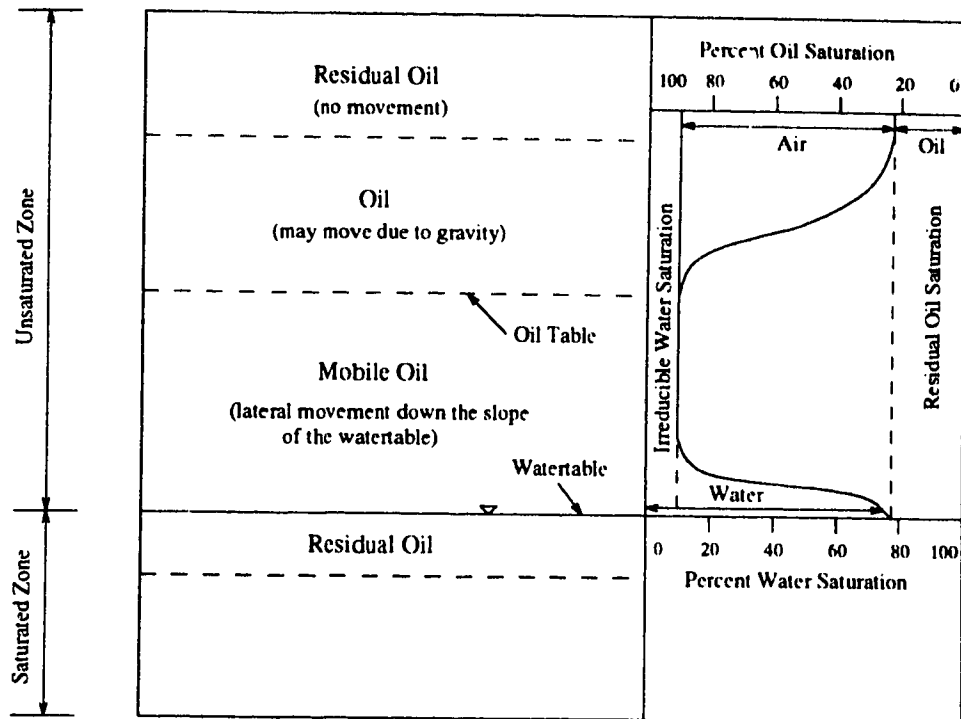


Figure 2.2: Approximation of the fluid distribution in the porous media when free product floats above the watertable (based on Fig. 5.19, Fetter, 1993).

port occurs when the extraction well is functioning (see Figure 2.1). The extraction well replenishes the system's oxygen supply leading to the biodegradation of the dissolved NAPL. This may also lead to an increase in the size of the microbial population in the zone of contamination. Both vapourization and volatilization are also enhanced because the air extraction removes contaminant from the system in the gaseous phase. The hydrocarbon mass is thus removed from the unsaturated zone by some combination of microbial degradation, vapourization, and volatilization.

2.2 Mathematical Model

The mathematical model necessary to describe the bioventing process is composed of several distinct, but interrelated, equations. To ease the computational burden, yet adequately represent the radial flow of air to extraction wells, axisymmetric (cylindrical) coordinates are used throughout the study. A three-dimensional analysis would

be preferred; however, the computations would be lengthy and the much greater number of required parameters would be difficult to quantify. The axisymmetric model will account for any horizontal layering and will therefore give a close representation of many three-dimensional problems of practical interest, and in particular the Strachan site.

2.2.1 Air Flow

Steady-state, laminar flow of air due to pressure gradients imposed by extraction wells is assumed throughout the study. Steady-state flow implies the magnitude and the direction of the flow are constant with time at any point in the flow field (Freeze and Cherry, 1979); however, from point to point in the domain the velocity may change. Because it is commonly observed that steady-state flow is achieved within a relatively short period of time, on the scale of hours to a day (Johnson *et al.*, 1990), and because this is also observed at the Strachan field site (Moore *et al.*, 1995), the steady-state flow assumption will be reasonable when the extraction rate is held constant over a time frame much longer than the response time of the system.

Assuming the principal directions of permeability are aligned with the coordinate axes and that vertical density effects are insignificant relative to the imposed pressure gradients, the steady-state flow equation in axisymmetric-coordinates for porous granular unsaturated media is given by (modified from Mendoza and Frind, 1990):

$$\frac{1}{r} \frac{\partial}{\partial r} \left(r k^* k_{rr} \frac{\rho_0 g}{\mu} \frac{\partial h}{\partial r} \right) + \frac{\partial}{\partial z} \left(k^* k_{zz} \frac{\rho_0 g}{\mu} \frac{\partial h}{\partial z} \right) = 0 \quad (2.1)$$

where r and z are the radial and vertical coordinate directions; k^* and k_{rr} , k_{zz} are the relative and intrinsic permeabilities; ρ_0 is the density of the uncontaminated soil gas; μ is the viscosity of the mixture; and g is the gravitational constant. The viscosity is calculated by a simple linear mixing model. The fresh-air head is defined as:

$$h = \frac{P}{\rho_0 g} + z \quad (2.2)$$

where P is the gas pressure relative to atmospheric pressure.

Darcy's law can be used to describe airflow during bioventing assuming both the air compressibility effects and the gas slippage (the Klinkenberg effect) are negligible. The assumption of incompressible gas flow is valid when the pressure difference for the inducing flow is less than approximately 50% of atmospheric pressure (Massmann, 1989; Brusseau, 1991; Croise *et al.*, 1989; Wilson *et al.*, 1988). Within that pressure range, the Klinkenberg factor can be ignored (McWhorter, 1990; Massmann, 1989). Due to the lower viscosities of gases, much smaller pressure gradients are required to generate significant gas flow (compared to groundwater flow) (Brusseau, 1991) and a pressure range of 20% of atmospheric pressure is found for most in-situ venting remediation techniques (Massmann, 1989; McWhorter, 1990). Massmann (1989) found the effects of gas slippage are small relative to viscous flow for low permeability soils (fine silt size) under the pressure and temperature conditions typical for most in-situ venting remediation techniques and therefore gas slippage can be neglected for flow in coarser sand and gravel materials.

The relative permeability may be calculated using the relationship given by Brooks and Corey (1934) for non-wetting fluids:

$$k^* = (1 - \theta_e)^2 (1 - \theta_e^{\frac{2+\lambda_B}{\lambda_B}}) \quad (2.3)$$

where λ_B is the Brooks-Corey pore size distribution index. The effective porosity, θ_e , is given by:

$$\theta_e = \frac{\theta_w - \theta_r}{\theta - \theta_r} \quad (2.4)$$

where θ_w is the soil moisture content; θ_r is the residual moisture content; and θ is the total porosity. For this study the necessary data for both the soil moisture content and the residual moisture content is not available. The soil moisture content is thus assumed to equal the residual moisture content and the relative permeability is equal to one. The effective permeability is thus calculated using inverse modelling techniques.

For flow there are two applicable boundary conditions. The first is a specified or

constrained head boundary (Type I, Dirichlet):

$$h = h_o \quad (2.5)$$

Because the elevation, z , is fixed, such boundaries may equivalently be expressed in terms of pressure, as shown in Figure 2.3. The second is a specified gradient boundary (Type II, Neumann):

$$\frac{\partial h}{\partial n} = g_o \quad (2.6)$$

where n is the direction normal to the domain boundary and g_o is some arbitrary function or value along the boundary.

The boundary conditions for the conceptual model are illustrated in Figure 2.3. For flow, the boundary conditions are as follows. The ground surface boundary is open to the atmosphere and has a specified head boundary corresponding to atmospheric pressure. A specified head equivalent to atmospheric pressure is also applied to the far right lateral boundary. The watertable boundary has a specified gradient of zero since it is impermeable to gas flow. An extraction well may be represented by either a non-zero gradient corresponding to the volumetric flux of air caused by the extraction pump or a fixed head corresponding to the pressure measured in the well during extraction. If a non-zero gradient is specified, the gradient may be determined from the required volumetric flow rate (Q in Figure 2.3) and Darcy's Law. This boundary condition will apply only for the length of the well's screen and only during air extraction. The remainder of the extraction well boundary is a symmetry boundary having a normal pressure gradient equal to zero. The entire length of the well will be a symmetry boundary when air extraction is not occurring.

The far right lateral boundary is placed at a distance far enough from the region of interest that it has little influence on the flow behaviour. The placement of this boundary is determined by comparing the results from simulations having different lateral limits. The boundary is assumed to be at a sufficient distance when no difference in the position of equipotentials exists between two plots for the different-sized domains. For the Strachan site simulations, this distance was calculated to be 120m and less than 3% of the total flux into the system crossed this boundary.

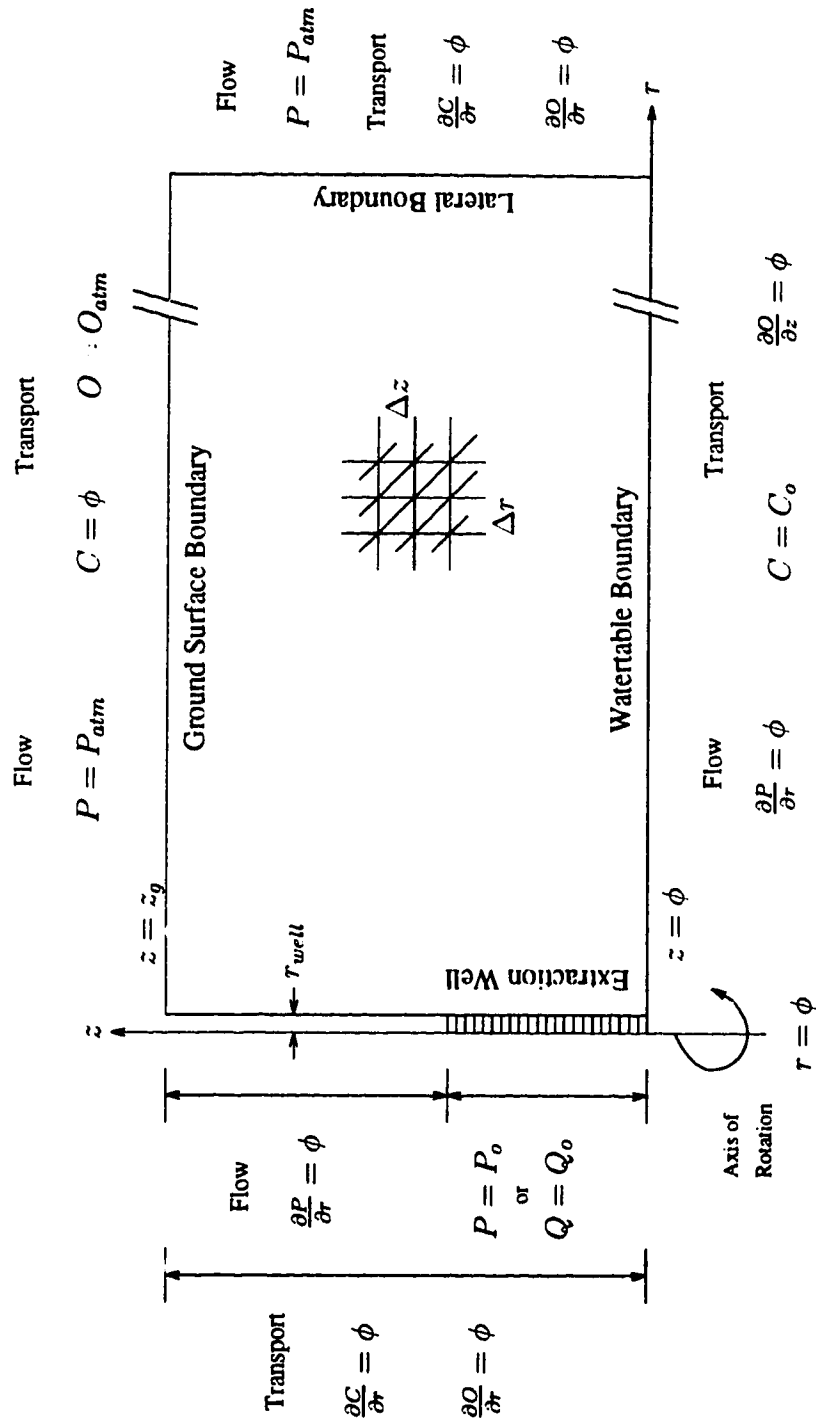


Figure 2.3: The boundary conditions of the conceptual model.

2.2.2 Transport

A pair of coupled, non-linear partial differential equations can be used to describe the transport of the oxygen and hydrocarbon gas phases. A third equation, required to describe the growth and death of the microorganisms, is discussed in the next section. Microbial consumption of both the hydrocarbon and the oxygen is a macroscopic term representing a natural sink in each of the transport equations. The advection-dispersion equation combined with Monod kinetics defines transport. The advection-dispersion equations for the two phases, hydrocarbon and oxygen, are as follows (modified from Borden and Bedient, 1986; Mendoza and Frind, 1990a; MacQuarrie *et al.*, 1990a):

$$\begin{aligned}
 & \frac{1}{r} \frac{\partial}{\partial r} (r \theta_a \mathbf{D}_{rr} \frac{\partial C}{\partial r}) + \frac{1}{r} \frac{\partial}{\partial r} (r \theta_a \mathbf{D}_{rz} \frac{\partial C}{\partial z}) + \frac{\partial}{\partial z} (\theta_a \mathbf{D}_{zr} \frac{\partial C}{\partial r}) + \frac{\partial}{\partial z} (\theta_a \mathbf{D}_{zz} \frac{\partial C}{\partial z}) \\
 & \quad - \theta_a v_r \frac{\partial C}{\partial r} - \theta_a v_z \frac{\partial C}{\partial z} \\
 & + \frac{1}{r} \frac{\partial}{\partial r} (r \frac{\theta_w}{H_C} D_{wr} \frac{\partial C}{\partial r}) + \frac{\partial}{\partial z} (\frac{\theta_w}{H_C} D_{wz} \frac{\partial C}{\partial z}) \\
 & = R_C \theta_a \frac{\partial C}{\partial t} + H_C \theta_w h_u \lambda M_t
 \end{aligned} \tag{2.7}$$

and

$$\begin{aligned}
 & \frac{1}{r} \frac{\partial}{\partial r} (r \theta_a \mathbf{D}_{rr} \frac{\partial O}{\partial r}) + \frac{1}{r} \frac{\partial}{\partial r} (r \theta_a \mathbf{D}_{rz} \frac{\partial O}{\partial z}) + \frac{\partial}{\partial z} (\theta_a \mathbf{D}_{zr} \frac{\partial O}{\partial r}) + \frac{\partial}{\partial z} (\theta_a \mathbf{D}_{zz} \frac{\partial O}{\partial z}) \\
 & \quad - \theta_a v_r \frac{\partial O}{\partial r} - \theta_a v_z \frac{\partial O}{\partial z} \\
 & + \frac{1}{r} \frac{\partial}{\partial r} (r \frac{\theta_w}{H_O} D_{wr} \frac{\partial O}{\partial r}) + \frac{\partial}{\partial z} (\frac{\theta_w}{H_O} D_{wz} \frac{\partial O}{\partial z}) \\
 & = R_O \theta_a \frac{\partial O}{\partial t} + H_O \theta_w h_u G \lambda M_t
 \end{aligned} \tag{2.8}$$

where C and O are the concentrations of the gaseous hydrocarbon and oxygen respectively; v_a and θ_w are the air- and water-filled porosities; R_C , R_O are the retardation factors for hydrocarbon and oxygen, respectively; t indicates time; and H_C , H_O are the dimensionless Henry's constants for hydrocarbon and oxygen which are used to transform gaseous concentrations into aqueous concentrations. The last term on the

right hand side of both Equation 2.7 and Equation 2.8 describes the decay due to microbial action and will be discussed in the next section.

The interstitial velocity is dependent on the gaseous Darcy flux, q , and is defined as:

$$v_i = \frac{q_i}{\theta_a} \quad i = r, z \quad (2.9)$$

The gaseous dispersion tensor is defined as (Bear, 1979):

$$D_{ij} = \alpha_\ell |v| \delta_{ij} + (\alpha_\ell - \alpha_t) \frac{v_i v_j}{|v|} + \tau_a D_{ai} \delta_{ij} \quad i, j = r, z \quad (2.10)$$

where α_ℓ and α_t are the longitudinal and transverse dispersivities; δ_{ij} is the Kronecker delta; τ_a is the air-phase tortuosity; and D_{ai} is the air-phase diffusion coefficient. The air-phase tortuosity is calculated using the equation developed by Millington and Quirk (1961):

$$\tau_a = \frac{\theta^{7/3}}{\theta^2} \quad (2.11)$$

where θ is the total porosity. This relationship is applicable for gases in sandy materials (Weeks *et al.*, 1982). The aqueous effective diffusion coefficients are defined as (modified from Mendoza, 1992):

$$D_{wi} = \tau_w D_w \quad i = r, z \quad (2.12)$$

where D_w is the free-solution aqueous diffusion coefficient and τ_w is the water-phase tortuosity calculated in the same manner as the air-phase tortuosity.

Assuming equilibrium phase partitioning, the retardation factor for the hydrocarbon gas phase is calculated by:

$$R_C = 1 + \frac{\theta_w}{\theta_a} \frac{1}{H_C} + \frac{\rho_b K_D}{\theta_a H_C} \quad (2.13)$$

where ρ_b is the porous medium bulk density. When adsorption onto the solid organic matter dominates the partitioning between the aqueous phase and solid phases (Mendoza *et al.*, 1996), the distribution coefficient may be approximated by:

$$K_D = f_{oc} K_{oc} \quad (2.14)$$

where f_{oc} is the soil organic content and K_{oc} is the organic carbon partitioning coefficient. In Equation 2.13, the second term on the right hand side describes the partitioning of vapours into the soil moisture according to Henry's Law; the third term describes the partitioning of organic compounds between the soil moisture and the solid phases (Mendoza *et al.*, 1996). Equilibrium phase partitioning between the air, water, and solids should be valid for weakly advective conditions to a first approximation (Johnson *et al.*, 1993). Linear adsorption and exchange reactions are assumed to be instantaneous and are described by equilibrium isotherms. The retardation factor for the oxygen gas phase is given by:

$$R_O = 1 + \frac{\theta_w}{\theta_a} \frac{1}{H_O} \quad (2.15)$$

which assumes no partitioning to the porous media solids.

For transport there are two applicable boundary conditions for this study. The first is a fixed concentration boundary (Type I, Dirichlet):

$$c = c_a \quad (2.16)$$

and the second is a zero-concentration gradient boundary (Type II, Neumann):

$$\frac{\partial c}{\partial n} = 0 \quad (2.17)$$

where c can represent either hydrocarbon (C) or oxygen (O) concentrations. The boundary conditions describing the conceptual model for hydrocarbon and oxygen transport vary and are illustrated in Figure 2.3.

The hydrocarbon contamination is conceptualized as an immobile, pooled NAPL source at the lower boundary. Thus, for hydrocarbon transport, the lower boundary has a constant concentration equivalent to the vapour pressure of the hydrocarbon condensate present. The ground surface boundary has a fixed hydrocarbon concentration of zero to represent removal into the atmosphere. The lateral boundary represents a zero-concentration gradient and is again placed at a distance where it does not influence transport. The extraction well, or exit, boundary has a zero-concentration gradient since the concentration removed is the same as that immediately adjacent

to the well screen (Mendoza, 1992). The unscreened part of this boundary behaves like a symmetry boundary and therefore has a zero-concentration gradient.

For oxygen transport, the watertable boundary is assumed to have an oxygen concentration gradient of zero. The ground surface boundary is defined by an oxygen concentration equivalent to the atmospheric oxygen concentration (21%). The lateral boundary and the extraction, or exit, boundary both have the same boundary conditions discussed for hydrocarbon transport.

2.2.3 Biodegradation Reaction

The microorganisms are assumed to be present only within the soil moisture and are immobile (MacQuarrie *et al.*, 1990). The size of the microorganism population varies within the domain since the growth and death of the organisms varies due to spatial variations in the concentrations of the aqueous-phase hydrocarbon and oxygen. Biodegradation is assumed to be a concentration-dependent, time-dependent, irreversible kinetic reaction. The coupled, non-linear partial differential transport equations discussed above each include the microbial decay term to account for biodegradation. The microbial growth and death are described by coupled, ordinary differential equations (Chen *et al.*, 1992) describing dual Monod kinetic formulation. Thus, biodegradation of the organic contaminants is potentially limited by microbial utilization rates as well as the availability of both the electron acceptor, oxygen, and the electron donator, hydrocarbon (Rittmann *et al.*, 1994). The following equations describe dual Monod kinetics (modified from Borden and Bedient, 1986; MacQuarrie *et al.*, 1990a):

$$\frac{\partial C}{\partial t} = -H_C \theta_w h_u \lambda M_t \quad (2.18)$$

and

$$\frac{\partial O}{\partial t} = -H_O \theta_w h_u G \lambda M_t \quad (2.19)$$

and

$$\frac{\partial M_t}{\partial t} = h_u Y \lambda M_t - b M_t + k_c Y C_{oc} \quad (2.20)$$

where M_t is the total aerobic microbial concentration; h_u is the maximum hydrocarbon utilization rate per unit mass of microorganisms; G is the ratio of oxygen to hydrocarbon consumed assuming that complete mineralization occurs; Y is the microbial yield coefficient; b is the microbial death rate; k_c is the first order decay rate of natural organic carbon; and, C_{oc} is the natural organic carbon concentration. The Monod decay term, λ , is defined by:

$$\lambda = \left(\frac{C_w}{K_C + C_w}\right)\left(\frac{O_w}{K_O + O_w}\right) \quad (2.21)$$

where C_w , O_w are the aqueous hydrocarbon and oxygen concentrations, and K_C , K_O are the hydrocarbon and oxygen half-saturation constants. Equation 2.18 and Equation 2.19 are incorporated as the last term on the right hand side of the Transport Equations 2.7 and 2.8 respectively.

Equation 2.18 and Equation 2.19 represent the changes in the concentrations of the aqueous-phase hydrocarbon and oxygen, respectively; Equation 2.20 represents the change in the concentration of the microbial population. The third term on the right hand side of this equation is assumed to have little effect on the microbial concentration since it is assumed that the microbial population exists primarily on the foreign hydrocarbon relative to the organic carbon. Preliminary model simulations indicated this assumption is realistic since the value for the soil organic content had little effect on the amount of hydrocarbon biodegraded. Also, a representative value for the first order decay rate of natural organic carbon was not found. It is assumed the microbial growth will not lead to clogging of the air flow paths.

There are no boundary conditions applicable for the microorganisms because the microbial population is considered to be immobile and therefore only grows and dies within the domain. The initial conditions for the concentration of the microbial population was calculated by the method outline by Chen *et al.* (1992). The initial concentration calculation was based on the microbial soil population density which was measured for each stratigraphic unit at the Strachan field site and is discussed in more detail in Chapter 4.

Chapter 3

Numerical Model

3.1 Model Description

The air flow, contaminant and oxygen transport, and microbial degradation equations discussed in the theory section have been incorporated into an existing finite-element computer model, VapourT (version 2.11, Mendoza, 1992). VapourT was originally designed to simulate the flow of gas and the transport of a single vapour phase contaminant, without decay, in the unsaturated zone. The necessary modifications to the model included the addition of a second transported gas phase (oxygen) coupled with non-linear microbial growth and death. Incorporating the microbial component allowed the capability of determining the biodegradation of hydrocarbon and utilization of oxygen. The code was written in Fortran77 and all simulations of the new model, Biovent, were performed on IBM RS/6000 workstations.

The Galerkin finite-element method with triangular elements having linear basis and weighting functions (Mendoza, 1992) was used to approximate the partial differential equations presented in the mathematical model. The Galerkin method, as implemented in VapourT, is described briefly by Mendoza (1989) and in more detail, for general cases, by Wang and Anderson (1982) and Huyakorn and Pinder (1983), among others. The finite-element method was chosen because different geologic and physical properties can be assigned to each element to account for spatial variability and the method inherently conserves mass. The finite-element method also accu-

rately represents the dispersive cross-terms that arise with advective transport, a feature that is not necessarily true of the finite-difference method.

For the contaminant and oxygen transport, a generalized finite-element equation can be expressed as:

$$c[R]\{X\}^{t+\Delta t} + (1 - c)[R]\{X\}^t = -[T]\left(\frac{X^{t+\Delta t} - X^t}{\Delta t}\right) \quad (3.1)$$

which can be rearranged to obtain:

$$(c[R] + \frac{1}{\Delta t}[T])\{X\}^{t+\Delta t} = -(1 - c)[R]\{X\}^t + \frac{1}{\Delta t}[T]\{X\}^t \quad (3.2)$$

where c is the weighting factor; R is the spatial derivative of the advective-dispersive transport matrix; X is the function representing either C or O ; T is the contaminant mass time matrix; and t represents the known time-step solution and $t + \Delta t$ the unknown solution.

The spatial derivative of the advective-dispersive transport matrix, R , may be weighted in time using explicit, implicit, or Crank-Nicolson methods. The fully explicit or forward difference method is evaluated at time t and has a weighting factor of $c = 0$; the fully implicit or backward difference method is evaluated at time $(t + \Delta t)$ and has a weighting factor of $c = 1$. The Crank-Nicolson or central difference method is evaluated midway between t and $(t + \Delta t)$ and has a weighting factor of $c = 0.5$. Although it is formally more accurate than explicit or implicit, Crank-Nicolson time weighting often suffers from small oscillations in the solution if the time step is much larger than that required for a stable explicit solution. For more difficult problems that deal with heterogeneities and non-linear coupling of equations, fully implicit time weighting is generally used because it guarantees a solution without oscillations. This study used fully implicit time weighting.

Equation 3.1 defines the function, X , as a time derivative on the interval t to $(t + \Delta t)$ using a finite-difference approximation in the temporal domain. In the method of weighted residuals, basis functions are used to define a solution vector over the entire domain. For the time derivative one generally has a choice as to whether these basis functions are used or whether nodal (point) concentration values

are used. If the basis functions are used to define the time matrix, T , the formulation is said to be consistent. Otherwise, the formulation is lumped and the time matrix effectively represents a spatial finite-difference approximation. The lumped formulation indicates the spatial weighting is only between two adjacent nodes; the consistent formulation indicates the spatial weighting is between all three nodes comprising an element (Daus *et al.*, 1985). For non-linear problems, such as those simulated here, the lumped time formulation is superior to the consistent form because it tends to dampen oscillations which can give rise to non-physical concentration results and is thus more stable (Seegerlind, 1984; Frind, 1982). The lumped time formulation is used in this study.

Because air flow is described as being at steady-state and is assumed to be independent of transport, flow solutions are obtained only at the beginning of each computer simulation. In contrast, the hydrocarbon and oxygen transport equations and the microbial degradation equation are transient, non-linear and coupled. That is, the solutions step forward in time and some parameters within each equation are dependent on solutions of the other equations. Specifically, the hydrocarbon and oxygen transport equations require the rate of biodegradation of the hydrocarbon and oxygen from the microbial degradation equation; yet the rate of biodegradation is dependent on the amount of hydrocarbon and oxygen available for consumption by the microbes. The coupled nature of these equations is accommodated through a sequential iteration scheme whereby the equations are initially solved within each time step using parameters based on the known concentration values from the previous time step. The solutions are then further resolved by successively updating parameter values based on updated concentrations obtained for each iteration. Iterations continue until all concentrations have converged within specified tolerances. The convergence tolerance used here requires that the maximum change in either hydrocarbon, oxygen, or microbial nodal concentration from one iteration to the next be less than 0.0001% of the final nodal concentration. For the simulations performed in this study, an average of 5 iterations were required per time step at early time

when the hydrocarbon degradation and oxygen utilization rates were high; at later time, when these rates slowed and the concentration solution became more spatially uniform, iterations were generally no longer required. The size of the time step also affected the convergence of the solution. A time step smaller than 1.0 hours was necessary for passive transport and 0.1 hours for advective-dispersive transport to prevent exceeding the maximum number of iterations (30).

3.2 Mass Balance and Mass Fate

Detailed mass balance and mass fate calculations are performed for both flow and transport. Mass balance calculations are required for three main reasons: to quantify mass input into and output from the domain; to determine the fate of mass within the domain; and, to verify mass conservation of the model. The mass conservation for transport essentially checks whether the implementation of the equations and their coupling is correct and also indicates whether the time step size is reasonable. For time steps which are too large, changes in the mass within the domain occur too quickly which often results in mass balance errors.

A boundary mass summary for flow and transport is calculated by determining both the advective and dispersive mass fluxes along all domain boundaries. This summary indicates the movement of air, hydrocarbon, or oxygen across the grid boundaries, which include: the ground surface, watertable, lateral, extraction well boundaries, and for transport, the amount of hydrocarbon degraded and the amount of oxygen utilized by the microbes. During transport calculations, the boundary mass summary is determined for each time step and is also accumulated through time. For transport, a stored mass summary is also calculated at the end of each time step and is accumulated over the length of the simulation. This summary of the stored mass within the domain indicates the amount of hydrocarbon in the vapour, aqueous, and sorbed phases and the amount of oxygen in the vapour and aqueous phases.

The overall transport mass balance calculations determine the changes in stored mass, changes in mass due to source addition or extraction, and changes in the mass

due to hydrocarbon and oxygen utilization by the microbes. More specifically, the calculation compares the changes in the amount of mass entering and exiting the boundaries to the corresponding changes in the amount of mass in storage. The net change in mass for the boundary and storage summaries for one time step should be zero.

Overall, the mass balance error was lower for oxygen transport than for hydrocarbon transport because there was an excess amount of oxygen in the system relative to the amount the microbes required. For each time step, the hydrocarbon and oxygen mass balance errors were generally around 0.004%. The cumulative mass balance error for oxygen was usually less than the time step mass balance error; however, in time the hydrocarbon cumulative mass balance error grew to a maximum of 3%. In most cases the error was significantly less.

For the hydrocarbon simulations, the flux of the hydrocarbon into the system occurred predominantly along the watertable with very little entering across the lateral boundary. As discussed later, most of the hydrocarbon was removed from the system by microbial degradation with smaller amounts exiting via the extraction well. This is in accordance with the objectives of the bioventing strategy. In contrast, oxygen predominantly exited via the extraction well and substantially less was degraded by microbial action. However, the flux of oxygen along the ground surface boundary was typically over an order of a magnitude higher than the flux of hydrocarbon into the system because of the significantly higher oxygen concentrations at the ground surface relative to the hydrocarbon concentrations at the watertable. This meant there was more oxygen mass within the system and exceeded the amount required by the microbes, resulting in better mass balance calculations. Stored mass summaries indicated that hydrocarbon and oxygen were predominantly stored in the vapour phase, with lesser amounts present in the aqueous and solid phases.

An air-flow boundary mass summary comparing the amount of air entering the system to the amount of air leaving the system is calculated once for each flow solution. For steady-state flow this net flow across the boundaries should be zero. Air-

flow mass balance calculations showed an error of less than $10^{-6}\%$ for all simulations performed. By considering the fluxes along the different boundaries separately, the source of air may also be discriminated. This allowed the ability to calculate the placement of the far right lateral boundary at a distance where less than 5% of the total source of air crossed this boundary. For most simulations presented here, 97% of the air flow entered the system along the ground surface boundary and 3% along the lateral boundary. All air exited via the extraction well.

3.3 Accuracy and Stability Criteria

The Peclet and Courant criteria are limits on dimensionless numbers that can be used to assess the potential accuracy and stability of numerical transport models with a given spatial and temporal discretization. The Peclet number represents the effects of spatial discretization, while the Courant number represents the effects of temporal discretization in a time-stepping scheme. Satisfaction of constraints on the Peclet and Courant numbers help minimize numerical dispersion and oscillations in the numerical solution leading to the increased accuracy and stability. These criteria were originally developed for solutions of the one-dimensional, linear advection-dispersion equation, and thus are used only as an approximate guide in this study. The definition of the Peclet and Courant numbers, and their constraints, are (Daus *et al.*, 1985):

$$Pe = \frac{v\Delta x}{D} \leq 2$$

$$Cr = \frac{v\Delta t}{\Delta x} \leq \frac{Pe}{2}$$

where Δx and Δt are the spatial and temporal discretization respectively. In practice, the maximum Peclet and Courant numbers are calculated in each coordinate direction for every different time step size. For an optimal spatial discretization where $Pe = 2$, a Courant number less than one implies the advective front never traverses more than the length of a single element (Δx) in a time step. Acceptable numerical solutions are often achieved when the Peclet number is as high as 10 in most cases

involving nonuniform flow (Huyakorn and Pinder, 1983). Daus *et al.* (1985) found that the lumped formulation tends to be more sensitive to violations of the Peclet criterion rather than the Courant criterion. The Peclet and Courant numbers do not account for the steepness of the concentration gradient within any part of the domain; however, the overall accuracy of a simulation depends on the initial conditions existing prior to the start of a time step (Daus *et al.*, 1985). Thus, when steep gradients exist, most commonly at early times, the satisfaction of the criteria is critical. Generally, as the solution becomes smoother at later time, (*i.e.*, as the concentration gradient decreases due to dispersion), the criteria may be relaxed with no appreciable increase in error. For this study, the accuracy of the solution also depended strongly on the rate of biodegradation. For example, during passive transport simulations, if the Peclet and Courant criteria were just satisfied, the solution was unstable due to the high rate of biodegradation. Thus, for these cases, an even smaller temporal discretization than would be indicated by the Courant criterion was necessary.

3.4 Analytical Solution Comparison

Comparison of axisymmetric transport equations to analytical solutions is often difficult because analytical solutions are computationally complex and typically have restrictive boundary conditions (Mendoza, 1989). In this study, the numerical model results were compared to two simple, linear analytical solutions. Hydrocarbon and oxygen transport were simulated separately for comparison since no analytical solution incorporating simultaneous coupled hydrocarbon and oxygen transport is known.

The numerical model was first compared to the one-dimensional Ogata-Banks solution (Ogata and Banks, 1961) for transport in a semi-infinite domain with a constrained concentration source and no biodegradation. Although no results are shown, the numerical solution approximated the analytical solution for both passive and advective-dispersive transport very well.

The numerical model was then compared to the analytical solution for two-dimensional mass transport from a semi-infinite strip source (Cleary and Unga, 1994).

The solution was obtained from the Prince package coded by Waterloo Hydrogeologic Software. Cartesian coordinates were used for the numerical model simulations. For this suite of simulations, biodegradation was considered to be a first-order reaction in a manner similar to that employed by MacQuarrie *et al.* (1990). Using a Monod kinetics formulation, they approximated first-order hydrocarbon decay by maintaining a constant microbial population and a constant oxygen (electron acceptor) concentration. When $K_C \gg C_w$ and $K_O \ll O_w$, the biodegradation decay term (see Equations 2.18 and 2.21) can be approximated by:

$$\frac{\partial C}{\partial t} \approx -H_C \theta_w \frac{M_t h_u}{K_C} C \approx -\kappa C$$

which gives a first-order decay rate that is consistent with the representation of decay in the analytical solution. Figure 3.1 shows the boundary conditions and the parameters used for the hydrocarbon transport simulations. The comparison of the numerical model to the analytical solution is shown in Figure 3.2; the match between the numerical and analytical solutions is very good, which gives confidence that the basic coding of the transport model is correct. The two solutions also compare well for different times, for profiles off the centreline, and for approximating first-order oxygen decay when the hydrocarbon concentration is held constant.

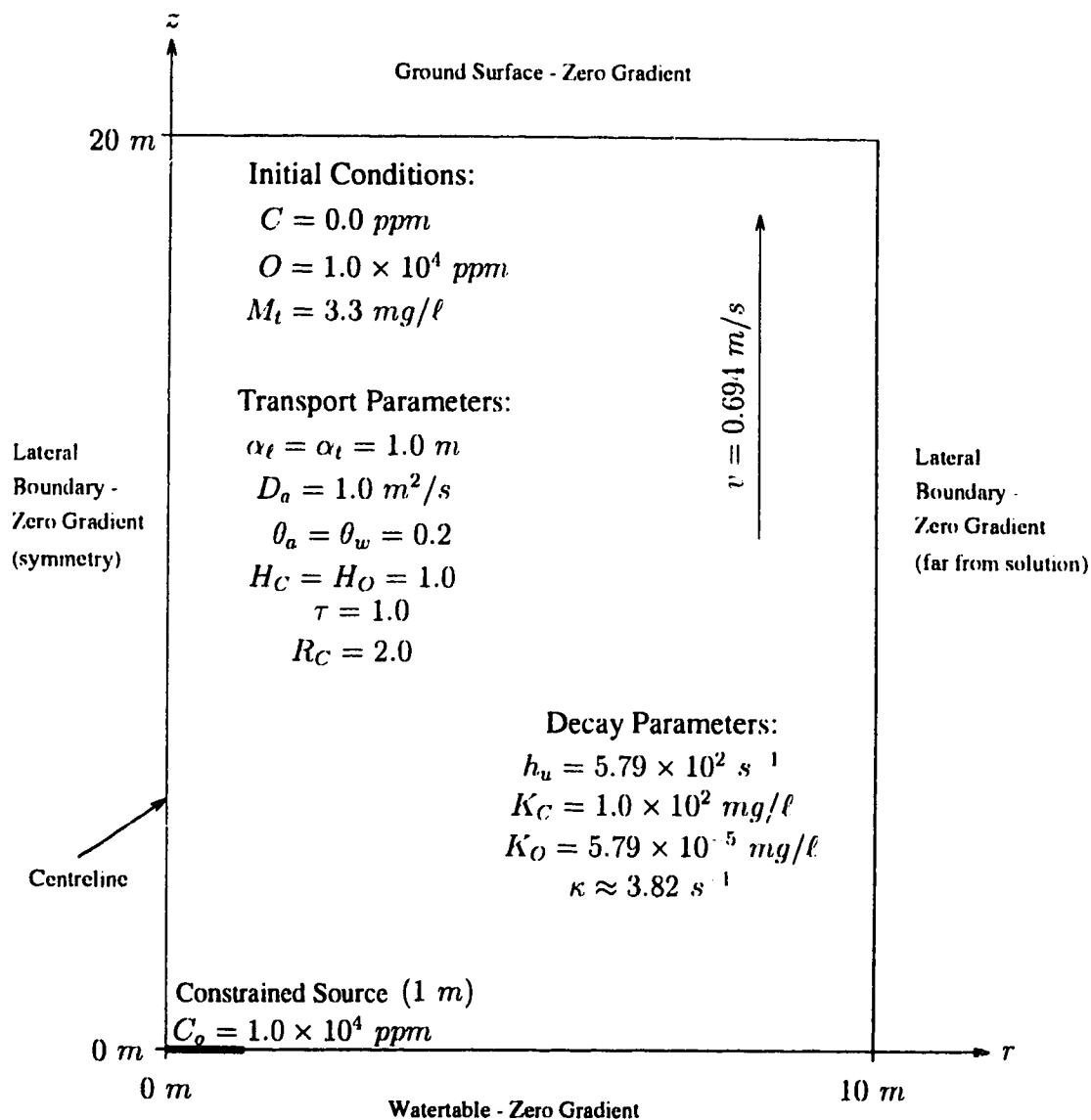


Figure 3.1: Summary of the boundary conditions and the parameters of the numerical model for the analytical comparison for hydrocarbon.

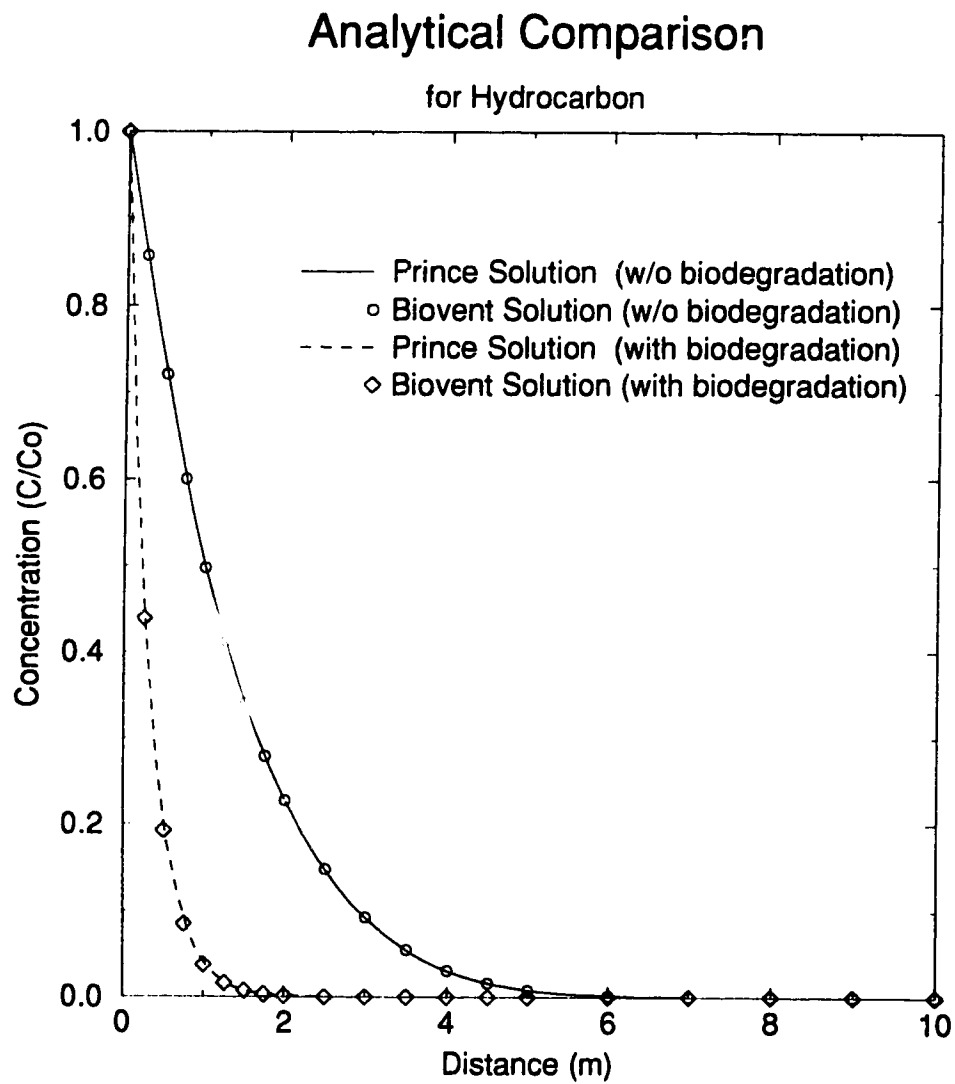


Figure 3.2: Numerical model compared to an analytical model for simple advective-dispersive transport with and without biodegradation for the centreline at $t = 2.0$ s.

Chapter 4

Comparison of the Numerical Model Results to Field Data

The geology, hydrogeology, hydrocarbon contamination, and microbial population determined from field data collected for a bioventing pilot test, performed by Komex International Ltd., are described in this Chapter. The air flow and transport and biodegradation of hydrocarbon and oxygen trends observed during the field tests are then compared to those trends calculated by the numerical model to establish its performance, predictability, and accuracy.

4.1 The Field Site

4.1.1 Site Location and Characterization

The field site is located near Rocky Mountain House, Alberta, 200 *km* northwest of Calgary, at the Gulf Canada Resources Limited Strachan Sour Gas Plant (Figure 4.1). Remediation activities at the Strachan gas plant are the result of a study initiated by the Canadian Association of Petroleum Producers (CAPP) and Environment Canada to demonstrate remedial technologies for groundwater and soil contamination at Alberta gas plants. The initial remediation technology used at Strachan was soil vapour extraction; however, the direction of the project turned to using bioventing upon observing indications of possible microbial degradation. The Strachan field site is an

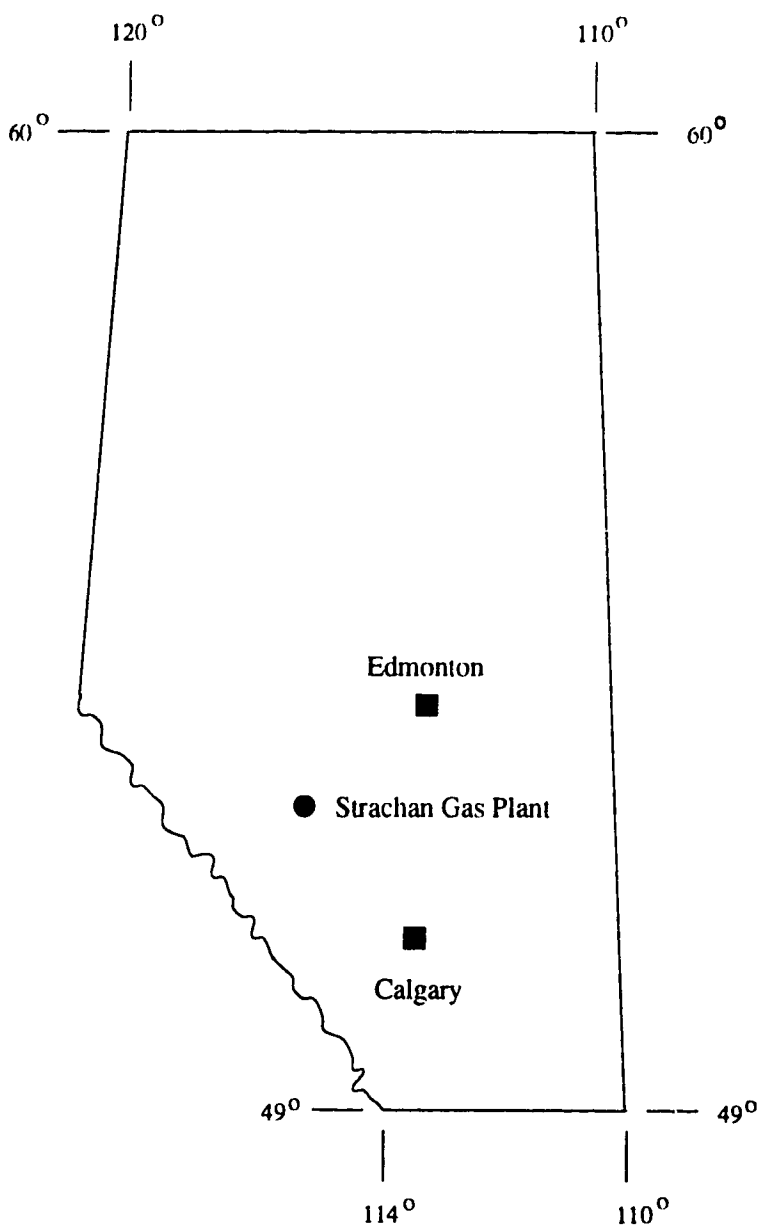


Figure 4.1: Location of the Gulf Canada Resources Limited Strachan Sour Gas Plant (T37, R9W5M).

example of an engineered bioremediation site (NRC, 1993) rather than an intrinsic bioremediation site, implying that the microbial activities are increased due to modifications made at the site such as well installation, air extraction, etc. This study uses field measurements taken by Komex International Ltd. after the shift in program direction towards bioventing during the time period June, 1993 to August, 1994.

Stratigraphy

The unsaturated zone at this field site consists of two distinct geological units, a glacial till unit and an alluvial sand and gravel unit, determined from observations made during drilling with a large diameter rathole auger and from results of a geophysical study using the EM39 downhole conductivity tool. The uppermost unit is a highly electrically conductive glacial till which extends to 2.0 to 2.5 *m* below the ground surface. This light brown till is described as a silty clay till of low plasticity and possibly fractured, with some sand and gravel, and the occasional rounded cobble (Komex, 1994b). The glacio-fluvial sand and gravel unit underlying the till has a significantly lower electrical conductivity and extends to 6 to 12 *m* below the ground surface. The top 2 - 3 *m* of this unit has more observed heterogeneities than the lower 4 - 9 *m*. This tan to dark yellow (depending on the soil moisture content) sand and gravel unit has a silty clay matrix and contains rounded clasts up to cobble and boulder size (up to 0.4 *m* diameter) (Komex, 1994b).

The two surficial units are underlain by the Paskapoo Formation. This sedimentary bedrock is comprised of gray shales interbedded with fine-grained sandstone (Komex, 1994b).

Hydrogeology

The watertable is approximately 8 *m* below the ground surface in the glacio-fluvial sand and gravel unit and approximately 2 *m* above bedrock. Seasonal groundwater fluctuations up to 2.5 *m* per year have been observed which has resulted in significant smearing of the condensate, as discussed in Chapter 2, above and below the

watertable (Environmental Research Advisory Council, 1994). The water level measurements indicated the watertable was generally 1 to 2.5 *m* higher in the observation wells in July than in April (Komex, 1994b). The watertable elevation decreases from north to south indicating the direction of groundwater flow is towards the south at approximately 1 *m/day*.

Hydrocarbon Contaminants

At the Strachan gas plant, an estimated 10 000 *m*³ of condensate has been accidentally released to the subsurface over an extended period of time (Environmental Research Advisory Council, 1994) and has an areal extent of about 65 000 *m*² (Moore *et al.*, 1995). The thickness of appreciable hydrocarbon product floating on the watertable is on the order of 2 to 3 *m* and is spatially variable over distances of 5 to 10 *m*. As mentioned earlier, the condensate is composed mainly of intermediate light hydrocarbons (*C*₅ to *C*₁₂), but may contain some *C*₁₂ to *C*₂₂ components. The liquid, soil, and vapour compositions of the light non-aqueous phase liquid (LNAPL) have varying amounts of straight chain (*S*), branch chain (*B*), and cyclic (*C*) aliphatic, and aromatic (*A*) hydrocarbons. The liquid portion of the condensate is approximately 37% *S*, 20% *B*, 27% *C*, and 16% *A*. The vadose zone sorbed hydrocarbon composition is 30 - 90% *S* with a variable distribution of the remaining *B*, *C*, and *A*; the vadose zone vapour hydrocarbon composition is 10 - 80% *S* or *C* with the remainder being predominantly *B*. The spatial variations and uncertainties in these fractions will significantly affect the determination of hydrocarbon transport and mass removal because of both the uncertainty in the source condition and nonuniform hydrocarbon mass removal. Different groups such as the straight chain aliphatic and the aromatic (*C*₉ or less) hydrocarbons will be removed preferentially according to their respective solubility, volatility, adsorption, and biodegradation characteristics. Therefore, to help simplify this problem and to focus attention on the more mobile hydrocarbon fraction, hexane was used as a generic hydrocarbon to represent and describe the volatilization, vapourization, and biodegradation occurring at the site during the field

tests. The behaviour of heavier compounds is considered briefly in the sensitivity analysis presented in Chapter 5.

4.1.2 Temperature

The subsurface temperature was monitored with thermistors installed at a depth of 6.1 *m* below the ground surface in the extraction well. The subsurface temperature range at the Strachan field site during 1993 was measured to be from 3°C to 10°C. The average subsurface temperature for May was 5.5°C; for September, 9°C to 10°C; and, for December, 6.5°C (Komex, 1994a). In contrast, the surface air temperature ranged from 20°C to 30°C in the summer to -10°C to -30°C in the winter, showing the effect of seasonal variations in temperature on the subsurface diminished with depth (Komex, 1994a), as expected.

It was originally believed that lower biodegradation rates would coincide with lower subsurface temperatures. However, it is now believed that different microbes can acclimatize to different temperature ranges and can be as productive as the microbes associated with warmer temperatures. Therefore, because the range in temperature was approximately 5°C for the time period of interest and since lower temperatures did not appear to impede biodegradation (Moore *et al.*, 1995), temperature was not considered to be a major factor in this study. An average subsurface temperature of 8°C was assumed.

4.1.3 Data Collection

All the information reported in this study that specifically describes the Strachan field site was collected by Komex International Ltd. The data collected include soil moisture content, temperature, air pressure distributions, extraction rates, both hydrocarbon and oxygen concentrations, and microbial counts. The Komex reports, 1993 Soil Vapour Extraction Program Summary Report (1994b) and 1993 Soil Vapour Extraction Program Bioventing (1994a), provide details on the methods of collecting and measuring the data and the accuracies of the measurements. Thus the following

is an overview. During field monitoring, the accuracy of the measurements was assessed by performing duplicate and triplicate analyses on a regular basis, especially for the hydrocarbon and oxygen concentrations. The accuracy of the analytical equipment was monitored by using calibrated standards each day. In June, the oxygen content was analyzed by a gas chromatograph with a thermal conductivity detector (GC/TCD); in December, the oxygen content was analyzed by a handheld Nova oxygen/carbon dioxide analyzer (infrared detector for oxygen analysis). The hydrocarbon concentration was measured by a GasTech Trace-Tector calibrated for hexane gas. The measurements prior to December should be considered accurate to within $\pm 2.0\%$ and after December accurate to within $\pm 0.4\%$.

4.1.4 Site Parameters

The values for the parameters used to describe site properties are listed in Table 4.1 while the parameter values which describe transport are listed in Table 4.2. Those parameters which are shown with a range of values were deemed to be important variables when describing biodegradation and are most extensively analyzed during this part of the study. The 'High' and 'Low' designations refer to the values which contribute to increased biodegradation (High) and those which contribute to decreased biodegradation (Low). The remaining parameters without ranges in values are simply representative averages. Bulk densities of 1.75 g/cm^3 for the till and 1.65 g/cm^3 for the sand and gravel were assumed. Those transport properties relating to the hydrocarbon were calculated using hexane, which has a molecular weight of 86.2 g/mol , as the representative hydrocarbon. The molecular weights of air and oxygen are 28.96 and 32.0 g/mol , respectively. The soil moisture content and the amount of nutrients available for the microorganisms are assumed to be at appropriate levels for microbial degradation at the site. It is further assumed that the water produced during the biodegradation of hexane vapourizes, otherwise the residual water contents would need to continually change in some unknown fashion. The biodegradation parameters are listed in the section discussing the microbial population.

Parameter	Units	High	Average	Low	Reference
θ sand	-	-	0.35	-	(Freeze and Cherry, 1979)
θ till	-	-	0.34	-	(Freeze and Cherry, 1979)
θ_w sand	-	0.10	0.062	0.038	(Komex, 1994c)
θ_w till	-	0.15	0.077	0.040	(Komex, 1994c)
f_{oc} sand	-	0.00055	0.00074	0.001	(Domenico and Schwartz, 1990)
f_{oc} till	-	0.0063	0.011	0.02	(Domenico and Schwartz, 1990)
k_h sand	m^2	-	2.5×10^{-10}	-	calculated
k_r sand	m^2	-	1.5×10^{-10}	-	calculated
k_h till	m^2	-	6.0×10^{-12}	-	calculated
k_v till	m^2	-	6.0×10^{-12}	-	calculated
α_t	m	-	1.0	-	(pers. comm. Mendoza, 1995)
α_t	m	-	0.10	-	(pers. comm. Mendoza, 1995)
μ_a	$Pa \cdot s$	-	1.8×10^{-5}	-	(Green, 1984)

Table 4.1: Parameters used to describe the site properties, where 'High' indicates increased biodegradation and 'Low' indicates decreased biodegradation.

Parameter	Component	Units	High	Average	Low	Reference
μ_c	hc	$Pa \cdot s$	-	6.00×10^{-6}	-	(Green, 1984)
D_{ai}	hc	m^2/s	-	6.99×10^{-6}	-	(Green, 1984)
D_{ai}	O_2	m^2/s	-	1.80×10^{-5}	-	(Green, 1984)
D_{wi}	hc	m^2/s	-	5.0×10^{-10}	-	(pers. comm. Mendoza, 1995)
D_{wi}	O_2	m^2/s	-	1.0×10^{-9}	-	(pers. comm. Mendoza, 1995)
H_C	hc	-	61.6	72.2	82.8	(Mackay <i>et al.</i> , 1992)
H_O	O_2	-	-	31.1	-	(Borden and Bedient, 1986)
K_{oc}	hc	-	5500	6633	8000	(Mackay <i>et al.</i> , 1992)

Table 4.2: Parameters used for transport simulations where hc represents hydrocarbon and O_2 represents oxygen, and 'High' indicates increased biodegradation and 'Low' indicates decreased biodegradation.

4.1.5 Microbial Population

To determine whether or not hydrocarbon degrading microorganisms were present at the field site, soil samples were collected in December, 1993 from several locations in the subsurface and analyzed. Hydrocarbon degrading microorganisms were found to be present, with elevated populations within the soil vapour extraction test area (Komex, 1994c). Currently, no method to predict the length of time the microbes need to acclimatize exists (Alexander, 1994); therefore, it is assumed here that the microbes have acclimatized to their environment and, further, that no additional nutrients are necessary. It is believed that Psychrophilic bacteria, which are typically found in cold weather environments, are present; however, a mixed population of indigenous microorganisms is most likely. The microorganisms are assumed to consume the foreign hydrocarbon, hexane, and it is assumed that during biodegradation, toxic products which may be harmful to the microorganisms are not formed.

Microbial Counts

The size of the microbial population was determined from microbial counts from 14 soil samples collected in duplicate from 4 different boreholes. The total counts of the microbes varied from 10^6 to 10^8 viable cells / gram dry weight of sediment (Energy & Environmental Research Center, 1994) and changed little vertically. The microbial counts or the microbial soil population density were converted to microbial concentrations using the method outlined by Chen *et al.* (1992). By assuming a cell diameter of $1.0 \mu m$ and a microbial density of $1.0 g/cm^3$ the initial microbial concentration was calculated in *mg* active cell / *l* soil (Table 4.3).

Biodegradation Parameters

In general, microbial parameters depend on the characteristics of both the microorganisms and the hydrocarbon. Table 4.3 lists the microbial parameters and those parameters which highly influence biodegradation are again given a range of values. The first column of parameters indicates the values of each of the parameters

Parameter	Units	Biodegradation			Reference
		Increased (High)	Average (Average)	Decreased (Low)	
M_t sand	mg/l	165	16.5	3.30	(Komex, 1994c)
M_t till	mg/l		0.367		(Komex, 1994c)
h_u	s^{-1}	1.83×10^{-4}	1.029×10^{-4}	5.79×10^{-5}	(pers. comm. Rittmann, 1995)
K_C	mg/l	0.10	0.32	1.0	(pers. comm. Rittmann, 1995)
K_o	mg/l	0.05	0.16	0.50	(pers. comm. Rittmann, 1995)
G	mg/mg	-	3.5	-	calculated
Y	mg/mg	-	0.45	-	(pers. comm. Rittmann, 1995)
b	s^{-1}	1.16×10^{-8}	8.20×10^{-8}	5.79×10^{-7}	(pers. comm. Rittmann, 1995)

Table 4.3: Acceptable ranges of the biodegradation parameters, where 'High' indicates increased biodegradation and 'Low' indicates decreased biodegradation.

which will result in an increased rate of biodegradation (High) and the third column represents those values which result in a decreased rate of biodegradation (Low).

4.2 Conceptual Model

4.2.1 Grid and Domain

The numerical grid was 21 by 61 nodes for a total of 1281 nodes and 2400 elements (Figure 4.2). The glacial till unit extends from 0 *m* to 2.0 *m* and the extraction well extends from approximately 4.8 *m* to 7.5 *m* below the ground surface. The numerical grid is fixed at a depth of 8 *m* for all simulations. During advective-dispersive transport, concentration gradients are highest near the extraction well. To ease the numerical computations, the grid discretization in this area is tighter. Concentration gradients are smaller during passive transport and numerical computations are easier. Therefore, the grid necessary for advective-dispersive transport is also used for passive transport.

4.2.2 Boundary Conditions

The conceptual model in Chapter Two describes the boundary conditions for advective-dispersive transport. Passive transport is also studied and has slightly different boundary conditions, the main difference being flow boundary conditions are not applicable. In passive transport, the extraction well boundary behaves like a symmetry boundary, similar to the far right lateral boundary, and still has a zero concentration gradient.

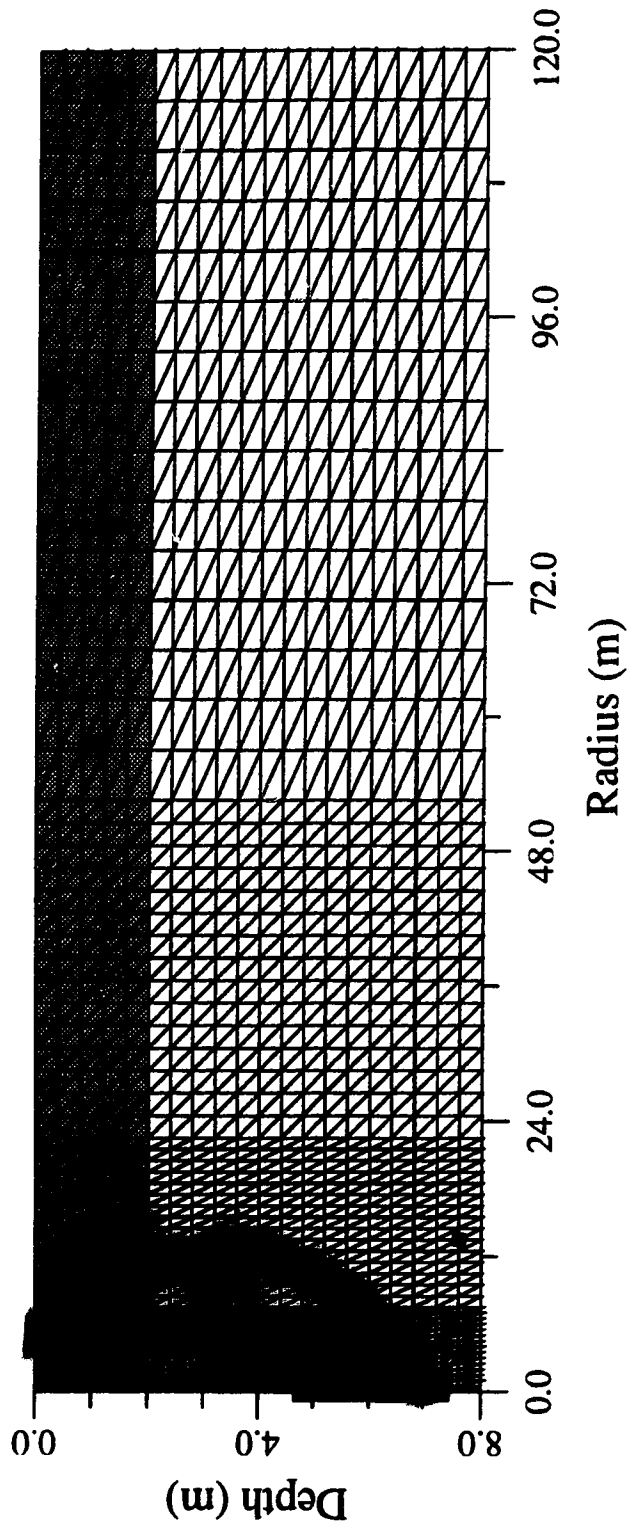


Figure 4.2: The numerical grid, where the glacial till is shaded, the extraction well is represented by the solid dark line, and the monitoring wells are indicated by solid black squares.

4.3 Modelling Results

4.3.1 Setup for Comparison to Field Data

During the bioventing remediation field tests, air extraction occurred only from one central well, SVE-1, and oxygen and hydrocarbon concentrations were measured at multi-level monitoring wells located outward at different radial distances (Figure 4.3). The multi-level monitoring wells were comprised of 3 nested wells with 0.3 m screens installed at 3 different depths, where the letter *C* is used to represent the shallowest screen, while *A* represents the deepest screen (Komex, 1994c). The extraction well had a 3 m screen which extended from 1.2 to 8.3 m below the ground surface. The numerical model simulations were designed to duplicate the field results specifically for ML-1A, ML-3A, and ML-4A since complete data sets were available for these wells and these wells were drilled to a depth of approximately 7 m into the zone of contamination, slightly above the watertable. The median screen depth for the wells of interest are 7.8 m for ML-1A, 7.4 m for ML-3A, and 7.5 m for ML-4A. Referring to Figure 4.2, ML-3A and ML-1A are located near the extraction well in the area of smallest grid discretization; ML-4A is located approximately at the halfway point in the next size of discretization of the grid mesh. In the field, the concentration is represented as an average concentration over the entire screen length; however, in the model, the concentration is taken from a point (node) located approximately at the midpoint of the monitoring well screen for each well.

4.3.2 Air Flow Comparisons

The soil permeabilities listed in Table 4.1 for both geologic units were determined by inverse modelling, where the pressure distribution calculated by the model was compared to the pressure distribution measured in the field site at several monitoring wells. It was determined that the till unit has a horizontal and vertical permeability of $6.0 \times 10^{-12} \text{ m}^2$; the sand and gravel unit has a horizontal permeability of $2.5 \times 10^{-10} \text{ m}^2$ and a vertical permeability of $1.5 \times 10^{-10} \text{ m}^2$. The calculated contrast in permeability

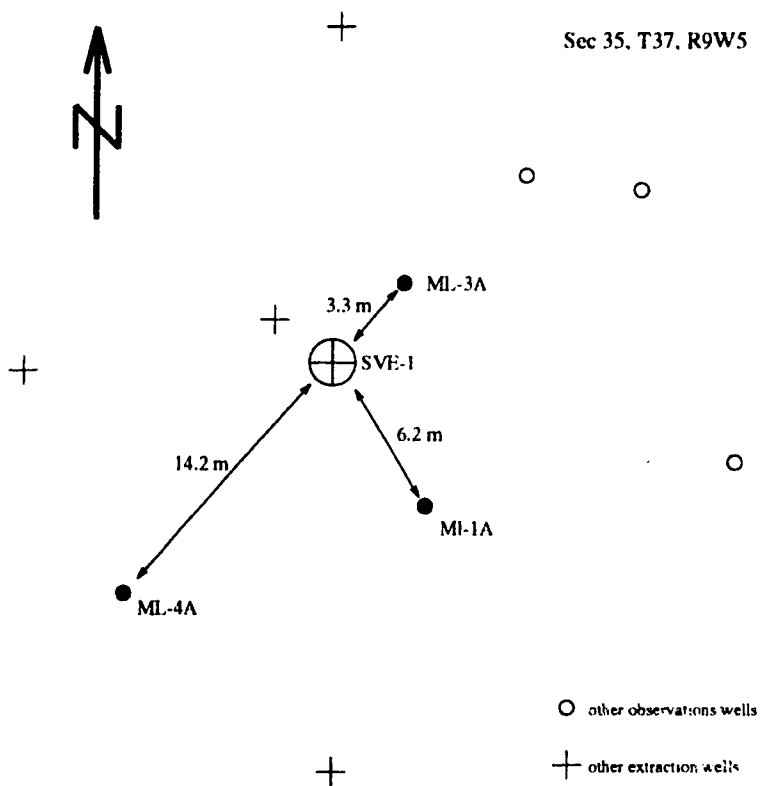


Figure 4.3: The distribution of the extraction well, SVE-1, and the monitoring wells, ML-1A, ML-3A, ML-4A, at the field site (not to scale).

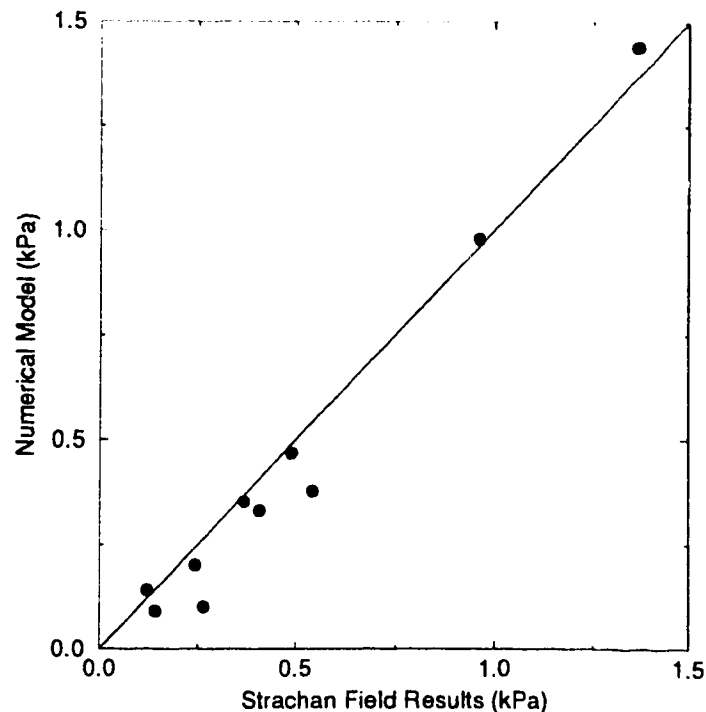


Figure 4.4: Comparison of the pressure distribution calculated by the numerical model and observed at the field in order to determine permeability. The straight line indicates exact correspondence between the field data and model calculations.

values between the till and sand units is lower than expected. The till permeability is higher than values given in Freeze and Cherry (1979) for a clay till. The discrepancy in the values is probably because of desiccation which resulted in fractures which would allow increase air flow through the unit. The weathered brown colour and the fact that the watertable lies significantly below the till unit further supports this hypothesis. For the reasonable match of the pressure distributions that was obtained (Figure 4.4), the values of the soil permeabilities used in the model were considered relatively good estimates and represented the permeabilities in all further simulations dealing with the Strachan field site. The resulting velocity distribution of these permeabilities is shown and discussed in more detail in Chapter 5.

A sensitivity analysis was performed to determine what affects the pressure drawdown curves. Aspects considered include: the effect of explicitly representing

the well radius in the domain and the effect of using a constrained pressure versus a constrained flux to define the extraction well. During the sensitivity analysis, it was determined that for constrained flux simulations, the pressure was the highest in the middle of the well screen (Figure 4.5). In the field, however, it is observed that for longer well screens (such as the one simulated here) larger amounts of air are extracted at the top of the well screen than at the bottom of the well screen.

The representation of the extraction well in the grid domain proved to be important for flow calculations. Two simulations were performed which used constrained pressures along the well screen to define the extraction well; however, one simulation explicitly accounted for a well radius of 10 *cm*, the approximate radius of the extraction well at the field site. Thus, instead of the axisymmetric model rotating the grid about a line during the simulation, the actual diameter of the field well is incorporated. Figure 4.6 shows that when the well radius is not included, the model underpredicted the pressure drawdown observed at the field site; thus it was concluded that the well radius should be explicitly included.

The results of two simulations comparing the effects of representing the extraction well screen as a constrained pressure boundary versus a constrained flux boundary are shown in Figure 4.7. Assuming a well radius of 10 *cm*, a total extraction rate of 0.305 *ℓ/s* was either calculated or specified for both simulations. The only difference in the results of the two simulations was in the pressure near the extraction well. The pressure was constrained at 4500 *Pa* for the one simulation; however, the pressures near the extraction well were slightly higher when the flux at each node was defined as 0.0436 *ℓ/s*. The constrained values of 4500 *Pa* or 0.0436 *ℓ/s* both yield suitable matches to the field data distant from the well and yield a total extraction rate (0.305 *ℓ/s*) that corresponds to the measured extraction rate. Because measuring the pressure at the extraction well in the field is impossible due to well and screen losses, a comparison of the calculated values to the measured value is not possible. Therefore, determining which simulation predicted the pressure better near the extraction well is not possible. Incorporating the size of the well's radius and using a constrained

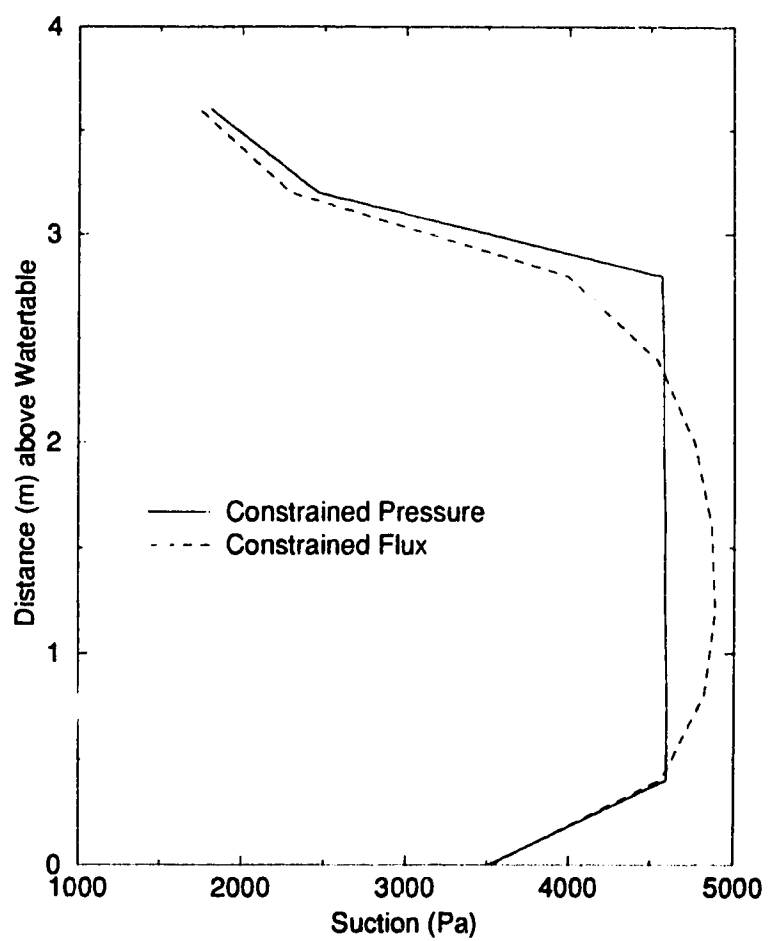


Figure 4.5: Distribution of pressure along the extraction well screen.

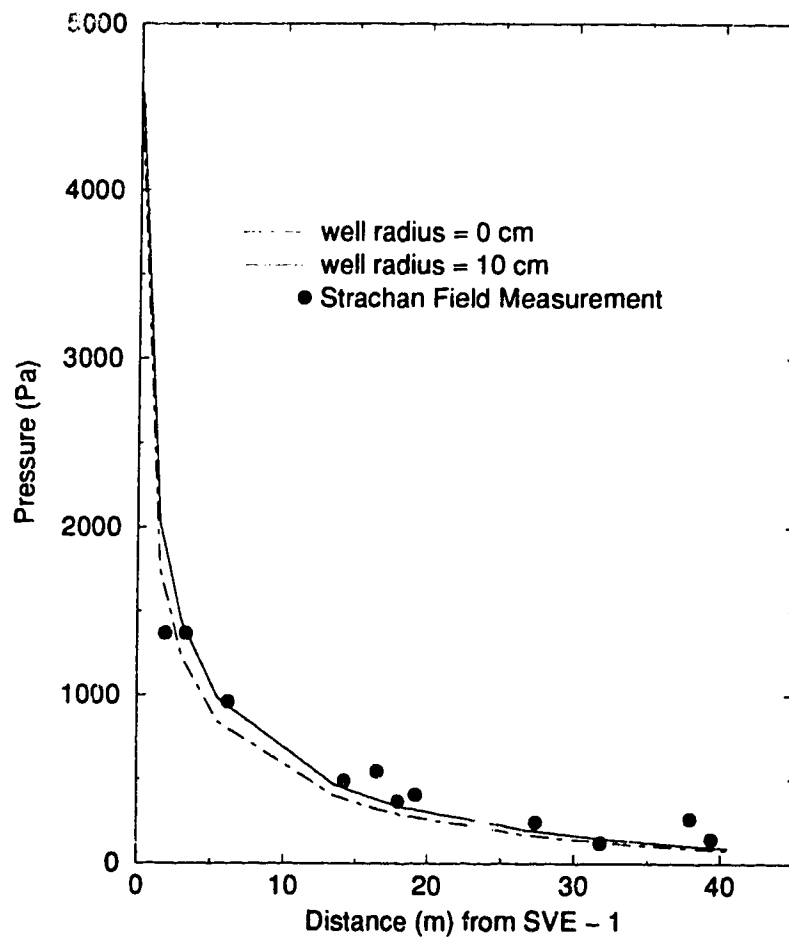


Figure 4.6: Comparison of the pressure distribution that results from having the well radius equal to 0 cm versus 10 cm.

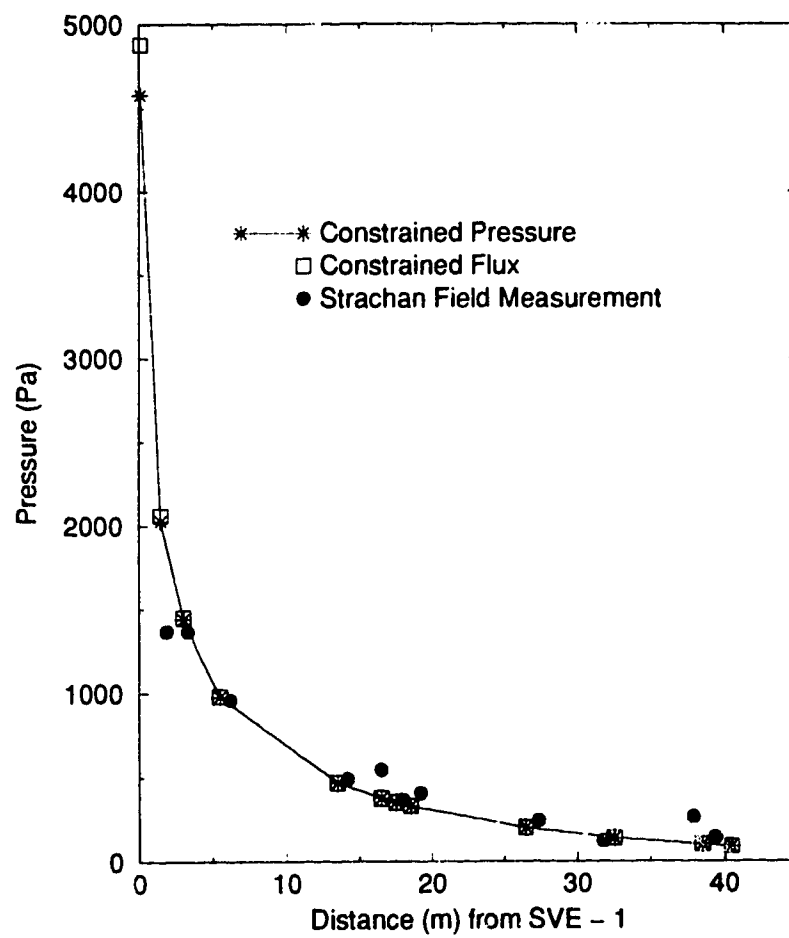


Figure 4.7: Comparison of the pressure distribution when the extraction well is defined as a constrained pressure versus a constrained flux.

pressure to represent the well screen appears to predict the pressure distribution more accurately; however, for most of the bioventing field test data, only the extraction rate was available, and therefore the simulations performed in this chapter used a constrained flux to represent the extraction rate.

4.3.3 Biodegradation Comparisons

At the Strachan field site, three fundamentally different tests were performed to study the bioventing remediation scheme and its effectiveness. The three field tests were: (a) a Recovery Test, with passive transport only; (b) a Variable Flow Rate Test, with advective-dispersive transport at different extraction rates; and, (c) a Respiration Test, with alternating passive and advective-dispersive transport. For all the tests, both hydrocarbon and oxygen concentrations were measured extensively; the concentrations of the microbes were measured only at one point in time. The initial conditions of each numerical simulation that represents one of the field tests try to duplicate the same hydrocarbon and oxygen distributions depicted during the start of that field test. The large hydrocarbon plume present at the field site extended beyond the area being bioremediated. Therefore, when the hydrocarbon concentrations decreased in the test site area, an influx of hydrocarbon mass probably occurred along the watertable. To represent this ongoing source, hydrocarbon contamination is represented as a continuous source along the watertable boundary during numerical simulations. To account for the smeared residual in the vicinity of the watertable in the field, the first three layers of elements, representing approximately 1.2 *m*, in the numerical grid have some initial hydrocarbon concentration. The hydrocarbon concentration is zero everywhere else in the domain. The initial oxygen concentration was 21% of an atmosphere everywhere in the domain to represent the oxygen levels at the start of each field test.

The axisymmetric numerical model assumes horizontal, radial uniformity. However, for each specific field test the three monitoring wells (ML-1A, ML-3A, ML-4A) displayed different trends in hydrocarbon and oxygen concentrations at essentially

the same elevation. This spatial variability is probably the result of heterogeneous residual hydrocarbon distributions and possibly due to variable porous media properties. Although a three-dimensional analysis of the problem would be ideal, this would require even more data that can not be adequately quantified during the field test. Thus, for each field test, three different simulations were performed to best represent the observed trends at each monitoring well. In this way, three best fits to the observed data were calculated; however, because of the unquantifiable heterogeneities, the behaviour of the system would best be represented and described by some combination of the three different simulations. This uncertainty in the final results is unavoidable given the spatial variability in the hydrocarbon distribution in the subsurface.

Since little information on the microbial population exists, a direct comparison of the field results to the numerical model results was not possible and the initial size of the microbial population was used as a fitting parameter. The till unit had an initial microbial concentration of $0.367 \text{ mg active cell} / \ell \text{ soil}$ whereas the sand and gravel unit had an initial microbial concentration that was varied from 3.30 to 16.5 to $165 \text{ mg active cell} / \ell \text{ soil}$. Although the model results could be used to extrapolate what the behaviour of the microbes might have been, the behaviour of the microorganisms was not extensively studied due to the high uncertainties. This aspect is explored in more detail in the sensitivity analysis (Chapter 5). During the different simulations, the size of the microbial population varied spatially due to differential growth of the microorganisms, with the most growth experienced in the zone of highest hydrocarbon contamination.

The focus of this part of the study was to determine how the size of the initial microbial concentration and the values of the biodegradation parameters influenced the modelling results. The parameters which were studied extensively for the comparison of field data to the numerical model results were: the initial microbial population, M_i ; the initial hydrocarbon and oxygen concentrations, C_i and O_i ; the hydrocarbon Henry's constant, H_C ; the soil organic content, f_{oc} ; the organic carbon partitioning

coefficient, K_{oc} ; the soil moisture content, θ_w ; the maximum hydrocarbon utilization rate, h_u ; and the half-saturation constants, K_C and K_O .

Recovery Tests

The Recovery Test was the initial test performed in the field from June 10 to July 6, 1993 to determine if aerobic biodegradation of the hydrocarbon condensate was occurring. After 36 days of continuous pumping from various extraction wells to aerate the subsurface and bring oxygen concentration to atmospheric levels (21%), the air blower was turned off and spatial oxygen concentrations were monitored over time. No hydrocarbon concentration data was collected during the Recovery test. It was observed that the oxygen concentration changed significantly in all wells, dropping from 21% to approximately 2 - 5% during the four weeks of passive transport. This was taken to be a strong indication that aerobic biodegradation was occurring at the site (Komex, 1994c). The oxygen concentration dropped rapidly at the start of the test and then gradually declined with time indicating oxygen utilization was highest initially after the blower was turned off (Komex, 1994a).

For this first phase of the numerical modelling, the objective was to determine parameter ranges which result in calculated oxygen trends that are similar to the trends observed in the field. A series of simulations demonstrated the results were highly sensitive to the value chosen for the different parameters which affect biodegradation (M_L , h_u , K_C , K_O , θ_w , and H_C) and that different sets of values could produce similar results. Three simulations representing the three different ranges of values for the parameters closely matched the data obtained at the field test (Figure 4.8) and the parameter ranges are outlined in Table 4.4 (only the parameters which are different than the ones outlined in Tables 4.1, 4.2, and 4.3 are noted). The numerical simulations for Data Sets I, II, and III all displayed increased oxygen utilization (rapid decrease in oxygen concentrations) followed by a gradual decrease in the oxygen concentration similar to what was observed in the field. As a result, the three data sets (High, Average, and Low) were used to describe the Variable Flow Rate and

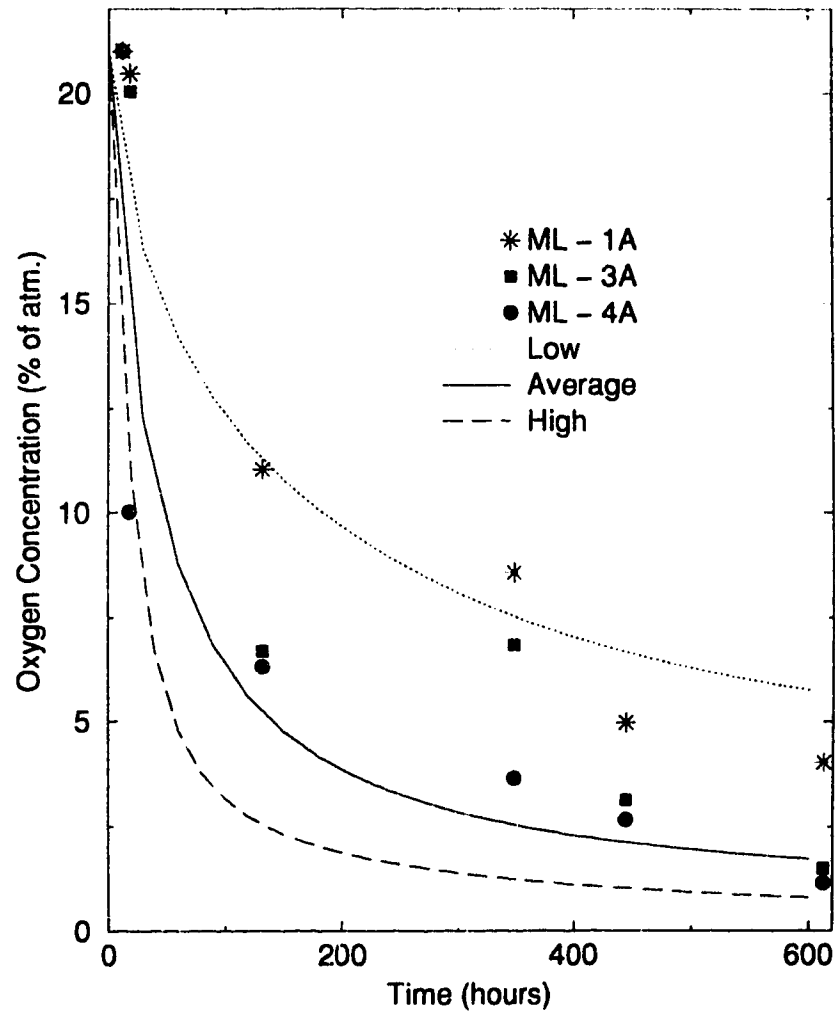


Figure 4.8: Oxygen concentration results for the Recovery Test, where 'High' indicates increased biodegradation and 'Low' indicates decreased biodegradation

	Data Set I	Data Set II	Data Set III	
Parameter	Units	High	Average	Low
C_i	ppm	5000	5000	5000
O_i	%atm	21	21	21
M_i	mg/l	3.30	16.5	165.0
H_C	-	61.6	72.2	82.8
$f_{oc\ sand}$	-	0.00055	0.00074	0.0010
$f_{oc\ till}$	-	0.0063	0.011	0.020
K_{oc}	-	5500	6633	8000
$\theta_w\ sand$	-	0.10	0.062	0.038
$\theta_w\ till$	-	0.15	0.077	0.040
h_u	s^{-1}	1.83×10^{-4}	1.029×10^{-4}	5.79×10^{-5}
K_C	mg/l	0.20	0.32	1.0
K_O	mg/l	0.10	0.16	0.50
b	s^{-1}	1.16×10^{-8}	1.16×10^{-8}	1.16×10^{-8}

Table 4.4: Parameters ranges for the three field tests, where 'High' indicates increased biodegradation and 'Low' indicates decreased biodegradation.

Respiration Tests as well.

The sensitivity of the numerical model results to the half-saturation constants and the size of the initial microbial population was briefly investigated. The sensitivity of the numerical model to these parameters, as well as others, is discussed in greater detail in Chapter 5. The values used for K_C and K_O are slightly higher for Data Set I than the lower end of the range depicted in Table 4.3 because using the lower values of 0.1 and 0.05 for K_C and K_O , respectively, overpredicted biodegradation (Figure 4.9). Thus, the values outlined in Table 4.4 for K_C and K_O were used. Figure 4.9 also shows the sensitivity to the initial microbial population. Using the parameters for Data Set III (Low), the initial concentration was changed from 165 mg/l to 3.30 mg/l. The difference between the two simulations indicates that when the biodegradation parameters are the same, oxygen and hydrocarbon utilization is greatest with a higher microbial population concentration, as expected.

Figure 4.10 shows the difference in hydrocarbon trends between a simulation using only vacuum extraction and a simulation which includes biodegradation. The concentration trends are clearly different if biodegradation is not considered. All three data sets give the same trends; therefore, only one simulation from one data set will be used to compare the hydrocarbon trends observed for the Variable Flow Rate and Respiration Tests.

Variable Flow Rate Test

The Variable Flow Rate Test consisted of a series of four step tests in which the extraction rate was decreased three times over a 17 week period from August to November. The two goals of the field test were to determine the effects of decreasing the extraction rate on the biodegradation and volatilization and to determine the lowest extraction rate which can replenish oxygen to sufficient levels (Komex, 1994c). Prior to the start of this test, all the air extraction wells had been pumping for approximately one month after the Recovery Test (Komex, 1994c). For the Variable Flow Rate Test, the blower was only attached to SVE-1 and the extraction rate

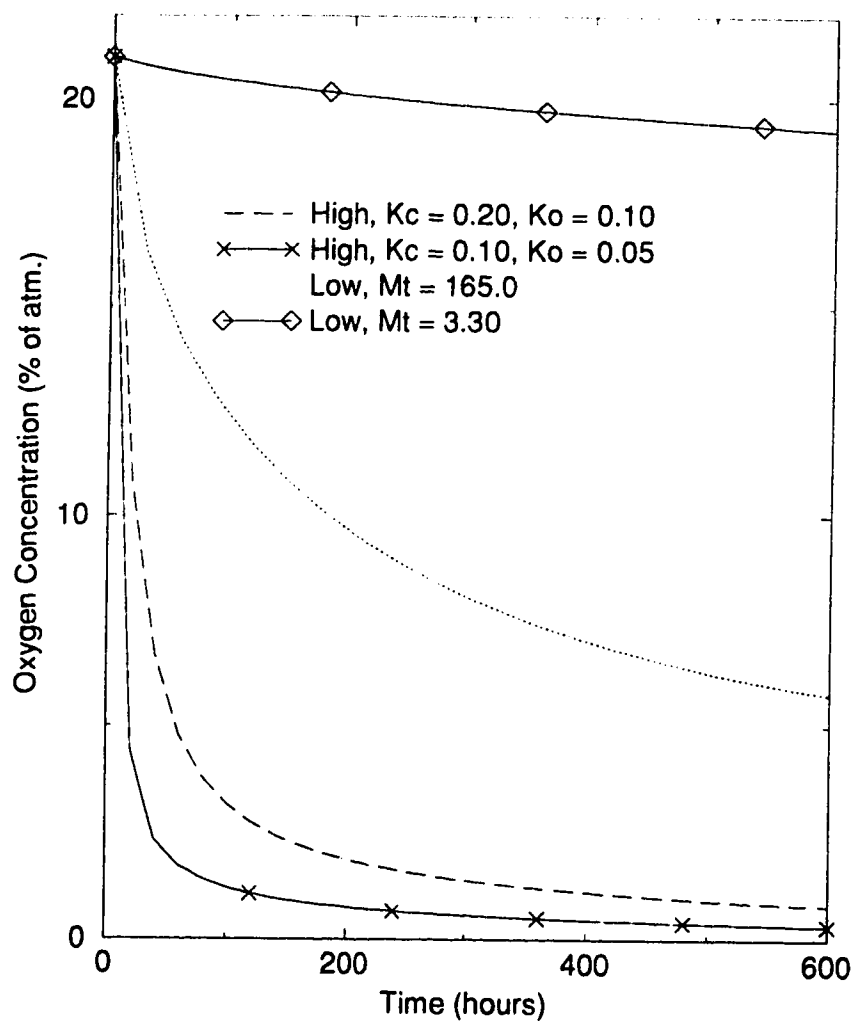


Figure 4.9: Comparing the difference between using different half-saturation constants for Data Set I and using a different initial microbial population for Data Set III in Table 4.4.

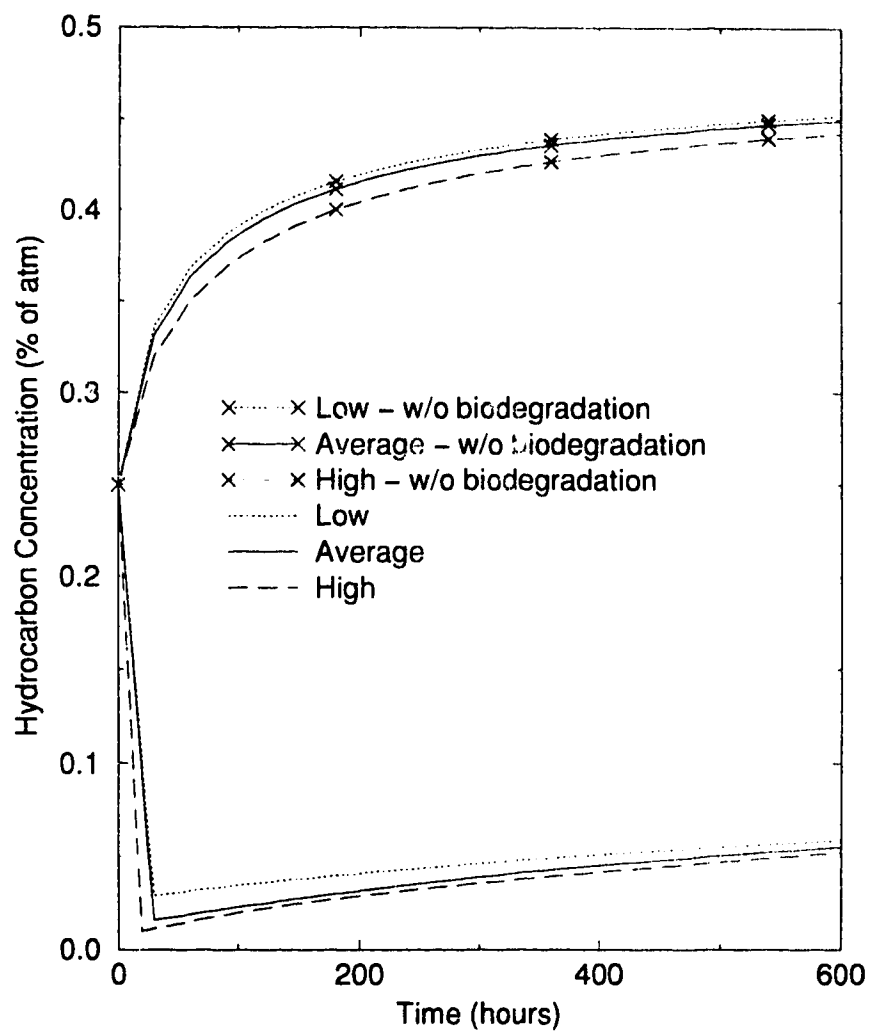


Figure 4.10: The difference in the hydrocarbon trends for the Data Sets in Table 4.4 between simulations with and without biodegradation, where 'High' indicates increased biodegradation and 'Low' indicates decreased biodegradation.

changed as follows: Step 1 - 118 ℓ/s for 1 week; Step 2 - 76 ℓ/s for 3 weeks; Step 3 - 42 ℓ/s for 4 weeks; and Step 4 - 24 ℓ/s for 9 weeks. Field observations tended to indicate that the optimal extraction rate was 76 ℓ/s because low hydrocarbon off-gas concentrations were observed and oxygen supply seemed sufficient.

The test simulations for the Variable Flow Rate Test used the same model input data sets as the Recovery Test (refer to Table 4.4); however, the source hydrocarbon concentration was substantially different for each simulation corresponding to each of the three monitoring wells: 5000 ppm at ML-4A, 75 ppm at ML-3A, and 200 - 500 ppm at ML-1A. Initial oxygen concentrations were specified as 21%, 20%, and 18% of an atmosphere for the simulations representing conditions at ML-4A, ML-3A, and ML-1A respectively. These concentration values are based on the observed concentration prior to the onset of the test. The oxygen trends calculated by the model for each data set (High, Average, Low) for each monitoring well duplicate the trends observed in the field reasonably well (Figures 4.11, 4.12, and 4.13). The shapes of the curves for the model simulations, especially for well ML-4A, indicate that when the extraction rate is decreased, more oxygen is utilized and biodegradation occurs at a higher rate until some later time at which oxygen utilization declines and biodegradation appears to reach steady-state. As well, after each decrease in the extraction rate, less oxygen becomes available in the system and the overall rate of oxygen utilization decreases. Figure 4.12 shows the oxygen concentration changed little during the variable flow rate test at ML-3A. This possibly indicates that the activity of the microbes is reduced with very low hydrocarbon concentrations.

Figures 4.11, 4.12, and 4.13 also demonstrate how important the initial concentrations are for both the hydrocarbon and oxygen. With lower initial hydrocarbon concentrations, less oxygen is utilized and therefore the biodegradation rate is lower. It is important then that the initial oxygen levels be representative of the initial levels observed in the field since too much oxygen initially in the system will overpredict the oxygen remaining in the system during the model simulation.

Figure 4.14 shows the difference in the hydrocarbon trends for wells ML-1A and

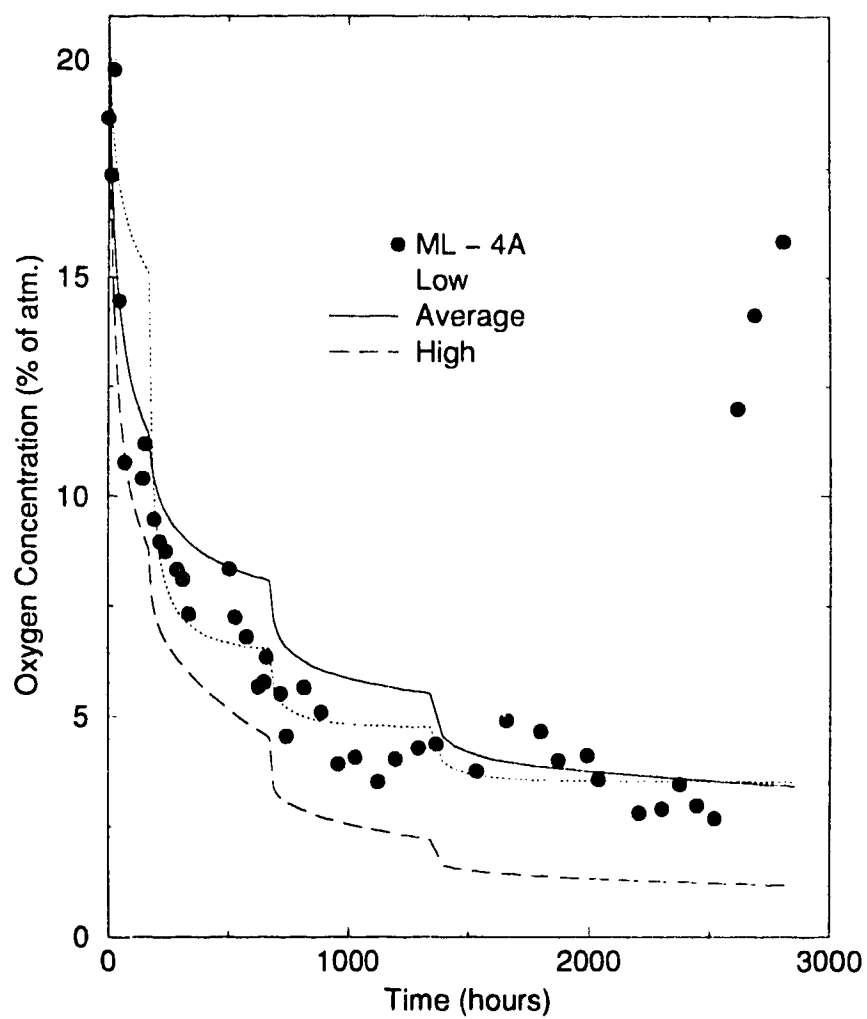


Figure 4.11: Oxygen concentrations results for the Variable Flow Rate Test for ML 4A, where 'High' indicates increased biodegradation and 'Low' indicates decreased biodegradation.

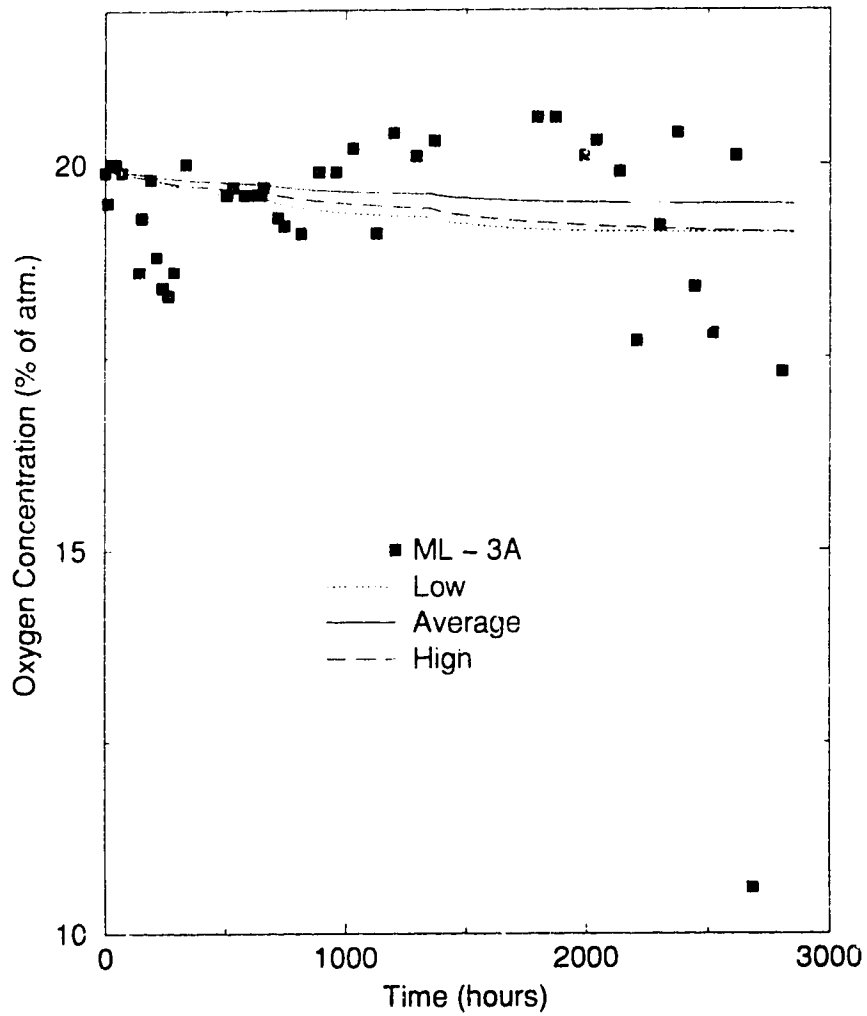


Figure 4.12: Oxygen concentrations results for the Variable Flow Rate Test for ML-3A, where 'High' indicates increased biodegradation and 'Low' indicates decreased biodegradation.

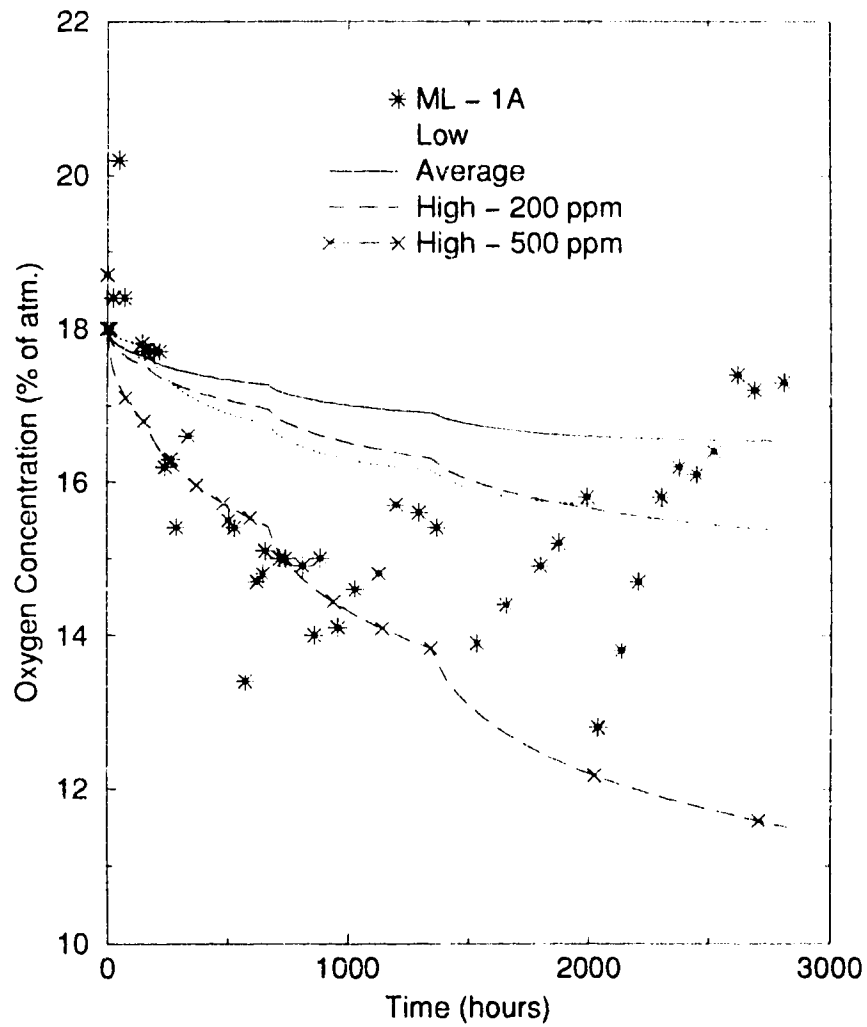


Figure 4.13: Oxygen concentrations results for the Variable Flow Rate Test for ML 1A, where 'High' indicates increased biodegradation and 'Low' indicates decreased biodegradation.

ML 3A for both the numerical model results with and without biodegradation and the field results. Data Set III, with an initial concentration of 500 *ppm* for well ML 1A, is used as the representative model simulation since similar trends were observed for all three data sets. This figure shows the hydrocarbon trends are best represented by the numerical simulations which incorporate biodegradation since those simulations without biodegradation overpredict the amount of hydrocarbon present at the monitoring wells.

Respiration Test

The Respiration Test began directly after the Variable Flow Rate Test and involved a series of tests which switched alternately between passive transport for approximately 10 days and advective-dispersive transport for approximately 4 days over a period of 6 months. The purpose of this test in the field was to determine if biodegradation continued throughout the winter months and the results showed temperature had little effect on the rate of biodegradation (Komex, 1991c) and the system appears to recover quickly when the extraction pump is turned off. The results of this test can also be used to look for kinetic effects that might indicate that equilibrium phase-partitioning does not represent the system in its entirety.

Although the Respiration Test was carried out from December 1993 to May 1994, only the time period from December 3 to February 1 was simulated because of the large amount of CPU time required for each simulation. Nonetheless, the reasonable match between the numerical results and the four cycles of field data for this time period indicate the numerical model could describe biodegradation occurring during the respiration tests adequately. The test began with a period of passive transport and, for the time of interest, a total of three periods of advective-dispersive transport occurred between four periods of passive transport. A high air extraction rate of 189 *l/s* was used in the field, and thus in the model, in order to aerate the subsurface quickly to increase the oxygen concentrations quickly.

Figures 4.15, 4.16, and 4.17 compare the model results and the field data for the

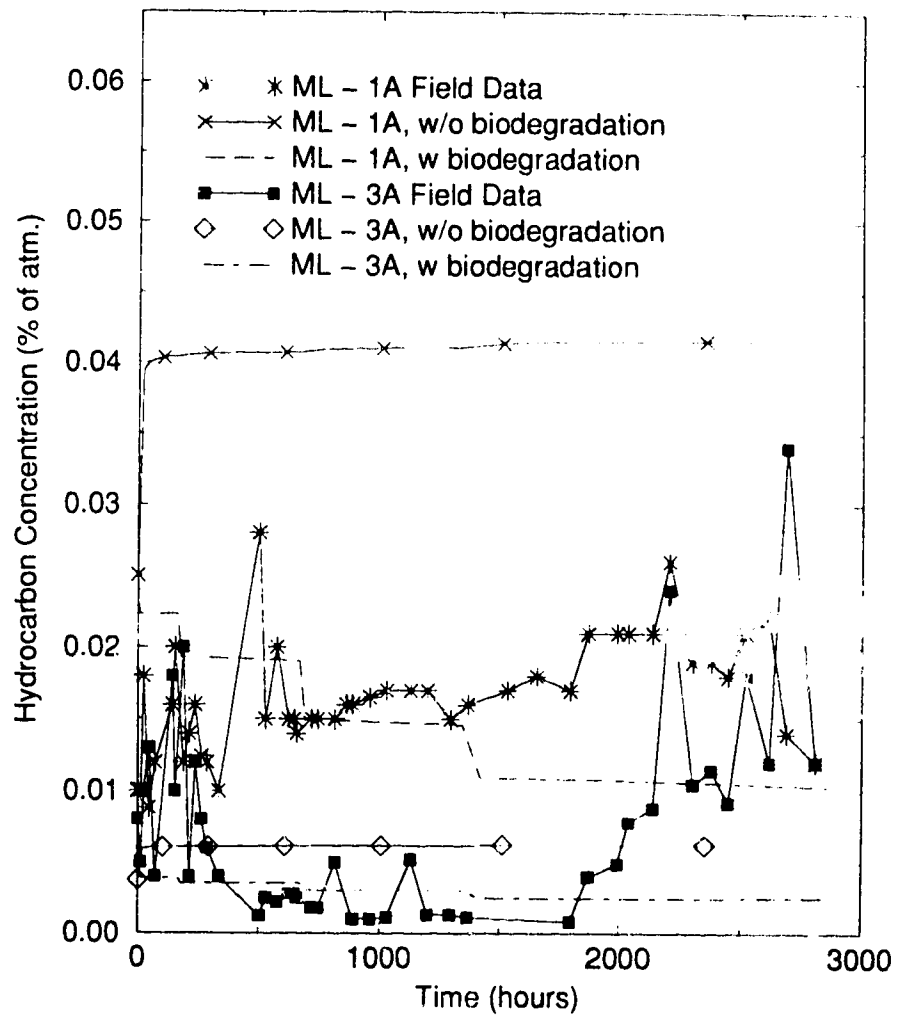


Figure 4.14: The different hydrocarbon trends for wells ML 1A and ML 3A for both with and without biodegradation.

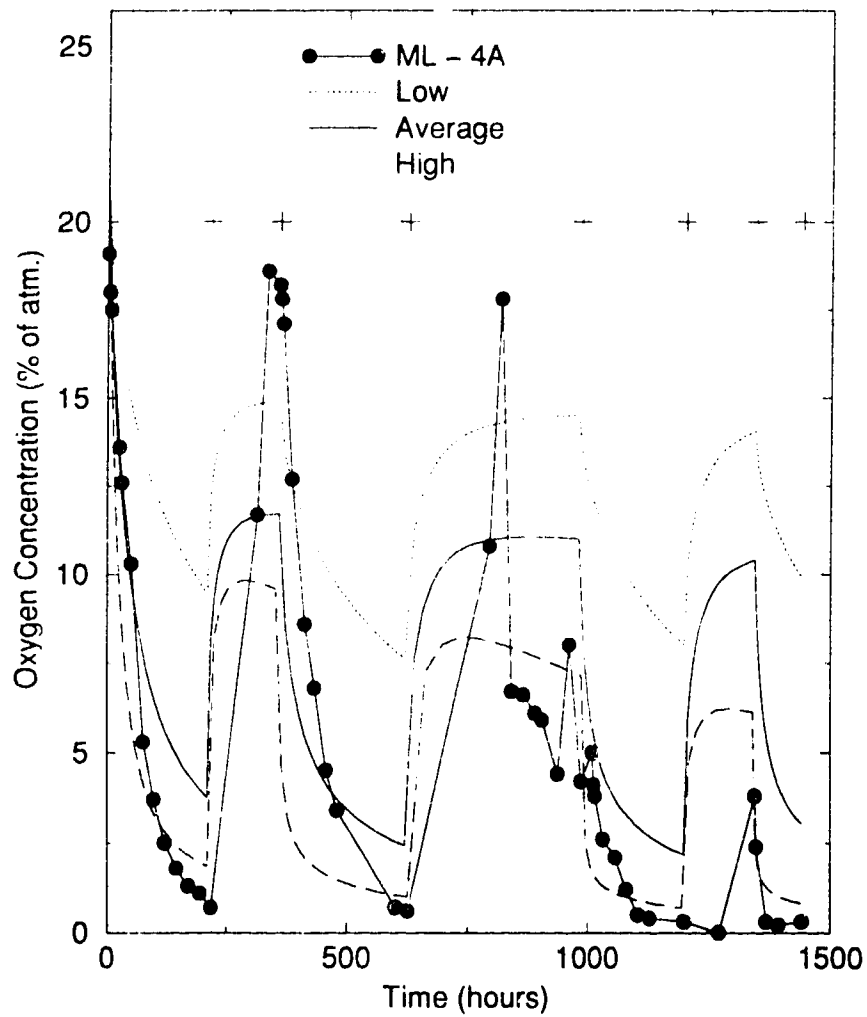


Figure 4.15: Oxygen concentration results for the Respiration Test for well ML-4A, where 'High' indicates increased biodegradation and 'Low' indicates decreased biodegradation.

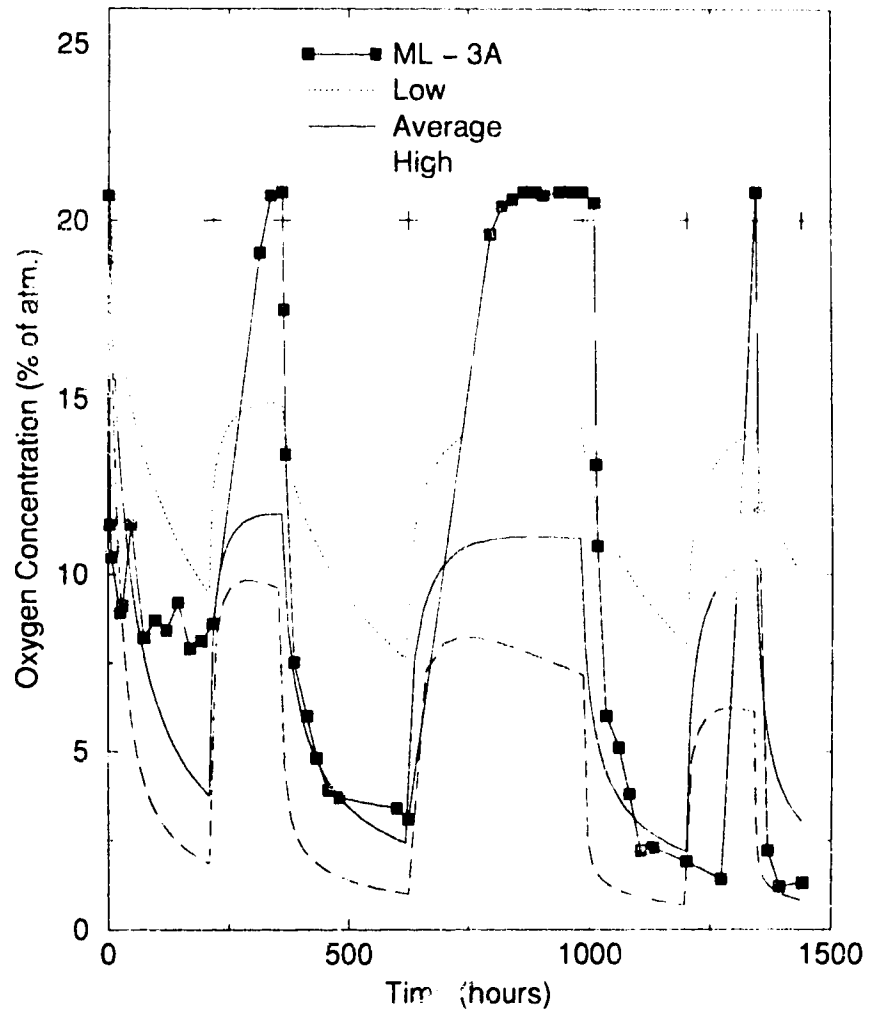


Figure 4.16: Oxygen concentration results for the Respiration Test for well ML 3A, where 'High' indicates increased biodegradation and 'Low' indicates decreased biodegradation.

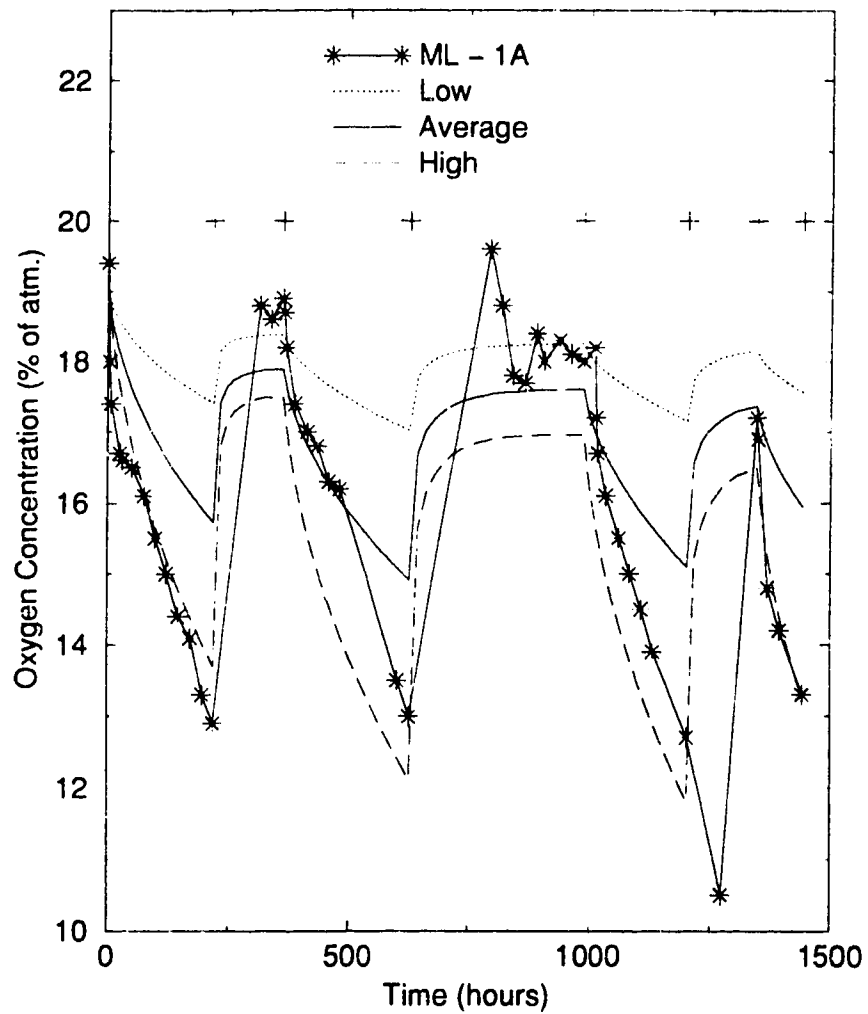


Figure 4.17: Oxygen concentration results for the Respiration Test for well ML-1A, where 'High' indicates increased biodegradation and 'Low' indicates decreased biodegradation.

Respiration Test, where the initial hydrocarbon concentration was 5000 ppm at wells ML-1A and ML-3A, and 500 ppm at well ML-1A. The hydrocarbon concentration measured at ML-3A at the start of the respiration test was much higher than the value measured at the start of the variable flow rate test. This is probably the result of a flux of hydrocarbon from an area of increased hydrocarbon concentration moving into the vicinity of ML-3A, previously an area of decreased hydrocarbon concentration, at some time between the two tests. The crosses on the figures indicate the time when the mode of transport changes from either advective-dispersive to passive or vice versa. Again, the same three sets of parameters (High, Average, Low) from Table 4.4 were used for the simulations of each well. It should be noted that the model simulations in Figures 4.15 and 4.16 are the same, but are plotted on two graphs to show how they compare to the two different sets of field data for those two wells. Both the model and field results for all three wells indicate the oxygen concentrations increase during advective-dispersive transport (the model does not quite increase to the levels observed in the field), and then rapidly decrease during passive transport. This means the extraction rate was sufficient to increase the oxygen supply to the microorganisms during air extraction. This also shows that pulse-pumping may be necessary to increase oxygen concentrations to maintain biodegradation if higher flow rates are used.

The hydrocarbon trends of the numerical model and the field data for ML-3A and ML-1A are compared in Figures 4.18 and 4.19. A simulation without biodegradation is also shown for comparison and Data Set II (Average) is taken as the representative data set. The numerical results indicate that during passive transport (*i.e.*, no air extraction) the hydrocarbon concentrations generally drop; however, the concentrations then increase during advective-dispersive transport (*i.e.*, air extraction). This means that the hydrocarbon concentrations are at their highest during advective-dispersive transport since the air flow allows increased amounts of hydrocarbon to move through the system. During passive transport, this mobile hydrocarbon is consumed by the microorganisms to decreased levels thereby preventing any significant contaminant

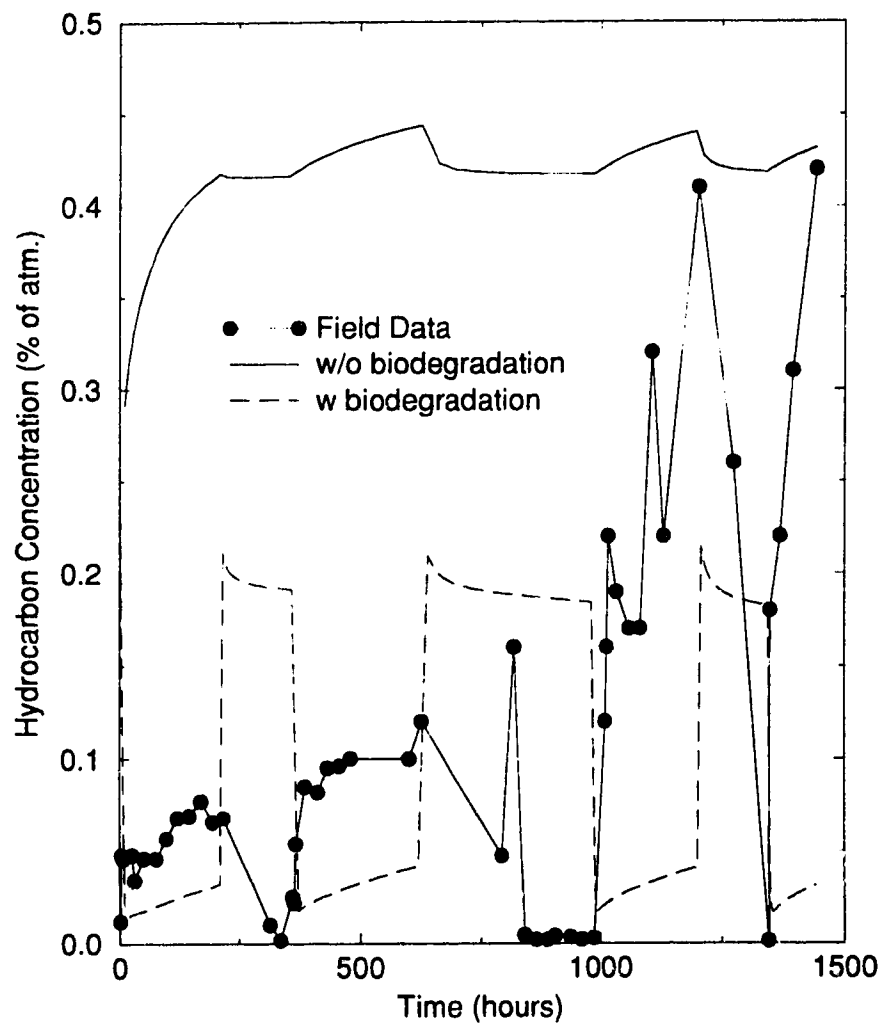


Figure 4.18: Comparison of the hydrocarbon concentration of the field data to the numerical results for well ML-3A with and without biodegradation.

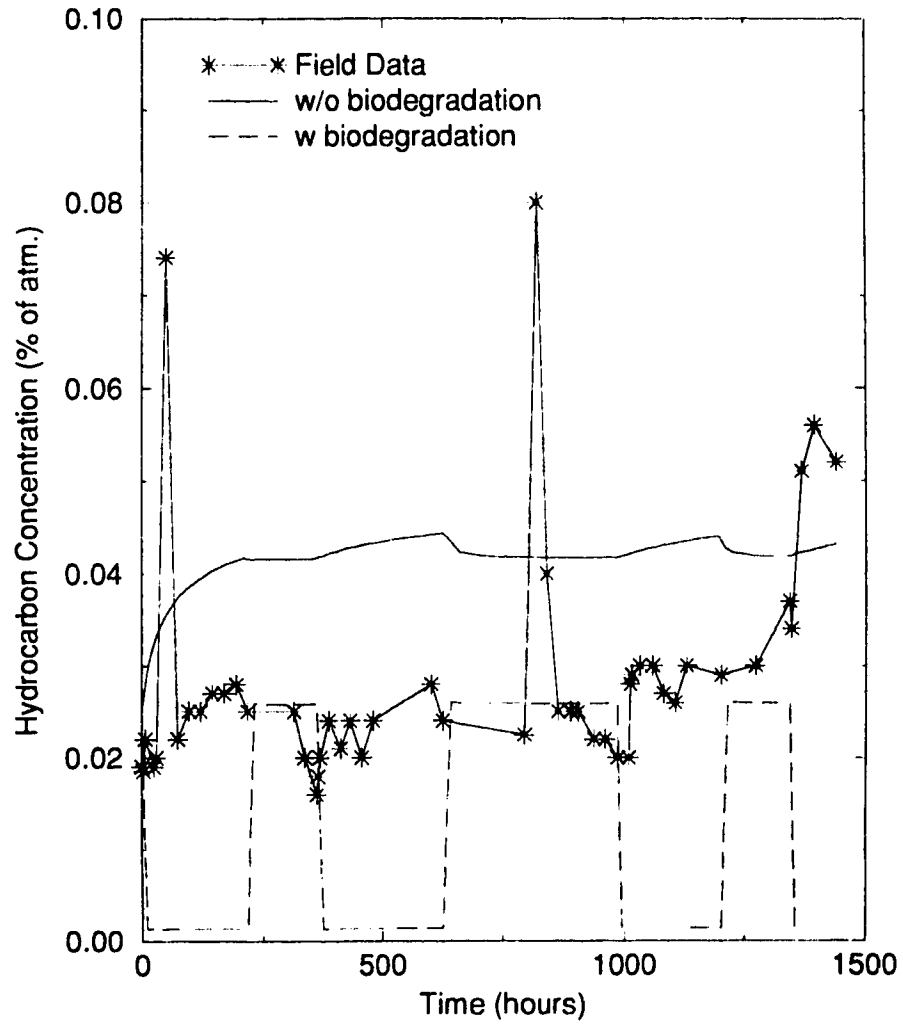


Figure 4.19: Comparison of the hydrocarbon concentration of the field data to the numerical results for well ML-1A with and without biodegradation.

migration. The numerical model slightly underpredicts the hydrocarbon concentrations observed at the field. This is probably because the hydrocarbon variability at the watertable can not be quantified adequately in the field and, therefore, cannot be incorporated into and described by the numerical model.

The three data sets do not absolutely represent the field data obtained from the Strachan field site, probably due to heterogeneities. This may also partly be due to inaccuracies in field measurements or due to Monod kinetics grossly oversimplifying the physical processes occurring in the field. Another reason may be that the biodegradation parameters are not identical during both passive and advective-dispersive transport. During advective-dispersive transport, the oxygen is moving quickly through the system and perhaps does not dissolve into the soil moisture as easily as compared to during passive transport, suggesting equilibrium phase-partitioning may not be a completely valid assumption. Further investigation into this area would be valuable, but, unfortunately, is beyond the scope of this study.

4.4 Summary

The numerical model compared well to the data from the three different field tests which studied biodegradation and bioventing. Oxygen utilization was generally fast at the start of the simulations and when the initial hydrocarbon concentration was high, whether a recovery test or a variable flow rate test was simulated. The oxygen utilization gradually decreased until steady-state conditions were nearly reached later in the simulations. The results of the model were sensitive not only to the biodegradation parameters, but also to the initial concentrations of the hydrocarbon, oxygen, and microbial population. The range of parameters chosen to describe the field site appear to adequately represent the processes occurring at the field site.

Several possibilities exist to explain why the parameter sets and the model results could not exactly duplicate the field data. Watertable fluctuations that may have occurred at the field site are not accounted for in the model and therefore temporal changes in the hydrocarbon concentration are not incorporated. Lateral movement

of the hydrocarbon along the watertable and the variable flow paths due to residual hydrocarbon vapourizing cannot be adequately quantified by field data and cannot be described by the numerical model. All heterogeneities present in the subsurface cannot be quantified in the model which may influence the oxygen flow path towards the zone of contamination and the amount available for microbial degradation. During the time frame studied at the field site, other fields tests outside of the ones modelled were performed (with very little data measured) and therefore may have affected the microbial conditions and these alterations cannot be duplicated by the model. Finally, and most importantly, due to heterogeneity and uncertainty, exact parameter values and their distributions cannot be obtained and thus exact computer simulations are not possible.

Chapter 5

Sensitivity Analysis

5.1 Approach

A sensitivity analysis was performed to determine which parameters have the greatest impact on transport and biodegradation. Through this analysis the uncertainty in the model due to the uncertainty in the estimates of the system's transport, microbial, and geologic parameters was studied. The analysis was centered around a base case scenario, similar to the domain modelled in Chapter 4, and both passive and advective-dispersive transport were considered.

The geology for the base case was the same as the domain depicted for the Strachan field data study which consisted of a 2 *m* glacial till unit overlying a 6 *m* glaciofluvial sand and gravel unit. The same boundary conditions described in Chapter 2 and Chapter 4 apply to the simulations performed throughout the sensitivity analysis. The hydrocarbon source is constrained as a constant concentration along the watertable boundary and the oxygen supply is constrained to atmospheric levels (21% of an atmosphere) along the ground surface. Both lateral boundaries have zero concentration gradients for both hydrocarbon and oxygen. The watertable boundary is also a zero concentration gradient boundary for oxygen and the ground surface boundary for hydrocarbon is a zero concentration boundary. The geology, microbial, and contaminant parameters chosen for the base case were those parameters which represented an average value for the ranges indicated in Tables 4.1, 4.2, and 4.3

with the one exception being the initial microbial concentration was $3.3 \text{ mg}/\ell$ for the sand and gravel unit and $0.367 \text{ mg}/\ell$ for the glacial till unit, the lower end of the values measured for the field site in Chapter 4. The base hydrocarbon contaminant considered was hexane and all properties were calculated assuming a constant temperature of 8°C . For advective-dispersive transport, a constant extraction rate of $118 \ell/s$ was assumed and the well screen was located in the same position as depicted in Chapter 4.

During the sensitivity analysis both passive and advective-dispersive transport were studied, where applicable, to gain an understanding of how the biodegradation process varies between the two different transport scenarios. The differences in the amount of hydrocarbon and oxygen consumed by the microbes and the distribution of hydrocarbon and oxygen during the two transport scenarios were analyzed. The effect that enhanced oxygen replenishment had during air extraction on the rate of biodegradation was also studied.

The sensitivity analysis focused on identifying those factors which primarily affect: (a) flow of air or the oxygen supply; (b) the amount and rate of biodegradation; and (c) the transport of hydrocarbon with the hydrocarbon concentration. The effect that the extraction rate, the well screen position, and the hydrocarbon concentration as well as the till layer thickness and permeability had on the flow of air and oxygen supply were studied. The rate and amount of biodegradation were studied as a function of the size of the initial microbial population, the soil moisture content, and the biodegradation parameters (K_C , K_O , h_u). Investigation into the effect of the microbe death rate (b) had on the biodegradation rate revealed that the b parameter has little effect on the amount of hydrocarbon and oxygen utilized and only affects whether the microbial population will grow or die. As a result, no emphasis was placed on the microbe death rate during the sensitivity analysis. Changing the hydrocarbon contaminant under consideration from the lighter hexane to heavier contaminants provided a combined study of both biodegradation rates and transport. The transport process was further analyzed from simulations that investigated the longitudinal and transverse dispersivities and

unconstrained sources.

During the sensitivity analysis oxygen and hydrocarbon transport were the predominant focus. The growth and death of the microbes were studied during comparison of different biodegradation rates. Unless otherwise specified, for each simulation the hydrocarbon, oxygen, and microbial concentrations were examined at 600 hours (25 days). The pressure and velocity distributions were also examined for those cases where the air flow field was modified.

5.2 Methods of Presenting Results

The hydrocarbon and oxygen concentrations are presented in two different formats depending on the parameter(s) being analyzed. The concentrations may be presented as relative concentration contours and depict the cross-sectional view of the domain. Recall, however, that because axisymmetric coordinates are used, these cross sections represent conditions in all radial directions from the vertical well. The hydrocarbon concentrations are represented by contours over three orders of magnitude, being 0.001, 0.01, and 0.1 to 0.9 (by increments of 0.2) where the watertable (lower) boundary represents a constrained source with a relative concentration of 1.0. The oxygen concentrations are represented by two orders of magnitude, with the contours being 0.01 (in only a few cases) and 0.1 to 0.9 (by increments of 0.2), and with the ground surface (upper) boundary having a fixed relative concentration of 1.0.

Ground surface to watertable profiles at 600 hours are the second method of portraying the results of the sensitivity analysis for both hydrocarbon and oxygen concentrations, as well as for microbe concentrations. For each case, for advective-dispersive transport, three profiles through the domain are represented: near the extraction well (A); either one quarter (B) or one half (C) the distance along the domain; and at the far end of the domain (D). The passive transport cases are only represented by one line (P) since this will indicate what is occurring along the entire domain. Note that the vertical coordinates for the profiles are distances above the

watertable, rather than depths below ground surface, and so the ground surface is indicated by 8 *m* while the watertable surface is indicated by 0 *m*. Hydrocarbon and oxygen concentrations are represented as a percentage of an atmosphere (*i.e.*, 0.5% is equivalent to 5000 *ppm*) and microbe concentrations are in the units of *mg/l*.

The steady-state velocity distribution for the cases examining how different parameters affect air flow are also represented by cross-sectional views of the domain. Only velocities which are greater than 0.1% of the maximum are plotted and a scale for the velocity vector is given in the bottom right corner of the figure in *m/s*. Where pressure distributions are given, the pressure in Pascals is shown by contours over four orders of magnitude: 0 to 10 (by 1); 10 to 100 (by 10); 100 to 1000 (by 100); and 1000 to 10000 (by 1000), where the extraction well represents the highest suction.

Mass fate tables are included to quantify the mass distribution (for hydrocarbon and oxygen) for certain simulations to emphasize differences relative to the base case. The hydrocarbon and oxygen boundary mass summaries indicate the cumulative movement of hydrocarbon and oxygen across all the boundaries as well as the amount of each utilized by the microbes. The 'source' for hydrocarbon is mass input at the constrained source along the watertable; the 'source' for oxygen is mass input from the atmosphere at the ground surface. Stored mass summaries are also presented for hydrocarbon and oxygen to indicate the distribution of the hydrocarbon in the aqueous, vapour, and sorbed phases and the distribution of oxygen in the aqueous and vapour phases. When applicable, the amount of air extracted from and added to the system is included. All mass values are in kilograms and are for the 600 hour time period.

5.3 Base Case

As mentioned previously, the base case is represented by the domain used in Chapter 4. Table 5.1 outlines the site parameters, the contaminant properties, and the biodegradation parameters. The initial hydrocarbon concentration is 0.5% of an atmosphere (5000 *ppm*) along the watertable and zero elsewhere. The initial oxygen

Site Property	Contaminant Property	Biodegradation Parameter
θ_w sand	-	MW 86.17 g/mol M_t 3.30 mg/ℓ
θ_w till	-	D_a 6.99×10^{-6} m^2/s h_u 1.029×10^{-4} s^{-1}
f_{oc} sand	-	μ 6.00×10^{-6} $Pa \cdot s$ K_C 0.32 mg/ℓ
f_{oc} till	-	H_C 73.2 - K_O 0.16 mg/ℓ
k_h sand	2.5×10^{10} m^2	K_{oc} 6633 - G 3.5 -
k_r sand	1.5×10^{10} m^2	Y 0.45 mg/mg
k_h till	6.0×10^{12} m^2	b 8.20×10^{-8} s^{-1}
k_r till	6.0×10^{12} m^2	
α_t	1.0	m
α_t	0.10	m

Table 5.1: Properties for the base case simulation.

concentration is 21% of an atmosphere everywhere.

Figure 5.1 depicts the hydrocarbon distribution for a) passive transport and b) advective-dispersive transport at 600 hours (25 days). The hydrocarbon contour closest to the ground surface is the 0.001 relative contour. Moving from this contour towards the watertable the 0.01, 0.1, 0.3, 0.5, 0.7, and 0.9 contours follow. The rightmost quarter of the domain for the advective-dispersive transport case behaves very similar to passive transport, confirming the extraction well has little influence in that area of the domain. This is also shown in the hydrocarbon profile in Figure 5.2 where diffusion (P) and advection in the far end of the domain (D) have similar hydrocarbon trends. The air movement during advective-dispersive transport allows for increased hydrocarbon migration near the extraction well in the zone of highest air flow (see the velocity distribution in Figure 5.3). This enhanced vertical transport of the hydrocarbon is largely the result of the vertical dispersivity value used; this aspect of the simulations will be examined in more detail later in the chapter. By comparing hydrocarbon distributions for both transport processes at 200 hours (8.3 days) and at 600 hours (25 days), steady-state appears to have been reached in each case. Oxygen transport will reach steady-state as well; however, steady-state was not reached during the time frame used for the simulations in the sensitivity analysis. When the transport for both hydrocarbon and oxygen reaches steady-state, the microbial growth will also be at steady-state. Note that steady-state can be achieved because of the fixed boundary conditions of the numerical model. The constrained sources, which will be realistic for hydrocarbon as long as appreciable amounts of product remains in the subsurface, provide essentially infinite supplies of hydrocarbon and oxygen. The amount of mass input into the system at the source is equivalent to the amount of mass extracted at the well and utilized by the microbes; therefore, these conditions allow for the attainment of steady-state concentrations.

Figures 5.4 and 5.5 depict the relative oxygen distribution for passive and advective-dispersive transport, respectively, at 200 hours and 600 hours. At 600 hours, the contour closest to the watertable is the 0.5 contour, moving towards the ground surface,

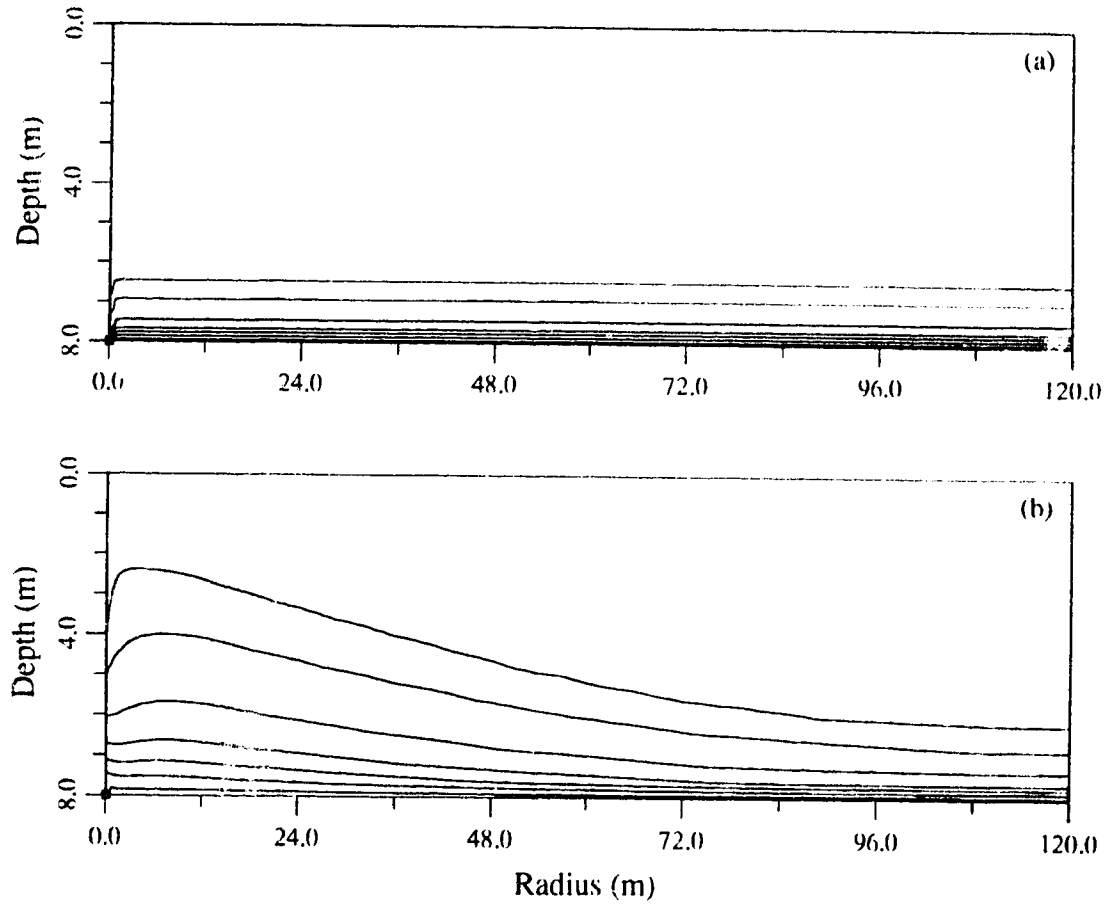


Figure 5.1: Hydrocarbon distribution for a) passive transport and b) advective-dispersive transport at 600 hours for the base case simulation. See Section 5.2 for the description of the contour labelling.

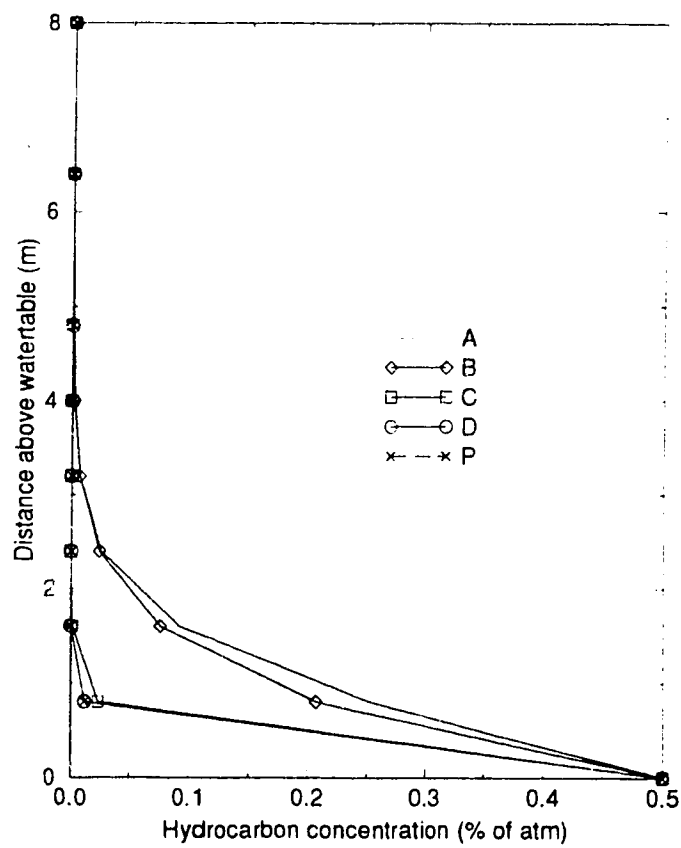


Figure 5.2: Hydrocarbon concentration profile for the base case simulation. See Section 5.2 for the location in the domain each letter represents.

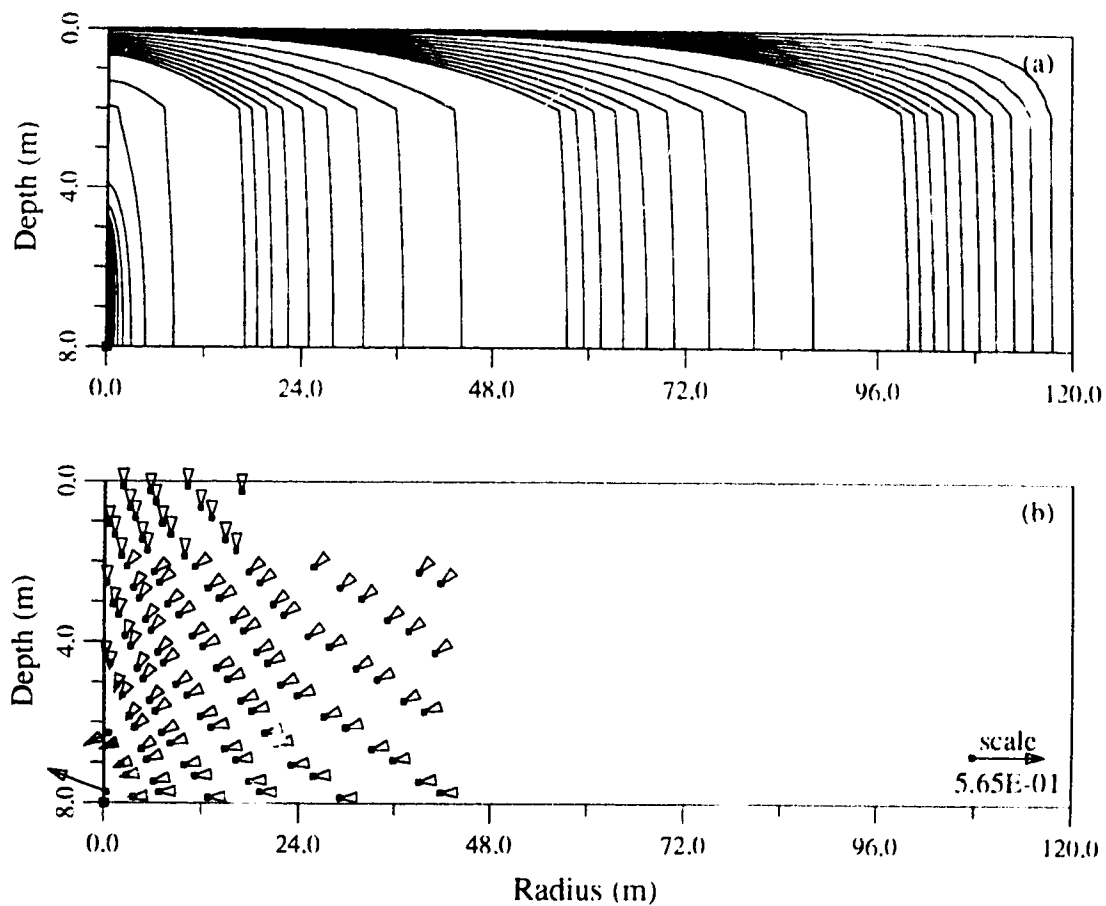


Figure 5.3: a) Pressure and b) velocity distributions for the base case simulation. See Section 5.2 for the description of the contour labelling.

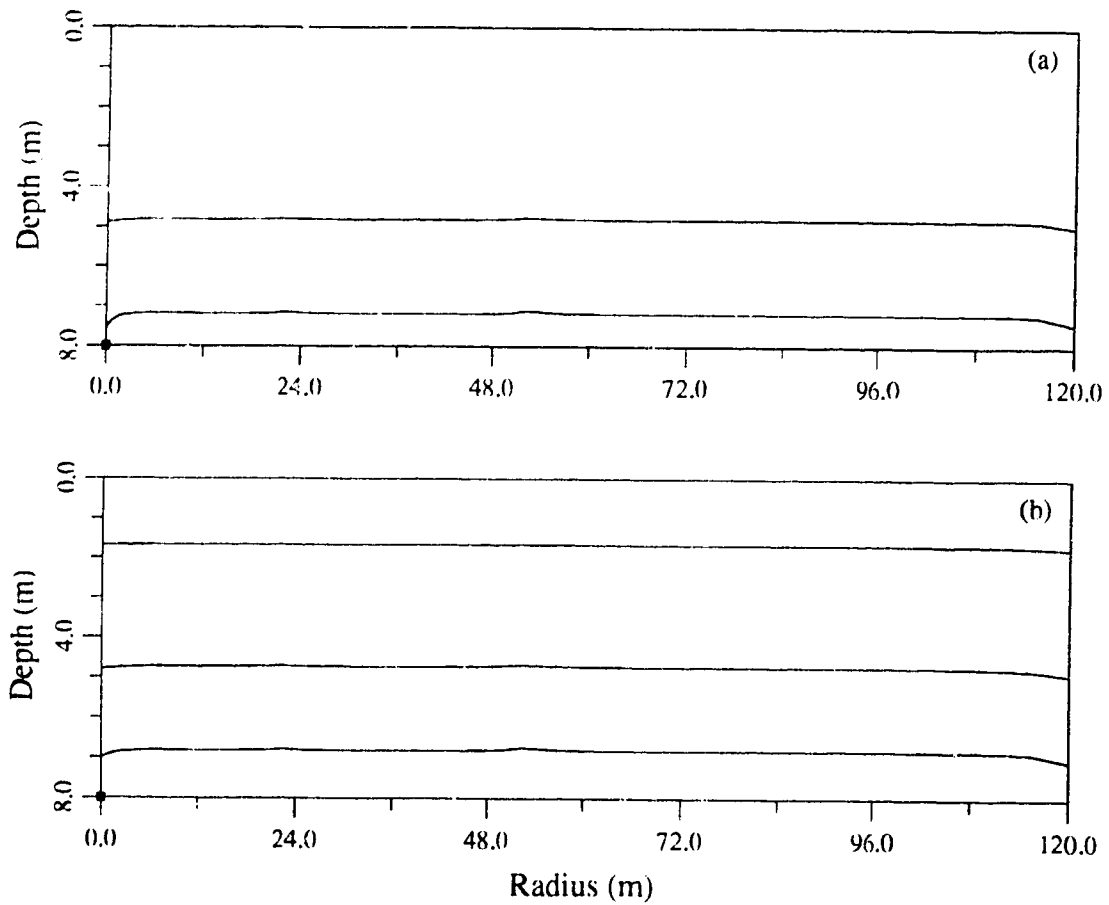


Figure 5.1: Oxygen distribution for passive transport at a) 200 hours and b) 600 hours for the base case simulation. See Section 5.2 for the description of the contour labelling.

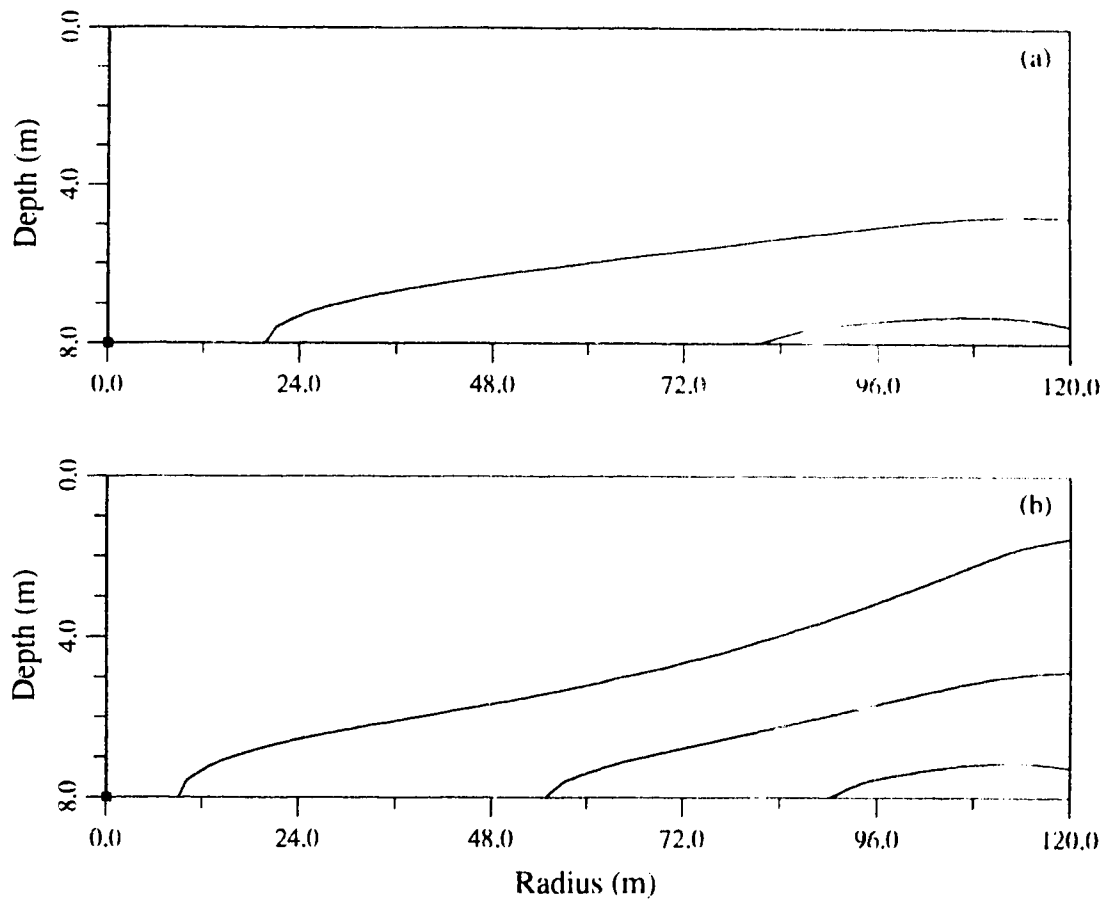


Figure 5.5: Oxygen distribution for advective-dispersive transport at a) 200 hours and b) 600 hours for the base case simulation. See Section 5.2 for the description of the contour labelling.

the 0.7 and 0.9 contours follow with the ground surface representing 1.0. These two figures indicate the oxygen concentrations are continually decreasing through time as a result of microbial degradation. For passive transport, the oxygen decreases conformably across the entire domain; however, for advective-dispersive transport, only the area of low air flow experiences significant drops in oxygen levels (Figure 5.6). Near the well, advective flow is able to replenish the oxygen supply. Oxygen concentrations decrease by the same magnitude for both passive and advective-dispersive transport in the right side of the grid, again indicating that diffusion is the dominant transport mechanism in this area.

Because steady-state air flow is specified, the amount of air flow entering the system along the ground surface and the right lateral boundary must be equivalent to the amount of air flow exiting the system via the extraction well. Only 3% of the total input mass crosses the far right lateral boundary which indicates that the domain is sufficiently large and that the specification of atmospheric pressure is justified along that boundary. Table 5.2 summarizes the mass fate for the hydrocarbon and oxygen for both transport scenarios. Air extraction results in the addition of a substantial amount of oxygen (two orders of magnitude more than the passive case) into the system. In correspondence with the conceptual model, this increase in oxygen availability allows for more hydrocarbon utilization by the microbes during advective-dispersive transport. Because oxygen has a lower Henry's constant than the hydrocarbon, more oxygen is available to the microbial population in the aqueous phase.

The microbial population experiences an overall decrease in size which may indicate the initial size of the microbial population may be too large or the microbe death rate is too high. Over this time interval, the microbial population either linearly increases in size in areas of high hydrocarbon concentrations or decreases in size in areas of low hydrocarbon concentrations, and do not yet reach steady-state concentrations. Figure 5.7 shows that along the watertable, near the hydrocarbon source where the hydrocarbon concentrations in the aqueous phase are highest, the microbial popula-

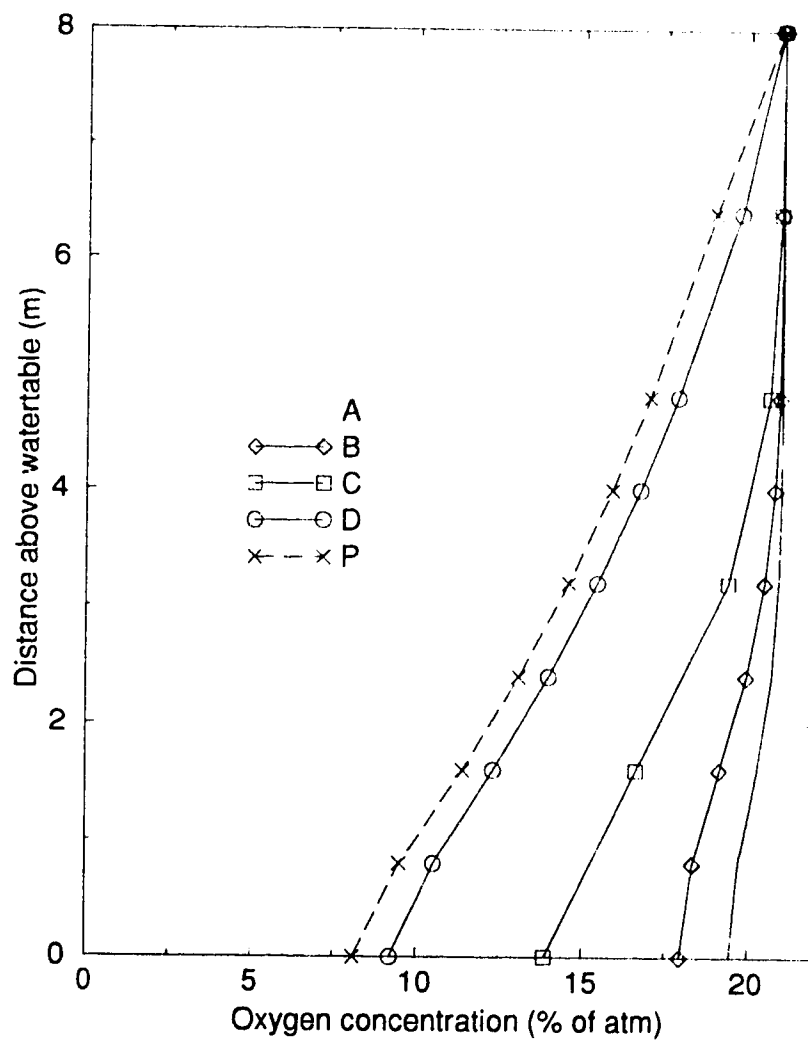


Figure 5.6: Oxygen concentration profile for the base case simulation. See Section 5.2 for the location in the domain each letter represents.

	Passive Transport		Adv-Disp. Transport	
	Hydrocarbon (kg)	Oxygen (kg)	Hydrocarbon (kg)	Oxygen (kg)
Boundary Mass Summary				
lateral	0.0	0.0	2.2×10^1	1.3×10^1
'source'	1.7×10^4	1.1×10^3	4.0×10^2	5.1×10^2
extracted	NA	NA	-9.6×10^3	-5.1×10^3
utilized	-1.7×10^1	-9.5×10^3	-3.0×10^1	-1.7×10^1
Stored Mass Summary				
vapour	6.6×10^1	2.2×10^1	1.0×10^2	2.5×10^1
aqueous	2.0×10^1	1.7×10^2	3.1×10^1	1.9×10^2
sorbed	2.6×10^1	NA	1.0×10^1	NA

Table 5.2: Mass fate for the base case simulation.

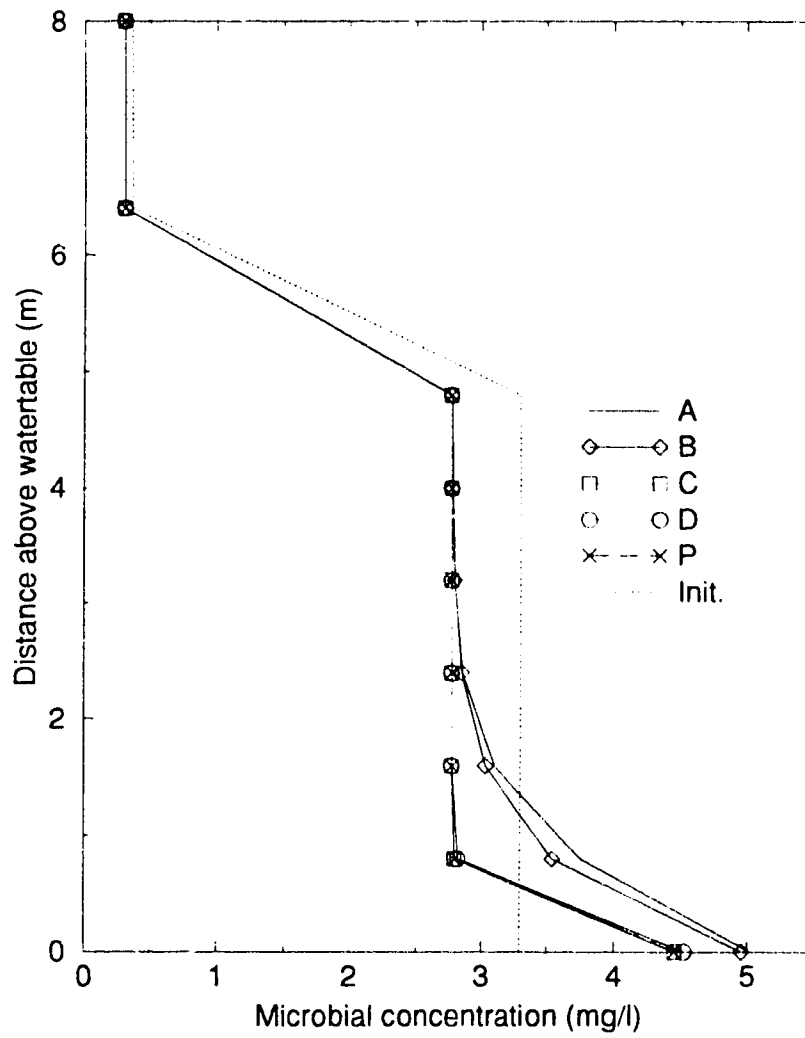


Figure 5.7: Microbial concentration profile for the base case simulation (Init. represents the initial concentration). See Section 5.2 for the location in the domain each letter represents.

tion increases. The most growth is experienced in the area immediately adjacent to the extraction well during advective-dispersive transport. The increased hydrocarbon biodegradation in the area near the source results in decreased oxygen concentrations, especially in the right side of the grid (area of lowest flow during advection) and as a result the microbial growth is slower in this area compared to near the extraction well. Elsewhere in the domain, where lower hydrocarbon concentrations are present, the microbial population declines and less oxygen is utilized.

For comparison to the base case, Figure 5.8 shows the hydrocarbon distribution for a) passive and b) advective-dispersive transport at 600 hours for simulations without biodegradation. The hydrocarbon distribution for Figure 5.8 shows significantly higher travel distances and unlike the base case, steady-state has not yet been achieved, indicating that at this extraction rate, vacuum extraction alone is insufficient to remove the hydrocarbon effectively. The mass removed during vacuum extraction is four times less than the total mass extracted at the well and utilized by the microbes for the base case simulation with biodegradation. In order to remove equivalent amounts of mass, remediation projects using straight vacuum extraction would need much larger extraction rates (and possibly larger extraction pumps) compared to bioventing projects and would require more surface treatment, thus increasing costs. This figure therefore demonstrates the important role biodegradation plays in hydrocarbon transport and suggests that remediation schemes should consider using bioventing for more viable programs.

5.4 Till Layer Thickness and Permeability

The importance of the thickness of the till unit and the permeability contrast between the two layers is explored in this section. Because the soil moisture content was assumed to be independent of permeability, the passive transport behaviour for both oxygen and hydrocarbon did not differ from the base case results. Thus passive transport results are not shown.

Simulations were performed to examine the effects of varying the thickness of the

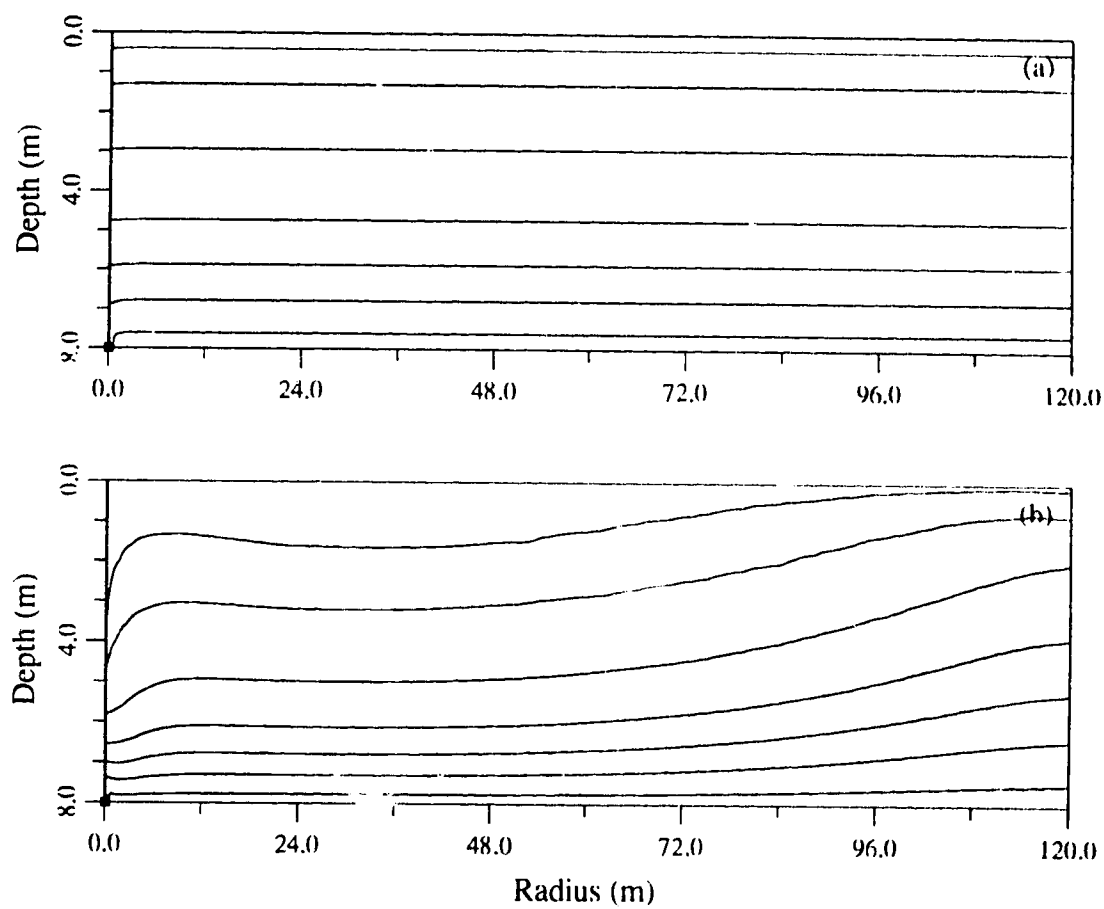


Figure 5.8: Hydrocarbon distribution for a) passive transport and b) advective-dispersive transport without biodegradation at 600 hours for the base case simulation. See Section 5.2 for the description of the contour labelling.

till layer from 4 m to 2 m (base case) to where no lower permeability unit was present. Pressure and velocity distributions are shown in Figure 5.9 for an absent till layer and in Figure 5.10 for a 4 m thick till layer. When no layer is present, the radius of influence of the extraction well decreases dramatically and the area of highest air flow is reduced by half. For this case, no air flow crosses the far right lateral boundary and therefore all oxygen supply comes directly from the ground surface in the vicinity of the well. The thicker till layer exhibits a slight increase in the radius of influence and a doubling of the calculated air flow (and oxygen supply) entering the system from the far right lateral boundary.

Figure 5.11 shows the hydrocarbon distribution for advective-dispersive transport for a) no till layer and b) a thicker till layer. Over half the domain behaves similar to passive transport for the simulation without a till unit because the radius of influence is smaller. In contrast, for the thicker till layer simulation, a slightly smaller portion of the domain behaves similar to passive transport; vertical and lateral hydrocarbon migration is increased along the domain and more hydrocarbon is available to the microbes for utilization. Figure 5.12 shows that oxygen replenishment across the domain is also increased due to the slightly larger radius of influence of the extraction well. As expected the amount of hydrocarbon degraded is higher for this simulation relative to the base case. Without the till layer, oxygen replenishment occurs in a small area only and decreased amounts of both hydrocarbon and oxygen in the system means significantly less hydrocarbon is biodegraded during this simulation (Table 5.3).

To represent the radially-symmetric air flow caused by extraction wells in the field, the numerical model uses axisymmetric, or cylindrical, coordinates meaning the volume of the grid increases dramatically away from the well. Therefore, when the radius of influence of the extraction well is larger due to a lower permeability unit and more oxygen is added to the system further from the extraction well, overall the total mass added the system is substantial. To increase the effectiveness of bioventing a lower permeability unit is beneficial as indicated in Figures 5.11 and

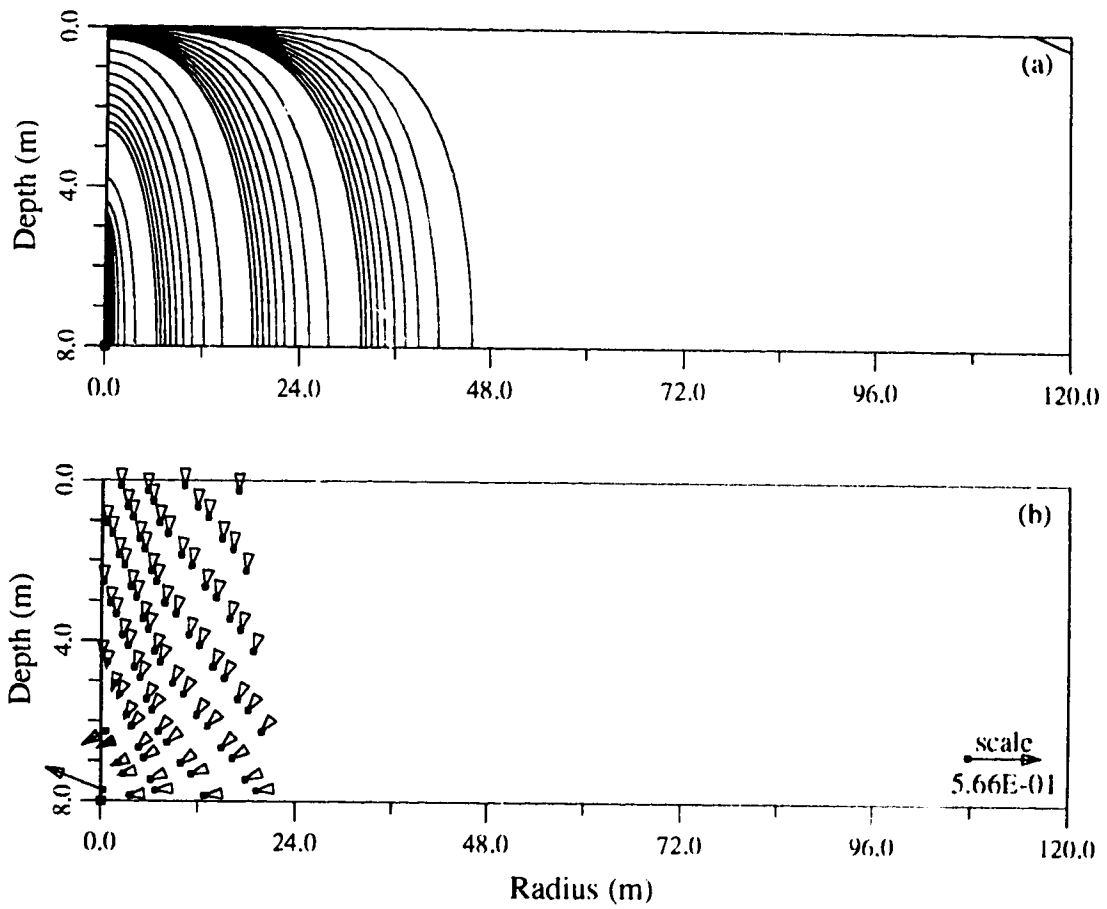


Figure 5.9: a) Pressure and b) velocity distributions for the no till layer simulation. See Section 5.2 for the description of the contour labelling.

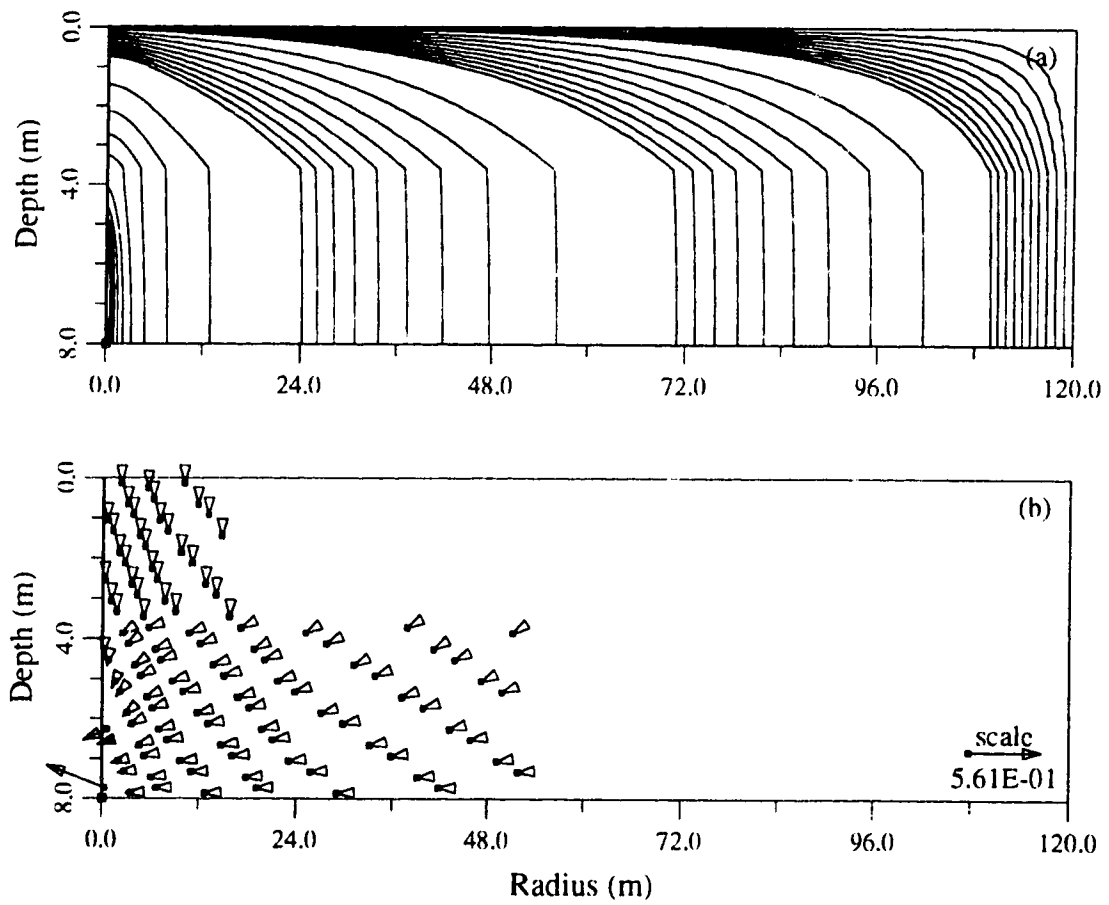


Figure 5.10: a) Pressure and b) velocity distributions for the thicker till layer simulation. See Section 5.2 for the description of the contour labelling.

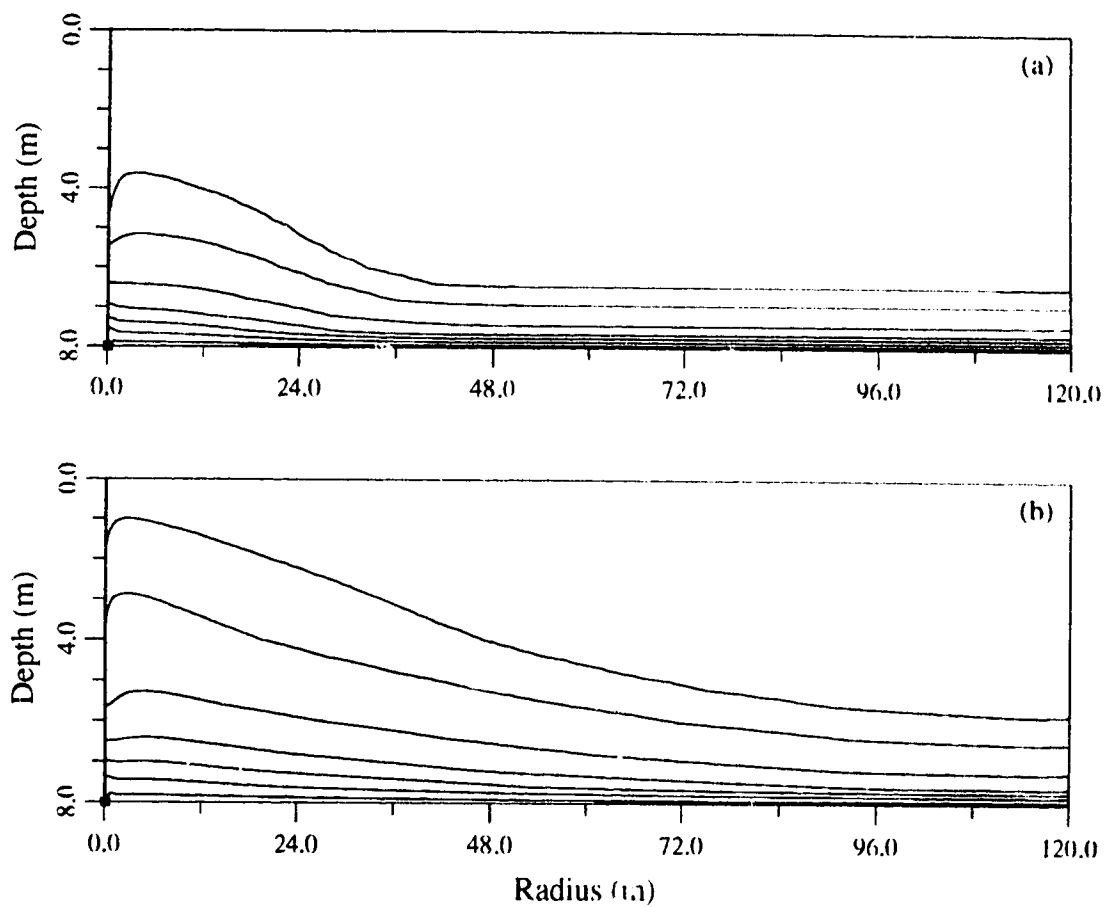


Figure 5.11: Hydrocarbon distribution for advective-dispersive transport for a) no till layer and b) a thicker till layer. See Section 5.2 for the description of the contour labelling.

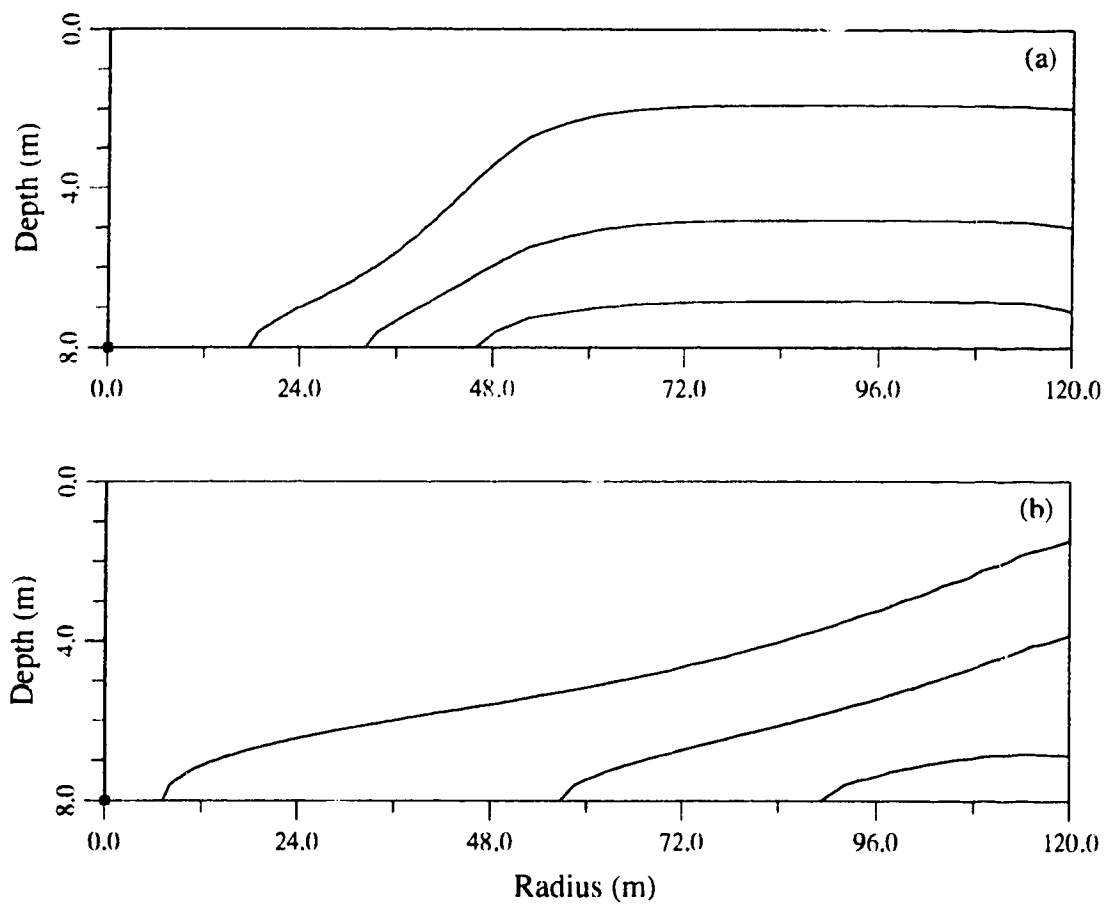


Figure 5.12: Oxygen distribution for advective-dispersive transport for a) no till layer and b) a thicker till layer. See Section 5.2 for the description of the contour labelling.

	No Till Layer		Thicker Till Layer	
	Hydrocarbon (kg)	Oxygen (kg)	Hydrocarbon (kg)	Oxygen (kg)
Boundary Mass Summary				
lateral	1.1×10^{-4}	8.0×10^{-2}	7.0×10^1	2.1×10^4
'source'	2.7×10^4	5.3×10^5	4.7×10^4	5.0×10^5
extracted	-7.6×10^3	-5.2×10^5	-1.2×10^4	-5.1×10^5
utilized	-1.9×10^4	-1.1×10^4	-3.5×10^4	-2.0×10^4

Table 5-3: Mass fate for the no till layer and the thicker till layer simulations.

5.12. For the base case simulation, the till layer can be considered as a leaky cover since air does move through this unit, possibly through fractures. This type of layer appears to be highly effective since oxygen can be replenished in the area of the extraction well. If the permeability contrast between the two layers was too high, the lower permeability layer would act as a relatively impermeable unit (as demonstrated below). For sites with little permeability contrast between layers, a surface cover could provide similar results. Providing the cover was not impermeable, the oxygen supply from the atmosphere along the ground surface is increased because the radius of influence of the extraction well is larger. At sites where surface covers are not applicable, increasing the number of vertical extraction wells is necessary to increase the areal extent of the oxygen supply in the area being remediated.

The mass fate for the simulations in Figure 5.11 is given in Table 5.3. The thicker till layer case experiences an increase in the amount of hydrocarbon into the system from the source which results in an increase in the amount of hydrocarbon present in the aqueous phase available for microbial degradation. More oxygen is utilized because more biodegradation occurs for this case. The oxygen supply is slightly replenished from the oxygen flux across the lateral boundary and this combined with the oxygen added to the system along the ground surface is insufficient to maintain the oxygen concentration at atmospheric levels for any of the cases.

The permeability contrast between the till unit and the sand and gravel unit is two orders of magnitude for the base case simulation. When the difference in the permeability contrast is increased to three orders of magnitude, horizontal flow through the sand and gravel unit, with minimal downward flow through the till unit, dominates the system. The air flux across the lateral boundary is now higher than the air flux across the ground surface boundary and consequently the solution is impacted by boundary effects because the grid is too small for this problem. Simulation results, then, can only provide gross generalizations for this case. Since horizontal flow dominates, transverse dispersion leads to increased hydrocarbon concentrations near the well and oxygen concentrations are the highest near the lateral boundary since

it acts as the oxygen source leading to increased oxygen utilization. Consequently, the area near the extraction well does not experience oxygen replenishment and the concentrations are half those of the base case.

5.5 Extraction Rate, Size and Position of the Well Screen

Determination of the optimal air extraction rate is often required for site remediation in order to decrease cleanup time, to increase the effectiveness, and ultimately to minimize the cost of the remediation scheme. Five different extraction rates were tested to determine which extraction rate best suited the base site to give the most favorable hydrocarbon and oxygen concentration distributions. Figures 5.13 and 5.14 compare the hydrocarbon and oxygen profiles, respectively, for two different extraction rates, 25 and 75 ℓ/s . Recall that the extraction rate for the base case was 118 ℓ/s . A decrease in the extraction rate decreases the vertical transport of both hydrocarbon and oxygen, which decreases the amount of hydrocarbon and oxygen added to the system and results in lower amounts of biodegradation (Table 5.4). Little difference in the hydrocarbon and oxygen distributions between an extraction rate of 75 ℓ/s and 118 ℓ/s is evident. However, the amount of hydrocarbon mass extracted from the well in the vapour phase is less at 75 ℓ/s and this would decrease the amount of off-gas surface treatment required. Based on the criteria that off-gas treatment be minimized while hydrocarbon losses be maximized, relative to the base simulation (Table 5.2), the mass fate summary for this simulation indicates an optimal extraction rate of 75 ℓ/s . For comparison, an optimal rate of 76 ℓ/s was estimated through the field tests at the Strachan field site (Komex, 1994c).

The hydrocarbon distribution is highly affected by changing the position of the well screen. When the bottom of the well screen is moved to 2 m above the watertable, the amount of vertical hydrocarbon transport near the extraction well increases by 2 m as well. Oxygen utilization is not significantly different since oxygen replenishment

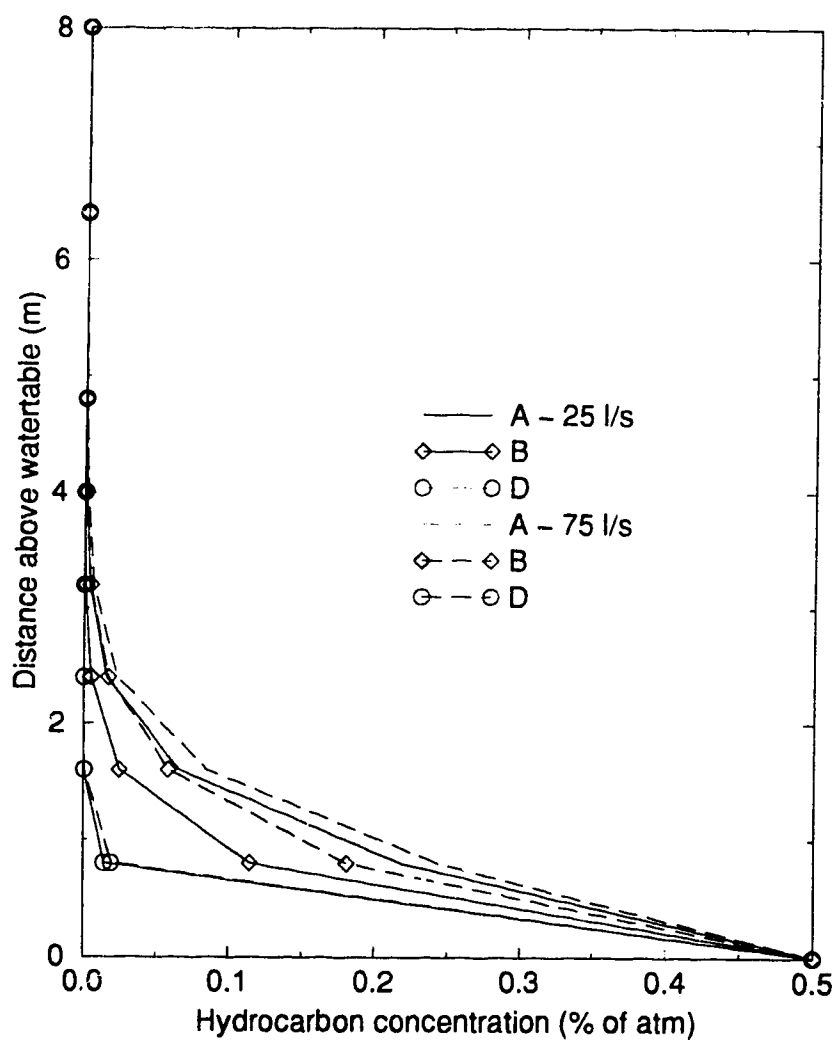


Figure 5.13: Hydrocarbon concentration profile for two different extraction rates, 25 and 75 l/s. See Section 5.2 for the location in the domain each letter represents.

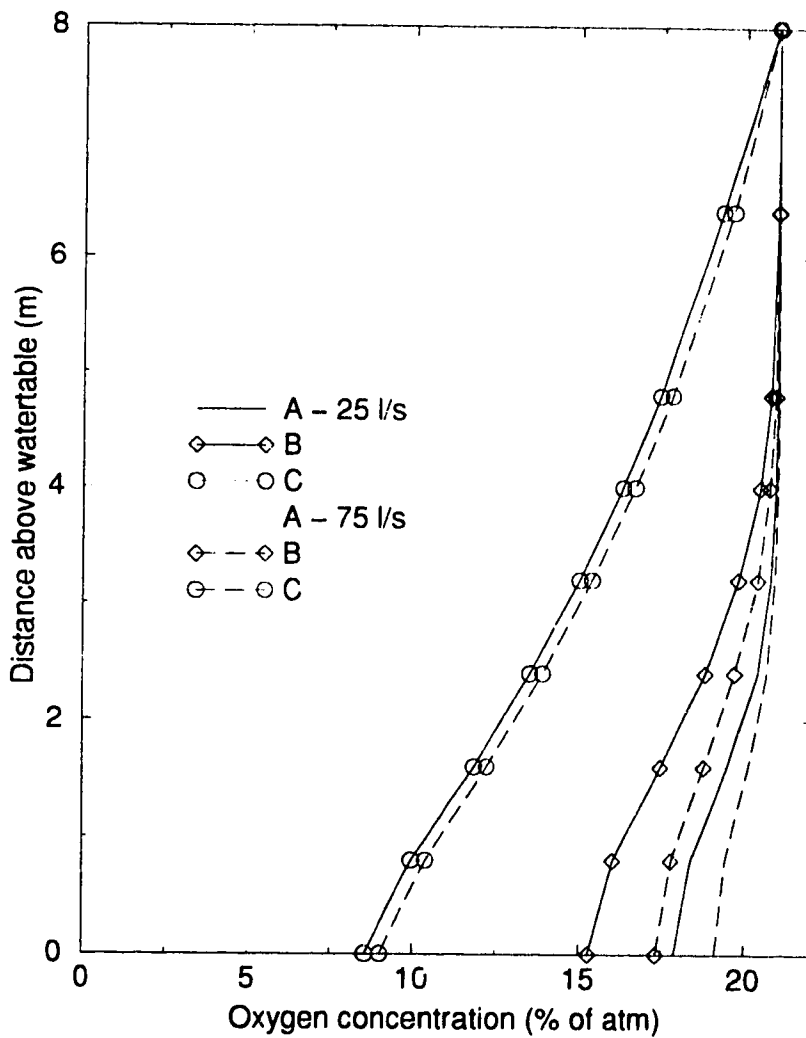


Figure 5.14: Oxygen concentration profile for two different extraction rates, 25 and 75 ℓ/s . See Section 5.2 for the location in the domain each letter represents.

	25 ℓ/s		75 ℓ/s	
	Hydrocarbon (kg)	Oxygen (kg)	Hydrocarbon (kg)	Oxygen (kg)
Boundary Mass Summary				
lateral	3.4×10^0	2.7×10^3	1.2×10^1	8.2×10^3
'source'	2.4×10^4	1.1×10^5	3.3×10^4	3.3×10^5
extracted	-1.8×10^3	-1.1×10^5	-5.9×10^3	-3.2×10^5
utilized	-2.2×10^4	-1.2×10^4	-2.7×10^4	-1.5×10^4
Stored Mass Summary				
vapour	8.0×10^1	2.4×10^4	9.4×10^1	2.5×10^4
aqueous	2.4×10^{-1}	1.8×10^2	2.8×10^{-1}	1.9×10^2
sorbed	3.1×10^1	NA	3.7×10^1	NA

Table 5.4: Mass fate the two different extraction rates, 25 and 75 ℓ/s .

occurs readily in this region of high air flow. The mass fate for this case and the base case are similar. As outlined below, however, the solution is more sensitive to well screen position if a shorter screen is used.

Various simulations were performed where the length of the extraction well screen was decreased by half, resulting in approximately half the volume of air moving through the system. This smaller screened interval was placed at various depths during the simulations. When the well screen was placed close to the watertable, the amount of vertical hydrocarbon transport decreased because air flow converges to a smaller point. When the well screen was placed close to the base of the till unit, the amount of vertical hydrocarbon transport increased as only small flow rates are induced deeper in the system (below the level of the well screen). Figure 5.15 shows the oxygen distribution for the simulations where the well screen is a) near the watertable and b) near the base of the till unit. When the extraction well is closer to the base of the till unit and does not extend to the watertable, an area of decreased air flow develops between the watertable and the bottom of the well screen. In this area, oxygen replenishment is decreased resulting in decreased oxygen concentrations compared to the base case. The oxygen and hydrocarbon distributions for the smaller well screen close to the watertable and the base case are quite similar. The base case removes 1.2 times more hydrocarbon and utilizes almost the same amount of oxygen. However, the amount of mass extracted by the smaller well screen close to the watertable simulation is 1.5 times less, indicating that less surface off-gas treatment is required. Thus, a relatively short well screen closer to the watertable is better in order to maximize hydrocarbon extraction and hydrocarbon and oxygen utilization near the extraction well.

5.6 Initial Microbial Concentrations

The size of the microbial population strongly influences the amount of hydrocarbon and oxygen utilized. Increasing the initial concentration of the microbes from 3.3 to 16.5 to 165 mg/ℓ changes the mass fate for these scenarios. Higher microbial

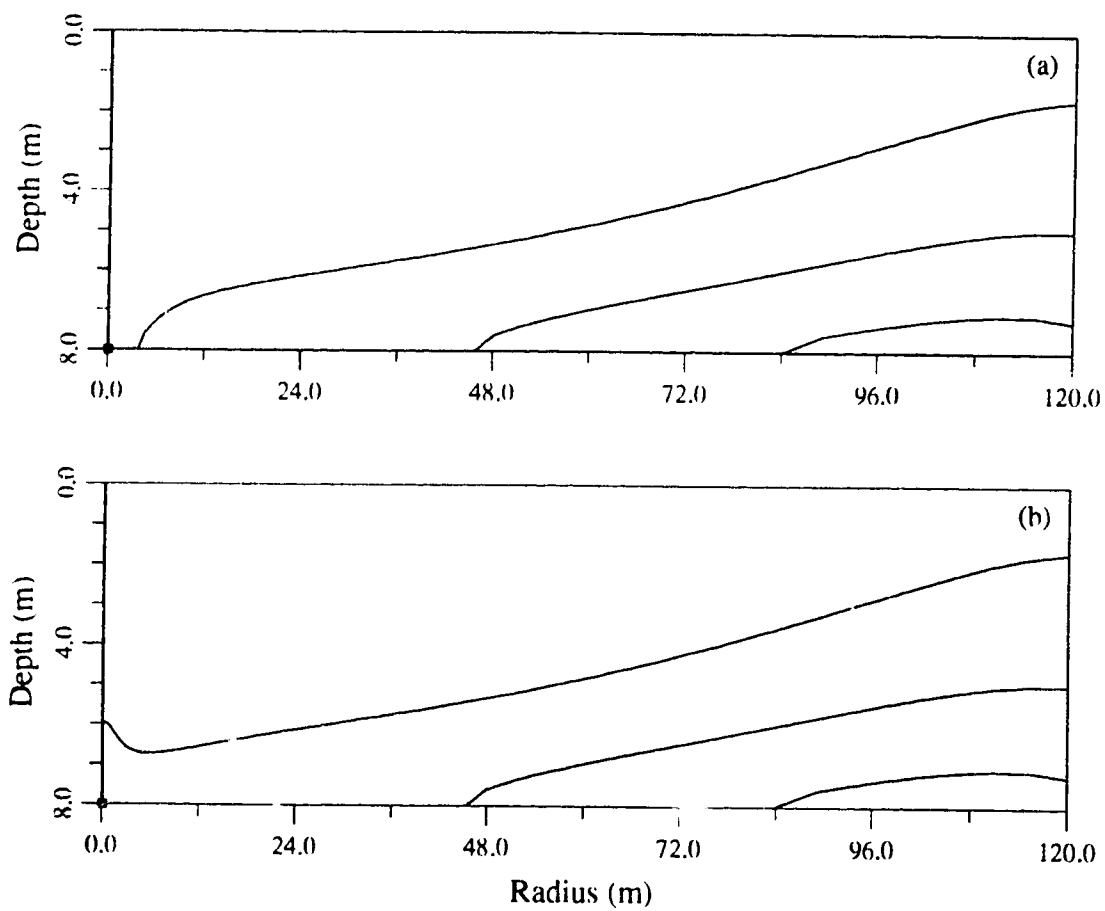


Figure 5.15: Oxygen distribution for advective-dispersive transport for the simulations where the smaller wellscreen is a) near the watertable and b) near the base of the till unit. See Section 5.2 for the description of the contour labelling.

Advective-Dispersive Transport		
	Hydrocarbon (kg)	Oxygen (kg)
Boundary Mass Summary		
lateral	4.9×10^0	7.6×10^3
'source'	1.7×10^5	5.1×10^5
extracted	-6.0×10^3	-4.4×10^5
utilized	-1.6×10^5	-8.9×10^4
Stored Mass Summary		
vapour	6.0×10^1	2.0×10^4
aqueous	1.8×10^{-1}	1.5×10^2
sorbed	2.3×10^1	NA

Table 5.5: Mass fate for a higher microbial concentration.

concentrations utilize more hydrocarbon and oxygen and less mass is extracted from the system (Table 5.5). Increasing the initial microbial concentration by two orders of magnitude (to 165) results in five times as much hydrocarbon and oxygen utilized during advective-dispersive transport and twice as much utilized during passive transport. Relative to the base case, lesser amounts of hydrocarbon and oxygen are available in the aqueous phase for the microbial population. However, overall, more mass has been added to the system at the constrained source due to the increased amount of mass removed from the system. Through time, greater amounts of hydrocarbon and oxygen have been available to the microbial population for utilization and thus more biodegradation occurs for increased microbial populations. As well, compared to the base case, the amount of vertical hydrocarbon transport as indicated by the 0.001 relative contour is less for both passive (1 *m* lower) and advective-dispersive transport (2.5 *m* lower).

Figure 5.16 shows the oxygen distribution for the increased microbial population. The increased size of the population requires more oxygen and the oxygen concentrations are decreased compared to the base case, even in the area near the extraction well. Because of this, the concentration of the oxygen in the rightmost quarter of the domain decreases by two orders of magnitude. The oxygen supply decreases quickly

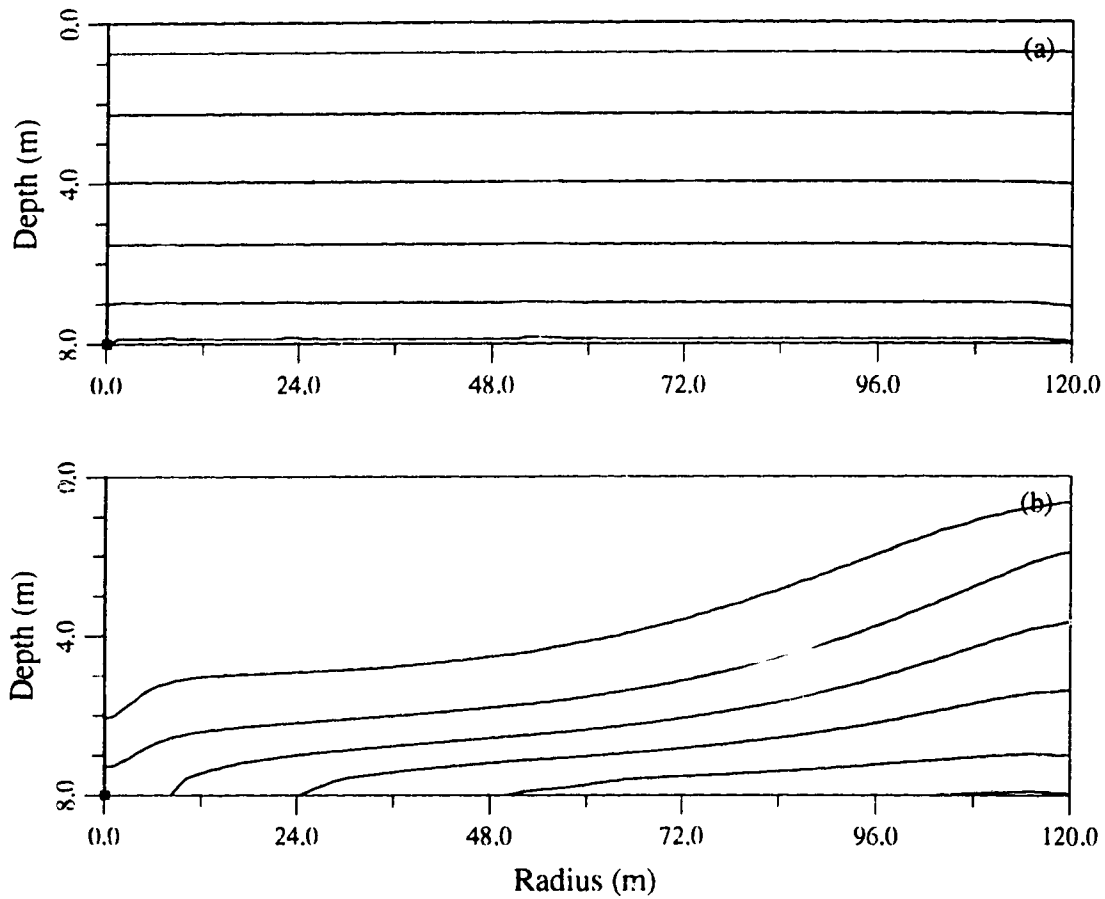


Figure 5.16: Oxygen distribution for a) passive transport and b) advective-dispersive transport for the increased microbial population size simulation. See Section 5.2 for the description of the contour labelling.

in this stagnant area and can no longer sustain microbial activities; therefore, unlike the base case, the size of the microbial concentration decreases. This may imply that $165 \text{ mg}/\ell$ is too large for the initial microbial condition everywhere in the domain, especially in areas of low air flow and low hydrocarbon concentrations, similar to what was indicated by the results for the base case simulation (Figure 5.7). During advective-dispersive transport, in the area of highest flow and increased oxygen supply, more oxygen is utilized by the microbes and therefore less mass is extracted in the vapour phase. The activities of a microbial population this size indicates that for optimal oxygen replenishment, an increase in the extraction rate or in the number of extraction wells should be considered to adequately aerate the area.

The overall mass summary for the microbes indicates a decrease in the total size of the microbial population over time. However, in areas, near the extraction well for example, the microbial population increases where ample hydrocarbon and oxygen in the aqueous phase are accessible to the microbes. In areas with an insufficient supply of oxygen and with low hydrocarbon concentrations, the microbial population decreases (Figure 5.17). When the hydrocarbon concentrations are at low levels for most of the domain, a decrease in the overall size of the microbes is expected since the substrate concentration is unable to sustain microbial activity.

5.7 Soil Moisture Content

Because the microbial population is assumed to exist only within the soil moisture, the microbes utilize hydrocarbon and oxygen in the aqueous phase. Thus, the soil moisture content, or water-filled porosity, will have a strong influence over the rate of biodegradation.

Figure 5.18 compares the oxygen concentration profiles for two simulations where the soil moisture content is (a) increased to 15% in the till unit and to 10% in the sand and gravel unit and (b) decreased to 4% in both units. Recall the soil moisture content is 7.7% in the till unit and 6.2% in the sand and gravel unit for the base case. An increase in the soil moisture content corresponds to an increase in the hydrocar-

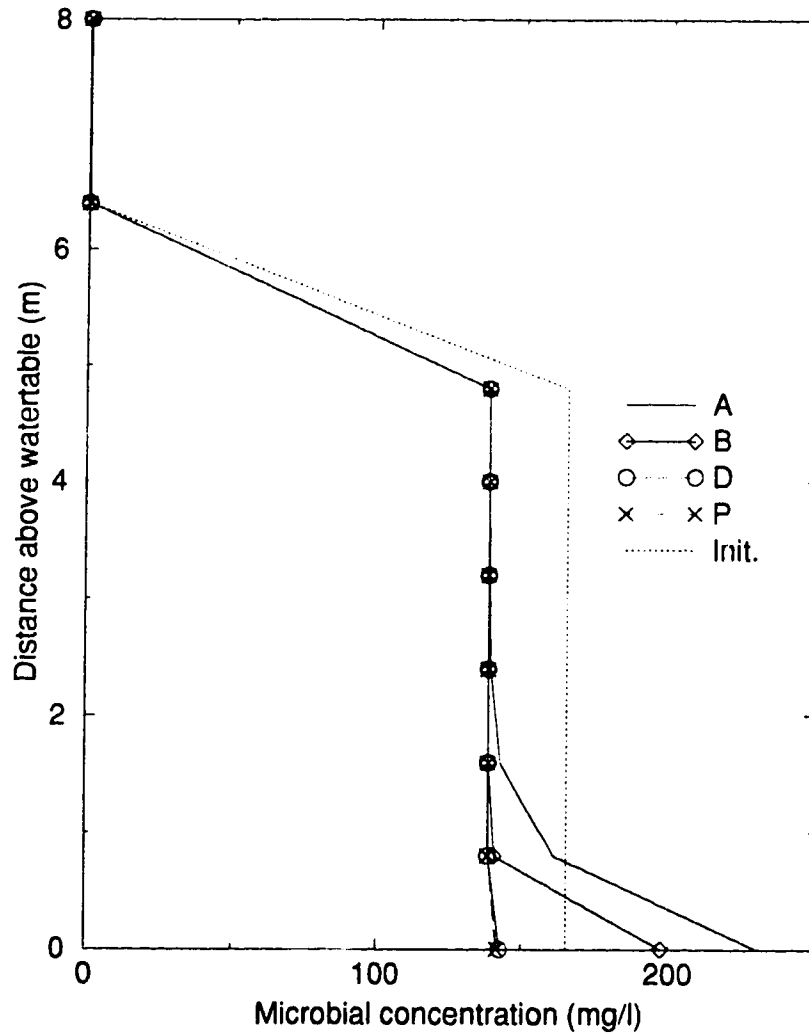


Figure 5.17: Microbial concentration profile for the increased microbial population size simulation (Init. represents the initial concentration). See Section 5.2 for the location in the domain each letter represents.

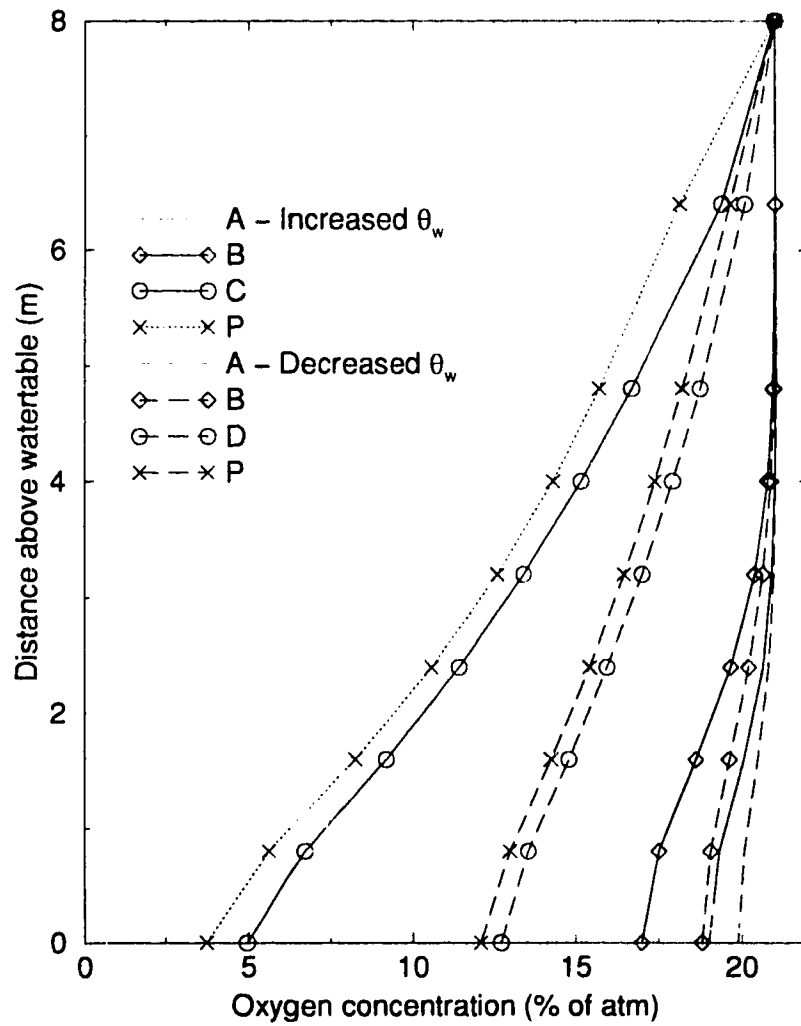


Figure 5.18: Comparison of the oxygen concentration profiles for the simulations with an increased and decreased soil moisture content. See Section 5.2 for the location in the domain each letter represents.

bon and oxygen concentrations per volume of porous medium available for microbial utilization which corresponds to an increase in the amount of biodegradation (Table 5.6). The increased amount of hydrocarbon utilized results in a decrease in the amount of hydrocarbon mass extracted from the well. A decrease in the soil moisture content corresponds to a decrease in the amount of biodegradation and slightly more vertical hydrocarbon migration occurs for both passive and advective-dispersive transport.

Table 5.6 indicates a greater amount of oxygen is utilized when the soil moisture content is increased. Although an increased soil moisture content increases the amount of mass biodegraded in the system, it also decreases the amount of oxygen in the system at a faster rate than the base case. Therefore, for sites with high soil moisture contents, oxygen replenishment may need to be enhanced.

5.8 Biodegradation Parameters

To determine the effect that the rate of biodegradation has on the amount of hydrocarbon and oxygen utilized, the microbial parameters (maximum utilization rate, hydrocarbon and oxygen half-saturation constants, and the microbial death rate) were varied over a range of values (Table 5.7) to give increased or decreased rates of biodegradation, where the average biodegradation rate case is equivalent to the base case.

Figure 5.19 illustrates the difference for advective-dispersive transport for hydrocarbon when a) an increased rate of biodegradation and b) a decreased rate of biodegradation is simulated. The passive transport simulations had similar variations in the hydrocarbon trends relative to the base case. The increased rate of biodegradation case exhibits similar trends in the hydrocarbon distribution as the advective-dispersive transport cases without a till layer (Figure 5.11) and with an increased size in the microbial population (not shown). The similarity with the latter case indicates that for these simulations a greater number of microbes biodegrade equivalent amounts of hydrocarbon (Table 5.5) to the same extent as a smaller number

	Passive Transport		Adv-Disp. Transport	
	Hydrocarbon (kg)	Oxygen (kg)	Hydrocarbon (kg)	Oxygen (kg)
Boundary Mass Summary				
lateral	0.0	0.0	1.4×10^1	1.2×10^4
'source'	1.8×10^4	4.4×10^2	4.7×10^4	5.1×10^5
extracted	NA	NA	-9.2×10^3	-5.1×10^4
utilized	-1.8×10^1	-1.0×10^1	-3.8×10^4	-2.1×10^4
Stored Mass Summary				
vapour	5.2×10^1	1.6×10^1	7.9×10^1	2.0×10^4
aqueous	2.9×10^{-1}	2.6×10^2	4.4×10^{-1}	3.1×10^2
sorbed	2.4×10^1	NA	3.5×10^1	NA

Table 5.6: Mass fate for the increased soil moisture content simulation.

Parameter	Units	Increased Biodegradation	Average Biodegradation (Base Case)	Decreased Biodegradation
h_u	s^{-1}	1.83×10^{-4}	1.029×10^{-4}	5.79×10^{-5}
K_C	mg/ℓ	0.10	0.32	1.0
K_O	mg/ℓ	0.05	0.16	0.50
b	s^{-1}	1.16×10^{-8}	8.20×10^{-8}	5.79×10^{-7}

Table 5.7: Biodegradation parameter ranges for the sensitivity analysis.

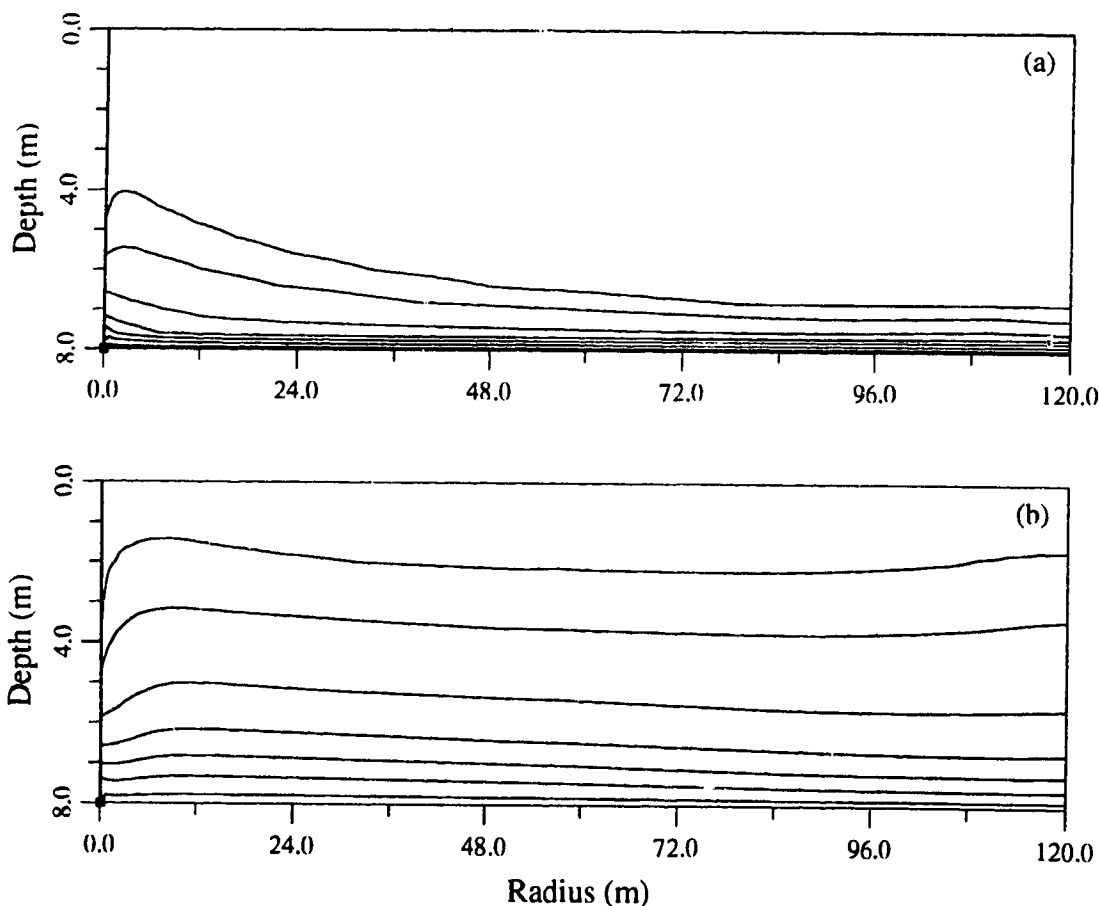


Figure 5.19: Hydrocarbon distribution for advective-dispersive transport for a) an increased biodegradation rate and b) a decreased biodegradation rate. See Section 5.2 for the description of the contour labelling.

Advective-Dispersive Transport		
	Hydrocarbon (kg)	Oxygen (kg)
Boundary Mass Summary		
lateral	8.4×10^0	8.2×10^3
'source'	1.6×10^5	5.1×10^5
extracted	-6.9×10^3	-4.5×10^5
utilized	-1.5×10^5	-8.4×10^4
Stored Mass Summary		
vapour	6.5×10^1	2.0×10^4
aqueous	1.9×10^1	1.5×10^2
sorbed	2.5×10^1	NA

Table 5.8: Mass fate for the increased rate of biodegradation and hexane transport.

of microbes which utilize hydrocarbon faster (Table 5.8). The microbial population in the decreased rate of biodegradation case utilize little hydrocarbon (almost an order of magnitude less than the base case) which results in increased hydrocarbon transport across the entire domain. Microbial activity is evident in this case since the amount of vertical hydrocarbon migration is still less than when no biodegradation is assumed to occur (Figure 5.8). At 600 hours, the hydrocarbon distribution had not yet achieved steady-state for the decreased rate of biodegradation simulation. A decreased amount of oxygen was utilized for this case as well; oxygen concentrations were greater than 19% of an atmosphere everywhere in the domain. Oxygen concentration levels for the base case decreased to 6% of an atmosphere in the area of low flow. In contrast, the oxygen concentration levels declined over one order of magnitude in this area for the increased biodegradation rate case and almost five times as much oxygen was utilized by the microbes.

The size of the microbial population was lowest for the decreased biodegradation rate case and highest (by approximately four times) for the increased biodegradation rate case. For all simulations, the size of the microbial population was only slightly larger for advective-dispersive transport than for passive transport which correlates to slightly higher amounts of hydrocarbon and oxygen being degraded

during advective-dispersive transport. Again microbial growth was greatest near the extraction well and close to the hydrocarbon source. For the increased biodegradation rate case, the microbes grew to $205 \text{ mg}/\ell$ (from $3.3 \text{ mg}/\ell$) in this area; for the base case with an average rate of biodegradation the microbes only grew to $5.0 \text{ mg}/\ell$. Growth did not occur anywhere for the decreased biodegradation rate case due to the low amounts of hydrocarbon and oxygen utilized and the microbial population decreased to $1.0 \text{ mg}/\ell$ across the entire sand and gravel unit, which may also indicate that the microbe death rate was too high. The other two simulations also experienced a decrease in the size of the microbial population in the area of the sand unit that extends 1.0 m above the watertable to the base of the till unit where low hydrocarbon concentrations were present. In this area, the microbial population decreased to $3.2 \text{ mg}/\ell$ for the increased biodegradation rate case and to $2.8 \text{ mg}/\ell$ for the base case.

5.9 Different Hydrocarbon Contaminants

This section of the sensitivity analysis compares transport and biodegradation for three different hydrocarbon contaminants: hexane, dodecane, and benzo[a]pyrene. The contaminants, dodecane and benzo[a]pyrene, were chosen as they both are manufactured in the petroleum refining industry and therefore may be present at sites similar to the Strachan Gas Plant where bioventing may be implemented for remediation. Table 5.9 outlines the chemical properties for the three hydrocarbons. With respect to this study, the differences in the Henry's constant, H_C , and the organic carbon partitioning coefficient, K_{oc} , which affect partitioning of hydrocarbon into the aqueous phase and the retardation factor of hydrocarbon, have the most influence on transport and the amount of hydrocarbon biodegraded. The ratio of oxygen to hydrocarbon consumed, G , is different for the three hydrocarbons due to the differences in their molecular weights and these values are also included in Table 5.9. To decrease the number of changing variables, the source concentration for all three contaminants was 5000 ppm . This concentration maybe too high for benzo[a]pyrene and as a result the amount of transport is probably less than what is described below.

Parameter	Units	Hexane			Dodecane			Benzo[a]pyrene		
		C_6H_{14}	$C_{12}H_{26}$	$C_{20}H_{12}$	C_6H_{14}	$C_{12}H_{26}$	$C_{20}H_{12}$	Reference		
MW	g/mol	86.17	170.33	252.32			calculated			
D_a	m^2/s	6.99×10^{-6}	4.83×10^{-6}	4.0×10^{-6}			(Green, 1984)			
μ	$Pa \cdot s$	6.0×10^{-6}	4.6×10^{-6}	3.9×10^{-6}			(Green, 1984)			
H_C	-	72.2	312	3.4×10^{-5}			(Mackay <i>et al.</i> , 1992)			
K_{oc}	-	6.663×10^4	2.75×10^5	4.4×10^5			(Mackay <i>et al.</i> , 1992)			
G	-	3.5	3.5	2.9			calculated			

Table 5.9: The chemical properties for hexane, dodecane, and benzo[a]pyrene.

Similar to hexane, three different simulations for dodecane were performed to determine the effects increased, average, and decreased biodegradation rates had on transport using the same parameters outlined in Table 5.7. To compare hexane and dodecane at effectively equivalent times, the simulations for dodecane were three times longer (1800 hours or 75 days) to account for the retardation factor which is three times greater for dodecane in the sand and gravel unit. The hydrocarbon distributions for both passive and advective-dispersive transport for dodecane at 1800 hours were basically identical to the distributions for hexane transport at 600 hours for all three biodegradation rates: increased, average, and decreased. The oxygen distributions for the three cases do have slight differences compared to hexane for both a) passive and b) advective-dispersive transport as shown in Figure 5.20 for the average biodegradation rate case. The oxygen concentrations are twice as high for this case compared to the base case. Both the increased and decreased biodegradation rate cases for dodecane also show higher concentrations of oxygen in the domain at the end of the simulation time. Dodecane has a larger Henry's constant compared to hexane and so less hydrocarbon partitions into the aqueous phase. Less oxygen is utilized and as a result an increased amount of oxygen is present in the aqueous and vapour phases throughout the domain. Mass balance calculations indicate that the microbes utilize greater amounts of hydrocarbon during the simulation for dodecane transport relative to hexane transport. At 1800 hours the amount of mass released from the source in the dodecane simulation is almost an order of a magnitude more than the base hexane case. Over the time period an increase in the amount of hydrocarbon utilized by the microbes occurs since more hydrocarbon has been available to the microbes, but the rate of biodegradation is slower as indicated by the decreased amount of oxygen utilized. Therefore, the oxygen supply can be replenished to higher levels in the simulations for dodecane than in the simulations for hexane.

The microbial population size for the dodecane simulations is substantially smaller due to less oxygen utilization and slower biodegradation compared to the hexane simulations. The lower amounts of hydrocarbon in the aqueous phase result in lower

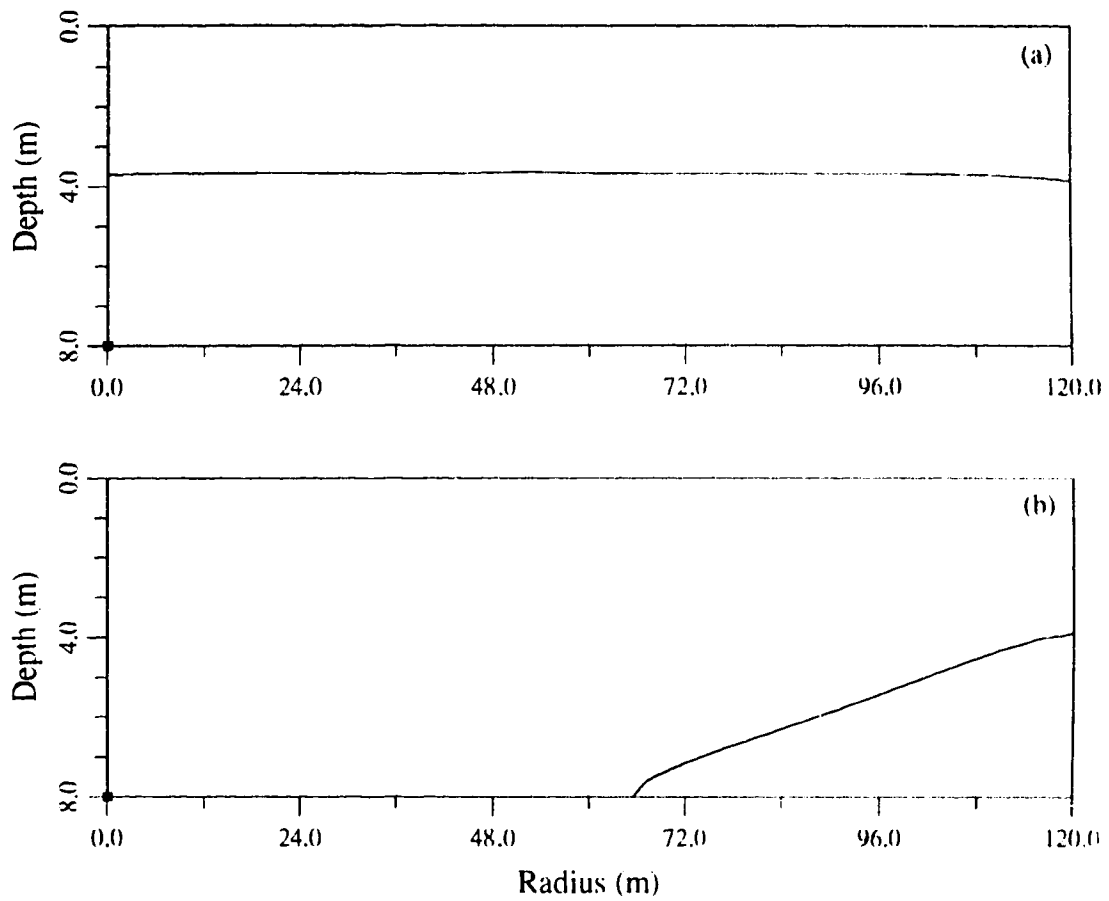


Figure 5.20: Oxygen distribution for a) passive transport and b) advective-dispersive transport at 1800 hours for dodecane with an average rate of biodegradation. See Section 5.2 for the description of the contour labelling.

amounts of substrate available for microbial growth. In the area of optimal conditions near the extraction well and the hydrocarbon source, three times less microbial growth is evident during dodecane transport compared to hexane transport.

Benzo[a]pyrene has a very large retardation factor (on the order of 10^8) due to a very small Henry's constant and a large organic partitioning coefficient. Hydrocarbon transport for benzo[a]pyrene is less than the base hexane passive transport case. For benzo[a]pyrene, no difference between advective-dispersive transport and passive transport is evident since this hydrocarbon is basically immobile due to the very high retardation factor and a very low vapour pressure. The slow transport of benzo[a]pyrene is therefore due to chemical properties and not due to biodegradation parameters. The mass fate calculations for these simulations indicate biodegradation is occurring, but the decreased amounts of oxygen and hydrocarbon utilization indicate a slow rate of biodegradation. The decreased oxygen concentrations in the area of the benzo[a]pyrene hydrocarbon distribution appear to indicate the microbes are utilizing oxygen at a high rate. Instead, the concentration of the hydrocarbon in the aqueous phase is so high that an increased amount of oxygen is utilized, but relative to hexane, the amount of hydrocarbon biodegraded is orders of magnitude less.

5.10 Dispersivities

The longitudinal, α_L , and transverse, α_T , dispersivities may exert considerable control over the shape of the hydrocarbon plume that develops during extraction at a contaminated site. However, values for dispersivities are difficult to quantify and are typically determined from curve fitting. For the base case simulation, the longitudinal and transverse dispersivities differ by a factor of 10, where α_L is 1.0 *m* and α_T is 0.10 *m*. When the transverse dispersivity is decreased to 0.05 *m* so the dispersivities differ by a factor of 20, less vertical transport occurs, as expected. For this case, the hydrocarbon 0.001 relative contour line has the same trend and lies approximately where the 0.01 relative contour line for the base case lies. The mass fate for hydrocarbon, relative to the base case, shows approximately 1.2 times less mass is extracted

at the well and also utilized by the microbes resulting in less mass placed into the system at the source. The oxygen distribution and mass fate for this case and the base case are basically the same.

5.11 Unconstrained Source

For all of the field simulations and the sensitivity analysis, a constrained source has been assumed. This is equivalent to a site with high levels of contamination where a limitless supply of hydrocarbon product is available in the area being remediated. At the end of a site's remediation program, nearly all the product should have been removed and all that would remain would be pockets of contamination throughout the domain. In order to replicate this scenario in a simplified manner, simulations were performed where the hydrocarbon source nodes were unconstrained after 200 hours and allowed to deplete. This enables a rough determination of the time required for hydrocarbon removal and how the removal would occur. The simulations indicate that removal of the hydrocarbon contaminant would be relatively fast; air extraction decreased the remediation time required and the hydrocarbon persisted in the domain 8 hours longer during passive transport. Equilibrium phase-partitioning is still being assumed; however, without a constrained source this assumption may become a less suitable approximation. Investigation of this aspect in future studies may be necessary.

Previously, the magnitude of the oxygen concentrations during transport were the same for both passive and advective-dispersive transport. However, for these simulations, the oxygen concentration levels dropped to 14% of an atmosphere during passive transport and only decreased to 18% of an atmosphere during advective-dispersive transport in the lower half of the grid. Biodegradation continually decreased the amount of hydrocarbon in the system so less oxygen was required by the microbes. The oxygen supply in the system could then increase towards atmospheric levels during advective-dispersive transport due to the continual supply from the ground surface.

During advective-dispersive transport, the hydrocarbon remains the longest in the area of low air flow in the lower right part of the domain. For an unconstrained source without a till layer, the hydrocarbon that remains extends twice as far across the domain compared to a simulation for an unconstrained source with a till layer and persists in the subsurface longer due to the decreased radius of influence of the extraction well when no cover or lower permeable unit exists. The oxygen concentrations for the simulation without a till layer decrease to 14% of an atmosphere, similar to the passive transport case with a layer, indicating in this area where hydrocarbon is still present only diffusion is occurring. The results of these simulations show the geology and surface structures which can act as covers are important factors to consider during bioventing. Without a cover or a lower permeable unit, remediating a site to acceptable levels may be difficult since the oxygen supply decreases in low air flow areas and is only replenished through diffusion. Optimization of the remediation by either adding more extraction wells or a temporary surface cover to increase the radius of influence of the extraction well is necessary in order to have increased oxygen replenishment in areas which otherwise have a low oxygen supply.

Chapter 6

Conclusions

Bioventing is a remediation technique that combines vacuum extraction with microbial degradation in such a way that mass removal is optimized while hydrocarbon extraction is minimized. Field observations and results from this study indicate bioventing is a promising technology to remove subsurface contamination. Although both vacuum extraction and bioventing remove hydrocarbon mass from the subsurface, it appears vacuum extraction is the superior remediation technique when pools of condensate and high hydrocarbon concentrations exist in the subsurface, generally at the start of remediation programs. However, bioventing is the superior remediation technique when the amount of hydrocarbon mass is low and spread discontinuously throughout the subsurface, generally near the end of remediation programs.

An axisymmetric finite-element model was developed to describe bioventing that incorporated air flow, hydrocarbon contaminant and oxygen transport, and microbial degradation. This study has made use of the realistic assumption that air flow may generally be considered to be at steady-state during air extraction and that the usual equations which describe groundwater flow and transport can be modified to describe advective-dispersive transport of both hydrocarbon and oxygen in the unsaturated zone. Biodegradation of hydrocarbon contamination in the subsurface may be described by dual Monod kinetics which also gives rise to non-linear coupling terms in the two transport equations.

The results of the numerical model simulations compare well to field data collected

for three different field tests which studied biodegradation and bioventing. Both the model results and the field data showed oxygen utilization by the microbial population was generally faster at the start of the simulations/tests when the initial hydrocarbon concentration was high. The initial concentrations of hydrocarbon, oxygen, and the microbial population affected the numerical results; therefore, obtaining accurate measurements of this information during field studies is important. The range of biodegradation parameters, including the size of the microbial population, used in the numerical model adequately described biodegradation at this field site and thus the model appears to represent the processes occurring during bioventing.

The size of the microbial population and the biodegradation parameters have the greatest impact on the amount of hydrocarbon degraded. The advantages of a large microbial population are increased amounts of hydrocarbon degraded and decreased amounts of hydrocarbon extracted; a corresponding disadvantage is that the oxygen is depleted faster and replenishment may need to be optimized for long term operations. The biodegradation parameters which highly affect the amount of hydrocarbon and oxygen utilized are the maximum hydrocarbon utilization rate and the hydrocarbon and oxygen half-saturation constants. Increasing the maximum hydrocarbon utilization rate and decreasing the hydrocarbon and oxygen half-saturation constants results in an overall increase in hydrocarbon biodegradation. The amount of biodegradation was comparable to the amount of hydrocarbon degraded when the microbial population was at its highest concentration for the parameters chosen for this study.

During advective-dispersive transport, almost twice as much hydrocarbon and oxygen are degraded relative to passive transport. As a result, the amount of hydrocarbon released to the unsaturated zone from the residual and pooled source is enhanced during advective-dispersive transport. Although the same magnitude of oxygen is utilized for both passive and advective-dispersive transport, oxygen replenishment during air extraction means higher concentrations of oxygen in the area of dominant flow, allowing for an increased amount of hydrocarbon degraded. There-

fore, more microbial growth is experienced during advective-dispersive transport, especially in areas close to the hydrocarbon source and the extraction well (area of increased oxygen replenishment).

After accounting for the retardation factor, transport for two of the contaminants, hexane and dodecane, chosen for this study behaved similarly. However, the rate of biodegradation is slower for dodecane because dodecane has a larger Henry's constant, resulting in less hydrocarbon partitioning into the aqueous phase. This indicates the chemical properties, such as the Henry's constant and the organic partitioning coefficient, are important to consider when analyzing how much biodegradation occurs at field sites with various hydrocarbon contaminants. For example, the slow transport of benzo[a]pyrene at a first glance may appear to be caused by increased biodegradation; however, in reality it is primarily due to the chemical properties of benzo[a]pyrene.

To optimize the efficiency of bioventing for site remediation, several factors should be considered. With high soil moisture contents, an increased amount of hydrocarbon is degraded since more oxygen and hydrocarbon are present in the aqueous phase. The extraction well should have a relatively short well screen placed as close as possible to the hydrocarbon source. An analysis of the amount of hydrocarbon and oxygen utilized versus the amount of hydrocarbon extracted is necessary to determine an optimal extraction rate. The most important factor to consider is the radius of influence of the extraction well. A site with an extraction well that has a large radius of influence will require a shorter remediation time. Therefore, fields site that have a lower permeability unit overlying the unit with hydrocarbon contamination will be remediated faster since the oxygen is supplied to the microbial population over a greater distance. A surface cover would provide similar results.

The values for the parameters describing hydrocarbon biodegradation in the unsaturated zone need to be investigated further. Currently, the values for these parameters reported in the literature are predominantly for saturated biodegradation. Using the same range of values determined in this thesis for the maximum hydrocarbon utilization rate, the hydrocarbon and oxygen half-saturation constants, and

the microbial decay rate for three different contaminants may oversimplify the problem, especially when a mixture of contaminants is present. Also, more bioventing field studies are required. This study was at times limited by the data available and detailed measurements of the hydrocarbon, oxygen, and microbial concentrations throughout the entire remediation project as well as detailed information on the geologic properties could have increased the accuracy of the model simulations. For example, the size of the microbial concentration controls the amount of hydrocarbon degraded; therefore, throughout a remediation project measurements of the subsurface microbial concentrations initially as well as through time will indicate if the numerical model is accurately predicting the changes in the size of the microbial population.

References

- Aelion, C. M., and Bradley, P. M. 1991. Aerobic Biodegradation Potential of Sub-surface Microorganisms from a Jet Fuel-Contaminated Aquifer. *Applied and Environmental Microbiology*, **57**(1), 57-63.
- Alexander, M. 1994. *Biodegradation and Bioremediation*. San Diego: Academic Press Inc.
- Armstrong, J. E., Frind, E. O., and McClellan, R. D. 1994. Nonequilibrium mass transfer between the vapor, aqueous, and solid phases in unsaturated soils during vapor extraction. *Water Resources Research*, **30**(2), 355-368.
- Bachr, A. L., and Baker, R. J. 1995. A Reactive Gas-Transport Model and Application to Determine Hydrocarbon Biodegradation Rates in Unsaturated Porous Media. *Water Resources Research*, **31**(11), 2877-2882.
- Bachr, A. L., Hoag, G. E., and Marley, M. C. 1989. Removing Volatile Contaminants from the Unsaturated Zone By Inducing Advective Air-Phase Transport. *Journal of Contaminant Hydrogeology*, **4**, 1-26.
- Bachr, A.L., and Corapcioglu, M. Y. 1987. A Compositional Multiphase Model for Groundwater Contamination by Petroleum Products 2. Numerical Solution. *Water Resources Research*, **23**(1), 201-213.
- Baveye, P., and Valocchi, A. 1989. An Evaluation of Mathematical Models of the Transport of Biologically Reacting Solutes in Saturated Soils and Aquifers. *Water Resources Research*, **25**(6), 1413-1421.

- Beak, Consultants Limited. 1990. *In-Situ Bioremediation: Considerations, Limitations, Potential, and Future Directions*. Burlington, Ontario: Burlington Environmental Technology Office, Canada Centre for Inland Waters.
- Bear, J. 1979. *Hydraulics of Groundwater*. New York, N.Y.: McGraw-Hill.
- Beausoleil, Y. J., Huber, J. S., Barker, G. W., and Neumann, S. N. 1993 (mar). *The Use of Air Sparging in the Remediation of a Production Gas Processing Facility*. Presented at SPE/EPA Exploration and Production Environmental Conference, San Antonio, Texas.
- Borden, R. C., and Bedient, P. B. 1986. Transport of Dissolved Hydrocarbons Influenced by Oxygen-Limited Biodegradation 1. Theoretical Development. *Water Resources Research*, **22**(13), 1973-1982.
- Borden, R. C., Bedient, P. B., Lee, M. D., Ward, C. H., and Wilson, J. T. 1986. Transport of Dissolved Hydrocarbons Influenced by Oxygen-Limited Biodegradation 2. Field Application. *Water Resources Research*, **22**(13), 1983-1990.
- Brooks, R.H., and Corey, A.T. 1964. *Hydraulic Properties of Porous Media*. Fort Collins, Colorado: Colorado State University, Hydrology Paper No. 3.
- Brusseau, M. L. 1991. Transport of Organic Chemicals by Gas Advection in Structured or Heterogeneous Porous Media: Development of a Model and Application to Column Experiments. *Water Resources Research*, **27**(12), 3189-3199.
- Chapelle, F. H. 1993. *Ground-water Microbiology and Geochemistry*. Toronto: John Wiley and Sons Inc.
- Chen, Y. M., Abriola, L. M., Alvarez, P. J. J., Anid, P. J., and Vogel, T. M. 1992. Modeling Transport and Biodegradation of Benzene and Toluene in Sandy Aquifer Material: Comparisons With Experimental Measurements. *Water Resources Research*, **28**(7), 1833-1847.

- Cleary, R.W., and Unga, M.J. 1991. *PRINCE*. User guide version 3.0 edn. Princeton Analytical Models of Flow and Mass Transport.
- Croise, J., Kinzelbach, W., and Schmolke, J. 1989. *Computation of Air Flows Induced in the Zone of Aeration During In Situ Remediation of Volatile Hydrocarbon Spills*. Rotterdam, Netherlands: Balkema. From *Contaminant Transport in Groundwater*, edited by H.E. Kobus and W. Kinzelbach.
- Daus, A. D., Frind, E. O., and Sudicky, E.A. 1985. Comparative Error Analysis in Finite Element Formulations of the Advection-Dispersion Equation. *Advances in Water Resources*, 8(6), 86-95.
- Domenico, P.A., and Schwartz, F.W. 1990. *Physical and Chemical Hydrogeology*. New York: John Wiley and Sons, Inc.
- Energy & Environmental Research Center, University of North Dakota. 1994 (sept). *Subsurface Sampling and Analysis of Contaminated Sediments at the Strachan Gas Plant*. Prepared for Project Steering Committee, CAPP. 94-EERC-09-05.
- Environmental Research Advisory Council, ERAC. 1994 (jul). *Subsurface Remedial Technologies Newsletter*. Edited by J. Armstrong, Komex International Ltd.
- Fetter, C.W. 1993. *Contaminant Hydrogeology*. New York: Macmillan Publishing Company.
- Freeze, R. A., and Cherry, J. A. 1979. *Groundwater*. New Jersey: Prentice-Hall, Inc.
- Frind, E.O. 1982. Simulation of Long Term Transient Density-Dependent Transport in Groundwater. *Advances in Water Resources*, 5(2), 73-88.
- Fyfe, W. S. 1996. The Biosphere is Going Deep. *Science*, **273**, 448.
- Green, D. W. 1984. *Perry's Chemical Engineer's Handbook*. New York: McGraw-Hill. 6th Edition.

- Hemond, H. F., and Fechner, E. J. 1994. *Chemical Fate and Transport in the Environment*. San Diego, California, USA: Academic Press, Inc.
- Hinchee, R. E., and Olfenbittel, R. F. 1991. *In Situ Bioreclamation Applications and Investigations for Hydrocarbon and Contaminated Site Remediation*. Columbus, Ohio: Butterworth-Heinmann.
- Hinchee, R. E., and Ong, S. K. 1992. A Rapid In Situ Respiration Test for Measuring Aerobic Biodegradation Rates of Hydrocarbons in Soil. *Journal of the Air and Waste Management Association*, **42**(10), 1305-1312.
- Huyakorn, P.S., and Pinder, G.F. 1983. *Computational Methods in Subsurface Flow*. Orlando, Florida: Academic Press.
- Johnson, P.C., Kemblowski, M.W., and Colthart, J.D. 1990. Quantitative Analysis for the Cleanup of Hydrocarbon-Contaminated Soils by In-Situ Soil Venting. *Groundwater*, **28**(3), 413-429.
- Johnson, R.L., Palmer, C.D., and Keely, J.F. 1993 (nov). *Mass Transfer of Organics between Soil, Water and Vapor Phases: Implications for Monitoring, Biodegradation and Remediation*. Proceedings, NWWA/API Conference on Petroleum Hydrocarbons and Organic Chemicals in Ground Water: Prevention, Detection, Restoration, Houston, Texas.
- Komex, International Ltd. 1994a (mar). *1993 Soil Vapour Extraction Program Bioventing*. Draft Appendix, A93-2327-5-1.
- Komex, International Ltd. 1994b (mar). *1993 Soil Vapour Extraction Program Summary Report*. Draft, KI93-2327-5-4.
- Komex, International Ltd. 1994c (jun). *Soil Vapour Extraction and Bioventing Program*. Summary Report.

- Lang, J. R., Rathfelder, K. M., and Abriola, L. M. 1995 (apr). *A Multiphase, Multicomponent Numerical Model of Bioventing with Non-equilibrium Mass Exchange*. Presented at The Third International Symposium for In Situ and On-Site Bioreclamation, San Diego, California.
- Mackay, D., Shiu, W.Y., and Ma, K.C. 1992. *Illustrated Handbook of Physical-Chemical Properties and Environmental Fate for Organic Compounds*. Boca Raton: Lewis Publishers. Volume III.
- MacQuarrie, K. T. B., and Sudicky, E. A. 1990. Simulation of Biodegradable Organic Contaminants in Groundwater 2. Plume Behavior in Uniform and Random Flow Fields. *Water Resources Research*, **26**(2), 223-239.
- MacQuarrie, K. T. B., Sudicky, E. A., and Frind, E. O. 1990. Simulation of Biodegradable Organic Contaminants in Groundwater 1. Numerical Formulations in Principal Directions. *Water Resources Research*, **26**(2), 207-222.
- Massmann, J. W. 1989. Applying Groundwater Flow Models in Vapor Extraction System Design. *Journal of Environmental Engineering*, **115**(1), 129-149.
- McWhorter, D. B. 1990. Unsteady Radial Flow of Gas in the Vadose Zone. *Journal of Contaminant Hydrogeology*, **5**, 297-314.
- Mendoza, C. A. 1992 (feb). *VapourT*. User's Guide.
- Mendoza, C.A. 1989. *Advective-Dispersive Transport of Heavy Organic Solvent Vapours in the Unsaturated Zone*. M.Sc. Thesis, University of Waterloo, Dept. Earth Sciences.
- Mendoza, C.A., Johnson, R.L., and Gillham, R.W. 1996. *Vapor Migration in the Vadose Zone*. Portland, Oregon: Waterloo Press. From *Dense Chlorinated Solvents*, by J.F. Pankow and J.A. Cherry.
- Miller, R. N., Vogel, C. C., and Hinchee, R. E. 1991. *A Field-Scale Investigation of Petroleum Hydrocarbon Biodegradation in the Vadose Zone Enhanced by Soil*

- Venting at Tyndall AFB, Florida*. Columbus, Ohio: Butterworth-Heinmann. From *In Situ Bioreclamation: Applications for Hydrocarbon and Contaminated Site Remediation*, edited by R. E. Hinchee and R. F. Olfenbuttel.
- Miller, R. N., Downey, D. C., Carmen, V. A., Hinchee, R. E., and Leeson, A. 1993. *A Summary of Bioventing Performance at Multiple Air Force Sites*. Houston, Texas: Water Well Publishing Company. 1993 *Petroleum Hydrocarbons and Organic Chemicals in Ground Water: Prevention, Detection, and Restoration*, Water Well Journal Publishing Company, Houston, Texas.
- Millington, R.J., and Quirk, J.P. 1961. Permeability of Porous Solids. *Transactions of the Faraday Society*, **57**, 1200-1207.
- Molz, F. J., Widdowson, M. A., and Benefield, L. D. 1986. Simulation of Microbial Growth Dynamics Coupled to Nutrient and Oxygen Transport in Porous Media. *Water Resources Research*, **22**(8), 1207-1216.
- Moore, B. J., Armstrong, J. E., and Hardisty, P. E. 1995 (apr). *The Effects of Temperature and Flow Rate Variations During Bioventing in Cold Climates*. Presented at the Third International Symposium for In Situ and On-Site Bioreclamation, San Diego, California.
- NRC. 1993. *In Situ Bioremediation - When Does it Work?* Washington, D.C.: National Academy Press. National Research Council.
- Ogata, A., and Banks, R.B. 1961. *A Solution of the Differential Equation of Longitudinal Dispersion in Porous Media*. Tech. rept. Paper no. 411-A. U.S. Geological Survey.
- Ostendorf, D. W., and Kampbell, D. H. 1991. Biodegradation of Hydrocarbon Vapors in the Unsaturated Zone. *Water Resources Research*, **27**(4), 453-462.
- Pederson, K. 1996. *Earth Science Review*, **34**(243).

- Rafai, H. S., and Bedient, P. B. 1990. Comparison of Biodegradation Kinetics With an Instantaneous Reaction Model for Groundwater. *Water Resources Research*, **26**(4), 637-645.
- Rafai, H. S., Bedient, P. B., Wilson, J. T., Miller, K. M., and Armstrong, J. M. 1988. Biodegradation Modeling at Aviation Fuel Spill Site. *Journal of Environmental Engineering*, **114**(5), 1007-1029.
- Rafai, H. S., Long, G. P., and Bedient, P. B. 1991. *Modeling Bioremediation: Theory and Field Application*. Columbus, Ohio: Butterworth-Heinmann. From *In Situ Bioreclamation: Applications for Hydrocarbon and Contaminated Site Remediation*, edited by R. E. Hinchee and R. F. Olfenbittel.
- Rathfelder, K., Lang, J.R., and Abriola, L.M. 1995 (jul). *Soil Vapor Extraction and Bioventing: Applications, Limitations, and Future Research Direction*. Tech. rept. International Union of Geodesy and Geophysics. *Reviews of Geophysics*, supplement.
- Riser-Roberts, E. 1992. *Bioremediation of Petroleum Contaminated Sites*. Chelsea, Mich.: C.K. Smoley.
- Rittmann, B.E., Seagren, E., Wrenn, B.A., Valocchi, A.J., Ray, C., and Raskin, L. 1994. *In Situ Bioremediation*. New Jersey: Noyes Publications. 2nd Edition, Source for microbial parameters.
- Schafer, W., and Kinzelbach, W. 1991. *Numerical Investigation into the Effects of Aquifer Heterogeneity on In Situ Bioremediation*. Columbus, Ohio: Butterworth-Heinmann. From *In Situ Bioreclamation: Applications for Hydrocarbon and Contaminated Site Remediation*, edited by R. E. Hinchee and R. F. Olfenbittel.
- Segerlind, L.J. 1984. *Applied Finite Element Analysis*. New York, New York: John Wiley and Sons. 2nd edition.

- Sleep, B. E., and Sykes, J. F. 1991. *Biodegradation of Volatile Organic Compounds in Porous Media with Natural and Forced Gas-Phase Advection*. Columbus, Ohio: Butterworth-Heinmann. From *In Situ Bioreclamation: Applications for Hydrocarbon and Contaminated Site Remediation*, edited by R. E. Hinchee and R. F. Olfenbuttel.
- Wang, H.F., and Anderson, M.P. 1982. *Introduction to Groundwater Modeling: Finite Difference and Finite Element Methods*. San Francisco: W.H. Freeman and Company.
- Weeks, E.P., Douglas, E.E., and Thompson, G.M. 1982. Use of Atmospheric Fluorocarbons F-11 and F-12 to Determine the Diffusion Parameters of the Unsaturated Zone in the Southern High Plains of Texas. *Water Resources Research*, **18**(5), 1365-1378.
- Widdowson, M. A., and Aclion, C. M. 1991. *Application of a Numerical Model to the Performance and Analysis of an In Situ Bioremediation Project*. Columbus, Ohio: Butterworth-Heinmann. From *In Situ Bioreclamation: Applications for Hydrocarbon and Contaminated Site Remediation*, edited by R. E. Hinchee and R. F. Olfenbuttel.
- Widdowson, M. A., Molz, F. J., and Benefield, L. D. 1988. A Numerical Transport Model for Oxygen- and Nitrate-Based Respiration Linked to Substrate and Nutrient Availability in Porous Media. *Water Resources Research*, **24**(9), 1553-1565.
- Wilson, D. J., Clarke, A. N., and Clarke, J. H. 1988. Soil Clean Up by in-situ Aeration I. Mathematical Modeling. *Separation Science and Technology*, **23**(11), 991-1037.
- Wu, J. C., Fan, L. T., and Erickson, L. E. 1990. Modeling and Simulation of Bioremediation of Contaminated Soils. *Environmental Progress*, **9**(1), 47-56.